MODELING AND SMALL SIGNAL STABILITY ANALYSIS OF SYNCHRONVERTER BASED DISTRIBUTED GENERATORS IN ISLANDED MICROGRID

MS (Research) Thesis

by

RAHUL RAJENDRA PAWAR

DISCIPLINE OF ELECTRICAL ENGINEERING
INDIAN INSTITUTE OF TECHNOLOGY INDORE

JULY 2022

MODELING AND SMALL SIGNAL STABILITY ANALYSIS OF SYNCHRONVERTER BASED DISTRIBUTED GENERATORS IN ISLANDED MICROGRID

A THESIS

Submitted in fulfillment of the

requirements for the award of the degree

of

Master of Science (Research)

by

RAHUL RAJENDRA PAWAR

DISCIPLINE OF ELECTRICAL ENGINEERING

INDIAN INSTITUTE OF TECHNOLOGY INDORE

JULY 2022

INDIAN INSTITUTE OF TECHNOLOGY INDORE

CANDIDATE'S DECLARATION

I hereby certify that the work which is being presented in the thesis entitled **Modeling and Small Signal Stability Analysis of Synchronverter based Distributed Generators in Islanded Microgrid** in the fulfillment of the requirements for the award of the degree of **MASTER OF SCIENCE (RESEARCH)** and submitted in the **DISCIPLINE OF ELECTRICAL ENGINEERING, Indian Institute of Technology Indore,** is an authentic record of my own work carried out during the time period from August 2020 to July 2022 under the supervision of Dr. Trapti Jain, Professor, Indian Institute of Technology Indore, India.

The matter presented in this thesis has not been submitted by me for the award of any other degree of this or any other institute.

13/09/2022

Signature of the student with date

(RAHUL RAJENDRA PAWAR)

This is to certify that the above statement made by the candidate is correct to the best of my knowledge.

13/09/2022

Signature of the Supervisor of MS (Research) thesis #1 with date

(Dr. TRAPTI JAIN)

Rahul Rajendra Pawar has successfully given his MS (Research) Oral Examination held on 13/09/2022

13/09/2022

Signature of Chairperson (OEB) with date

13/09/2022

Signature(s) of Thesis Supervisor(s) with date

13/09/22

Signature of Convener, DPGC with date

13 September 2022

Signature of Head of Discipline

ACKNOWLEDGEMENTS

I would like to express my sincere and deepest gratitude for my supervisor Dr. Trapti Jain (Professor, Discipline of Electrical Engineering, IIT Indore) for her valuable and constructive guidance throughout this research work. I am also immensely thankful for the constant support and motivation which she has provided me.

I would also like to express my sincere gratitude to my PSPC members; Dr. Srivathsan Vasudevan, and Dr. Shailesh Kundalwal for their continuous remarks and feedback. I am grateful to Dr. Amod C Umarikar and Dr. Vijay A S for their valuable comments which helped me a lot to widen my research perspectives.

It is also my pleasure to acknowledge the sincere advices, discussions and supports extended by all lab-mates and my friends. I really appreciate the support given by Mr. Ajinkya Sonawane and Mr. Yash Pandya and all others from time to time as and when required. Also, I would like to thank, my colleague and senior Mr. Adnan Iqbal for his valuable help in making this thesis a reality.

I would like to thank my parents, who educated me, for always believing in my capabilities and encouraging me to pursue my dreams; my brother, for his loving care and always being there for me during good and bad times. Last but not the least, I wish to thank all my family members and friends for their continues support and care.

RAHUL RAJENDRA PAWAR

Dedicated

To

My Mother & Father

Family

Friends

ABSTRACT

The growing trend in energy demand has led to the wide adoption of Distributed Generators (DGs) because of their environmental advantages, renewable sources, and economic feasibility due to the recent advancements in power electronics. Generation of electricity using DGs is in the form of either DC or a variable frequency AC. Hence, Power Electronic Converters (PECs) are needed to integrate DGs into the grid, also known as Inverter Interfaced Distributed Generation (IIDG). A group of these DG units with a cluster of local loads together forms a small power system called a microgrid.

Microgrids are the tiny structure of a centralized power grid containing DGs, transmission lines, and various loads that can be self-controlled and managed. A microgrid can operate in grid-connected mode or islanded mode. For grid-connected mode, voltage and frequency reference is provided by the grid, but in the case of islanded mode, DG should maintain its voltage and frequency output within a permissible range. Therefore, stability is a crucial concern in an islanded mode of operation.

RES-based DGs have very low or no rotating mass, resulting in low or no inertia. Increasing penetration of these DGs reduces the overall inertia of the power grid. Due to this, the effect of disturbance in the power grid will result in faster and more considerable variation in system frequency. Inertia plays a very important role in control of power system, since it is one of the essential factors in maintaining the stability of power system. Also, it slows down the effect of disturbance on the variation of frequency. Hence, to provide virtual inertia to the system, an inverter control scheme is designed to emulate virtual inertia. A Virtual Synchronous Generator (VSG) is one of the proposed solutions for the emulation of virtual inertia. Synchronverter is one of the many different models of VSG. The idea is to implement the synchronous generator equations in the control part of the converter.

The focus of this thesis is to analyze the stability of IIMG in island mode of operation with synchronverter as the local controller for DGs. This is accompanied by developing a linearized small-signal model for individual sub-modules and then combining all the sub-modules on a common reference frame to obtain the complete model of the microgrid. This methodology can be extended to a microgrid with n number of DGs. In a microgrid, the network dynamics can affect the microgrid's stability, so the network modeling is also included in this thesis. Small-signal modeling is formulated for multiple IIDGs connected to the transmission line network along with various passive loads. Analysis of the small-signal state-space model is conducted using MATLAB. Further, the control scheme is simulated in RSCAD within substep environment. To analyse the performance of the synchronverter dur-

ing various disturbances, various cases have been considered for both equal ratings as well as unequal rating of DGs. Besides, the comparison of the performance of the synchronverter control with the droop control scheme is presented.

Contents

List of Figures

List of Tables

List of Symbols

Δ Deviation in the variable

ω_c Cutoff frequency of low pass filter

ω_i Rotating speed of the synchronverter for i^{th} DG

ω_n Natural rated angular speed

ω_r Reference rotating speed of the synchronverter

ω_{comm} Common reference rotating angular speed

ψ_i Excitation flux of i^{th} DG

ψ_{ff}, Q_{ef} & T_{ef} Filter values for sensing parameters ψ_f, Q_e & $T_e, respectively$

τ Time constant of measurement filter

τ_f Time constant of active power loop

τ_v Time constant of reactive power loop

θ Angle between local and common reference frames (rad)

D_{pi} Frequency droop coefficient for i^{th} DG

D_{qi} Voltage droop coefficient for the i^{th} DG

I_{lDQ} DQ-axis components of filter inductor current (A) for i^{th} DG

I_{ldq} dq-axis components of filter inductor current (A) for i^{th} DG

$I_{lineDQi}$ DQ-axis component of the i^{th} line current

$I_{loadDQi}$ DQ-axis component of the i^{th} passive load current

I_{oDQ} DQ-axis components of output current (A) for i^{th} DG

I_{odq} dq-axis components of output current (A) for i^{th} DG

J_i Inertia constant for i^{th} DG

K_i Control parameter to adjust the speed of reactive power loop for i^{th} DG

P_i&Q_i Active power (W) & reactive power (VAR) of i^{th} DG unit

r_c & L_c Resistance (Ohm), inductance (Henry) of the coupling inductor

r_f, L_f & C_f Resistance (Ohm), inductance (Henry) and capacitance (Farad) of the filter

R_{linei} & L_{linei} Resistance (Ohm), inductance (Henry) of the i^{th} line

R_{loadi} & L_{loadi} Resistance (Ohm), inductance (Henry) of the i^{th} passive load

T_{ei} Electromagnetic torque for i^{th} DG

T_{mi} Mechanical input torque for i^{th} DG

V_{oDQ} DQ-axis components of output voltage (V) for i^{th} DG

V_{odq} dq-axis components of output voltage (V) for i^{th} DG

p_i&q_i Instantaneous active power (W) & reactive power (VAR) of i^{th} DG unit

List of Abbreviations

ACMG AC MicroGrid.

APL Active Power Loop.

CHIL Controller-Hardware-In-Loop.

CPL Constant Power Load.

DCMG DC MicroGrid.

DG Distributed Generation.

GTAI Giga-Transceiver Analog Input.

GTAO Giga-Transceiver Analog Output.

GTDI Giga-Transceiver Digital Input.

GTDO Giga-Transceiver Digital Output.

HADMG Hybrid AC/DC MicroGrid.

HIL Hardware-In-Loop.

IIDG Inverter Interfaced Distributed Generator.

IIMG Islanded Inverter-based MicroGrid.

MG MicroGrid.

PCC Point of Common Coupling.

PEC Power Electronic Converter.

PV Photo Voltaic.

R Resistive.

RES Renewable Energy Source.

RL Inductive.

RMS Root Mean Square.

RPL Reactive Power Loop.

RTDS Real Time Digital Simulator.

SG Synchronous Generator.

THD Total Harmonic Distortion.

UPS Uninterrupted Power Supply.

VSG Virtual Synchronous Generator.

VSI Voltage Source Inverter.

VUF Voltage Unbalance Factor.

Chapter 1

Introduction

1.1 Background

The use of Renewable Energy Sources (RESs) is increasing rapidly in electricity generation due to its environmental and economical reasons. Nowadays, wind energy and solar is getting more and more applications in the RES. Apart from this, few concerns about the existing conventional power system, such as greenhouse gas emission, nuclear waste production, construction of new transmission lines to transfer bulk amount of power and hence transmission losses, forced utilities and researchers to find other solutions. Due to all these reasons, power system is moving from the centralized generation to the Distributed Generation (DG) [1–6].

As per IEEE, DG is defined as, "Generation of electricity by facilities that are sufficiently smaller than the central generating plants so as to allow interconnection at nearly any point in the power system" [5, 6]. In the past, DGs were not required to regulate power generation as per the grid code [7]. DGs were operated to produce as much energy as possible with certain quality of the injected grid current. DGs used to be disconnected in case of fault condition. These standards were reasonable as there were low penetration of RES into grid. Presently, RES share in the power system has increased significantly and it is going to increase further in future.

The DGs are expected to provide benefits such as, reliability of power, power quality, reduction in pollution, environmental and economical power generation. DGs can not be integrated directly to the main grid due to the following issues.

- Generation of electricity using DGs is in the form of either DC or a variable frequency AC. Hence, Power Electronic Converters (PECs) are needed to integrate

DGs into grid, which is also known as Inverter Interfaced Distributed Generation (IIDG). To obtain the required voltage level at the output of IIDG, new control strategies are required.

- Conventional power grid has centralized power generation with power flow from transmission to distribution network. The direct integration of DG at distribution level causes power flow problems[8].

- RES are intermittent in nature and hence, produce fluctuating energy.

The issues in DGs are different than the conventional power system. To overcome these issues and to differentiate the DG from conventional power grid, Micro-Grids(MGs) are introduced [3, 9].

1.2 Microgrids

Microgrid (MG) is basically a scaled down version of centralized grid, which includes power generation, power transmission and power consumption. [10, 11]. A microgrid consists of low voltage DGs, storage devices and loads.

Microgrid can be operated in either grid connected mode or island mode of operation [10, 11]. The transition between the grid connected mode to island mode of operation, or vice verse, is controlled by the static switch at Point of Common Coupling (PCC). The advantages offered by microgrid is listed below.

- Reduced losses in transmission and distribution.

- Reduction in greenhouse gases due to RESs based DG.

- Increased reliability of power due to DGs.

- Improved power quality by managing local loads.

- Ability to work in islanded mode in case of grid failure.

- Ability of transition from grid connected mode to islanded mode of operation during faults or voltage fluctuation.

Classification of microgrid can be done based on various parameters. Based on the type

of grid voltage, MGs can be divided as, AC MicroGrids (ACMGs) [12, 13], DC MicroGrids (DCMGs) [14, 15] and Hybrid AC/DC MicroGrids (HADMGs) [16, 17]. ACMG proposed in [12, 13] uses the existing AC grid technologies along with protection and standards. However, most of the DGs use RESs and hence generate power in DC. This DC supply is converted to AC with the help of PECs. Moreover, this AC supply is again converted to DC to supply today's loads such as Uninterrupted Power Supply (UPS), variable motor drives, charging stations for electrical vehicles. Thus, PECs used at both the end (generation and load) causes the power losses and hence, ACMG may be less efficient.

Ref. [14, 15] proposed DCMG as an alternative to the ACMG to overcome disadvantages of ACMG mentioned earlier. But, the power generation from sources such as diesel generator, small hydro turbine etc, as well as, electrical load are mix of AC and DC power. Hence, the HADMGs [16, 17], which is a combination of ACMGs and DCMGs, is more beneficial in terms of connecting various AC and DC power sources and loads.

In MG, based on the operation, power converters are classified as grid-feeding, grid-supporting and grid-following converters[18, 19]. Grid-forming converters exhibit the properties of the grid such as ideal AC voltage with low output impedance and gives frequency and voltage amplitude reference to the other DGs working in the same ACMG. However, the grid-feeding converters are designed to supply power to the grid. They can be treated as an ideal AC current source with high impedance in parallel. Lastly, grid-supporting converters can be represented by both AC voltage source with low series impedance or AC current source in parallel with high impedance.

1.3 Major Challenges in Microgrid

One of the most important challenges in the MG is the stability of system. Power system stability can be defined as "the ability of electrical power system, for a given initial operating condition, to regain a state of operating equilibrium after being subjected to the physical disturbance, with most system variables bounded so that practically the entire system remains intact" [20, 21].

Along with the stability, some of the major challenges in MG can be listed as follows.

- Power sharing among DGs

- Voltage and frequency restoration
- Unbalanced and non linear loads
- Seamless transfer from islanded mode to grid connected mode and vice versa.
- Islanding detection of the microgrid
- Low inertia

When there are multiple DGs operating in MG, they should effectively share real and reactive power [22]. As per the IEEE standard, the voltage Total Harmonic Distortion (THD) and the Voltage Unbalance Factor(VUF) should be maintained within 5% and 2%, respectively. To supply unbalance loads, DG unit must inject negative sequence current to balance the voltage [23]. Islanding condition should be detected timely to ensure safety of the repair crew and power quality [24]. Further, the transition from islanded mode to grid connected mode and vice versa should be seamless as this transition will introduce severe transients to the system [25]. Moreover, low inertia due to the use of PEC causes barrier in stability of the microgrid.

1.4 Stability and Control of IIMG

Stability of ACMG is not a critical issue when operating in grid connected mode, since the grid would be responsible for its stable operation. But, in case of the island mode of operation, stability is an important concern because of low inertia support of IIDGs. For a given steady state condition, Islanded Inverter-based MicroGrid (IIMG) may become unstable when it is subjected to the large disturbance. However, for small disturbance, IIMG should remain in stable condition and operate satisfactory. Therefore, small signal stability analysis is widely used to analyse stability of the ACMG. This thesis also focuses on the small signal stability analysis of ACMG. A literature survey, relevant to the research work, is presented in the following subsections.

1.4.1 Concept of Virtual Inertia

Due to the recent developments in the power electronic technologies, energy generation using renewable sources are increasing exponentially. These sources generate electricity in the

form of DC or fluctuating AC, hence PEC is required to integrate DG into grid. One of the main issues with integration of large number of DGs into grid is decline in overall inertia. More penetration of RES in the power system is vulnerable to its stability. The concept of virtual inertia has emerged as a promising solution for this issue. The Virtual Synchronous Generator (VSG) is based on this concept.

The idea behind VSG is to emulate the behavior of Synchronous Generators (SG) in the control of DG, which includes inertia support and droop characteristics. Various techniques for VSG are proposed in literature [26–30]. According to these concepts, DG can control its active and reactive power output according to the frequency and amplitude of voltage, respectively. The inertial characteristics of control can contribute to the inertia of the grid. Synchronverter is one of the many different models of VSG.

1.4.2 Synchronverter

Synchronverter is a power electronic converter with mathematical model of SG embedded in the controller. It emulates rotor characteristics of the SG and contributes inertia to the grid [31]. Various studies have been done for the implementation of synchronverter and to analyze small signal stability of the system with synchronverter [31–41]. The whole intention of the synchronverter is to make VSG behave like SG. Synchronverter emulates swing equation and the excitation system of SG and manages active and reactive power output. Since synchronverter is not limited by the physical constraints of SG, the inertia constant and droop constant of synchronverter can be varied while it is operating.

The synchronverter with modified damping correction loop is given in [33]. It also gives the small signal model to analyse small signal stability and highlights the critical modes of system. [35] proposes the study of dynamic stability analysis for synchronverter based on the bifurcation theory. Furthermore, it gives analysis of the stability margin with the variation of parameters. Small signal analysis of synchronverter with PV is addressed in [37].

Synchronverter consists of the solid-state switches, LCL filter, and control part, which includes active and reactive power loops. Analysis of all the components are necessary to analyze the system behavior. For robust analysis, two parallel synchronverters are considered in [39]. It also gives the small signal analysis for LCL filter. The study of transient response

of synchronverter using dynamic phasor model is carried out in [41]. Moreover, it anticipates stability margin of the system.

1.5 Motivation and Objectives of Thesis

Due to the low inertial and intermittent nature of RES based DGs, stability is a vital concern for the operation of IIMG. Stability can be influenced by various parameters in the system such as type of load, controller parameters and transmission line network in system.

The literature review presented in previous section shows that most of the study is carried out considering synchronverter in the grid connected mode of operation. Island mode of operation is vulnerable to the disturbances and analysis of synchronverter in the island mode of operation is yet to be explored. Further, the analysis presented in the literature considered only a single DG, but in IIMG there may be multiple (more than two) DGs operating simultaneously. Moreover, when two or more DGs are operating in the same IIMG, they may be remotely placed and connected through the transmission line network. Conventional power system consists of large number of SG, induction motors and synchronous motors, which have large mass and rotating inertia. The dynamics of network is neglected in the conventional power system since the time constant of SG, induction motors and their controllers are high when compared to the time constant of the transmission network. But, in case of MGs, most of the DGs are connected using PEC, which has very low time constant. Network dynamics can influence the stability of the system. Hence, dynamics of network must be included in the analysis.

In view of the above observations, the main objectives of this thesis are

- Analyze stability of IIMG in island mode of operation with synchronverter as the local controller for DGs.
- To develop generalized small signal model of IIMG system, which has multiple DGs working simultaneously and connected through transmission lines, and feeding multiple loads.
- To study the behaviour of the system, when it is subjected to disturbances, through real-time simulations.

1.6 Organization of the Thesis

This thesis is organized into four chapters. The present chapter discuses few basic concepts of MGs, DGs, major challenges in MG, stability and control of IIMG. Further, the concept of virtual inertia and synchronverter is also introduced in this chapter. The survey of some important work, related to the control and stability analysis of IIMG, has been presented along with motivation and objectives of the work.

In Chapter 2, a generalized model is obtained for the IIMG consisting of n_M number of DGs, n_l no of loads and n_N no of transmission lines. To obtain the complete model, the IIMG is divided virtually into three modules, viz., generator model, network model and load model.

In Chapter 3, simulation results are presented for the test system. Eigenvalue analysis is performed on the system and the effect of parameter variation on eigenvalues is analyzed. Further, the results obtained from the real time simulations with various case studies are demonstrated.

Finally, **Chapter 4** concludes the finding of thesis and suggests few possible research avenues.

Chapter 2

Modelling of The Synchronverter in Islanded Microgrid

2.1 Introduction

Small signal modelling is extensively used to study stability analysis in power system. This involves development of the small signal state space model. This state space model is linearized at operating or steady state point and generally it is transferred in DQ reference frame. In this chapter , a similar approach is followed to obtain comprehensive small signal modelling of different components present in the system. The proposed system consists of 3 phase inverter, LCL filter, Active and reactive power loops with synchronverter control scheme, network lines and various passive loads.

2.2 Generalized Model Approach

The complete model of system has been developed in a synchronously rotating DQ reference frame. This modeling is divided in three sub modules, viz., generator sub-module, network sub-module and load sub-modules. The transformation used to convert ABC reference frame to the dq reference frame is given in fig. 2.1 . Transformation is done using (2.1).

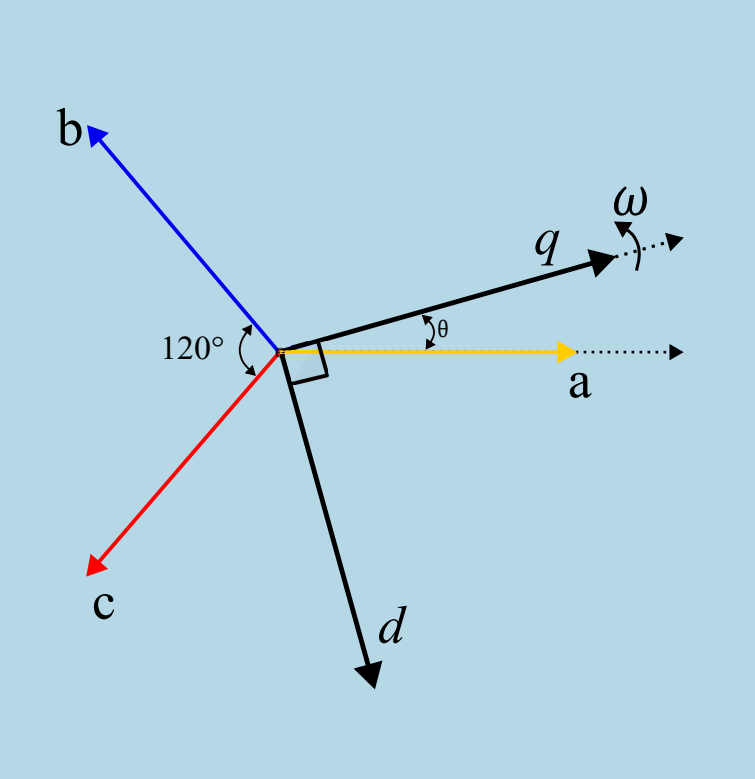

Figure 2.1: Reference frame transformation from ABC frame to dq frame

$$\begin{bmatrix} F_d(t) \\ F_q(t) \end{bmatrix} = [\mathbf{T_{dq}}] \begin{bmatrix} F_a(t) \\ F_b(t) \\ F_c(t) \end{bmatrix} \tag{2.1}$$

$$[\mathbf{T_{dq}}] = \sqrt{\frac{2}{3}} \begin{bmatrix} cos(\omega t+\theta) & cos\left(\omega t+\theta-\frac{2\pi}{3}\right) & cos\left(\omega t+\theta+\frac{2\pi}{3}\right) \\ -sin(\omega t+\theta) & -sin\left(\omega t+\theta-\frac{2\pi}{3}\right) & -sin\left(\omega t+\theta+\frac{2\pi}{3}\right) \end{bmatrix} \tag{2.2}$$

The dq to abc transformation is done using following formulas,

$$\begin{bmatrix} F_a(t) \\ F_b(t) \\ F_c(t) \end{bmatrix} = [\mathbf{T_{abc}}] \begin{bmatrix} F_d(t) \\ F_q(t) \end{bmatrix} \tag{2.3}$$

$$[\mathbf{T_{abc}}] = \begin{bmatrix} cos(\omega t+\theta) & -sin(\omega t+\theta) \\ cos\left(\omega t+\theta-\frac{2\pi}{3}\right) & -sin\left(\omega t+\theta-\frac{2\pi}{3}\right) \\ cos\left(\omega t+\theta+\frac{2\pi}{3}\right) & -sin\left(\omega t+\theta+\frac{2\pi}{3}\right) \end{bmatrix} \tag{2.4}$$

The generalized model is developed for the system shown in fig. 2.2, which contains n_M number of DGs with LCL filter and n_l number of loads and n_N number of transmission lines connecting buses. Block diagram representation of complete small signal state space model and small signal states, which connect different sub-modules on the common reference frame, is shown in fig. 2.3.

2.3 Generator Module

The generator sub module involves modeling of each DG unit on its individual local dq reference frame. Since there is more than one DG in the system, the first DG unit's reference frame is assumed as common DQ reference frame and all other DG units are transferred to this common reference frame using transformation technique given in (2.5).

Figure 2.4 shows the relation between individual reference frame and common reference frame. The axes (D – Q) represent the common reference frame whereas axes (d – q) represent individual reference frame.

$$\left[\mathbf{F_{DQ}}\right] = \left[\mathbf{T_i}\right]\left[\mathbf{F_{dq}}\right] \tag{2.5}$$

$$\left[\mathbf{T_i}\right] = \begin{bmatrix} cos(\theta_i) & -sin(\theta_i) \\ sin(\theta_i) & cos(\theta_i) \end{bmatrix} \tag{2.6}$$

Where θ_i is angle between common reference frame and individual reference frame. It is defined as,

$$\theta_i = \int (\omega_i - \omega_{com})dt \tag{2.7}$$

Synchronverter scheme for one DG is shown in fig. 2.5. Each DG consists of power processing unit and local control units as shown in fig. 2.6. Local control includes power calculation and synchronverter. Power processing section has 3 phase voltage source converters, an output LC filter with coupling inductor. The dc bus dynamics of VSI are neglected and constant dc voltage is assumed as an input to the VSI. The switching dynamics of VSI is also neglected with the realization of high switching frequency [42].

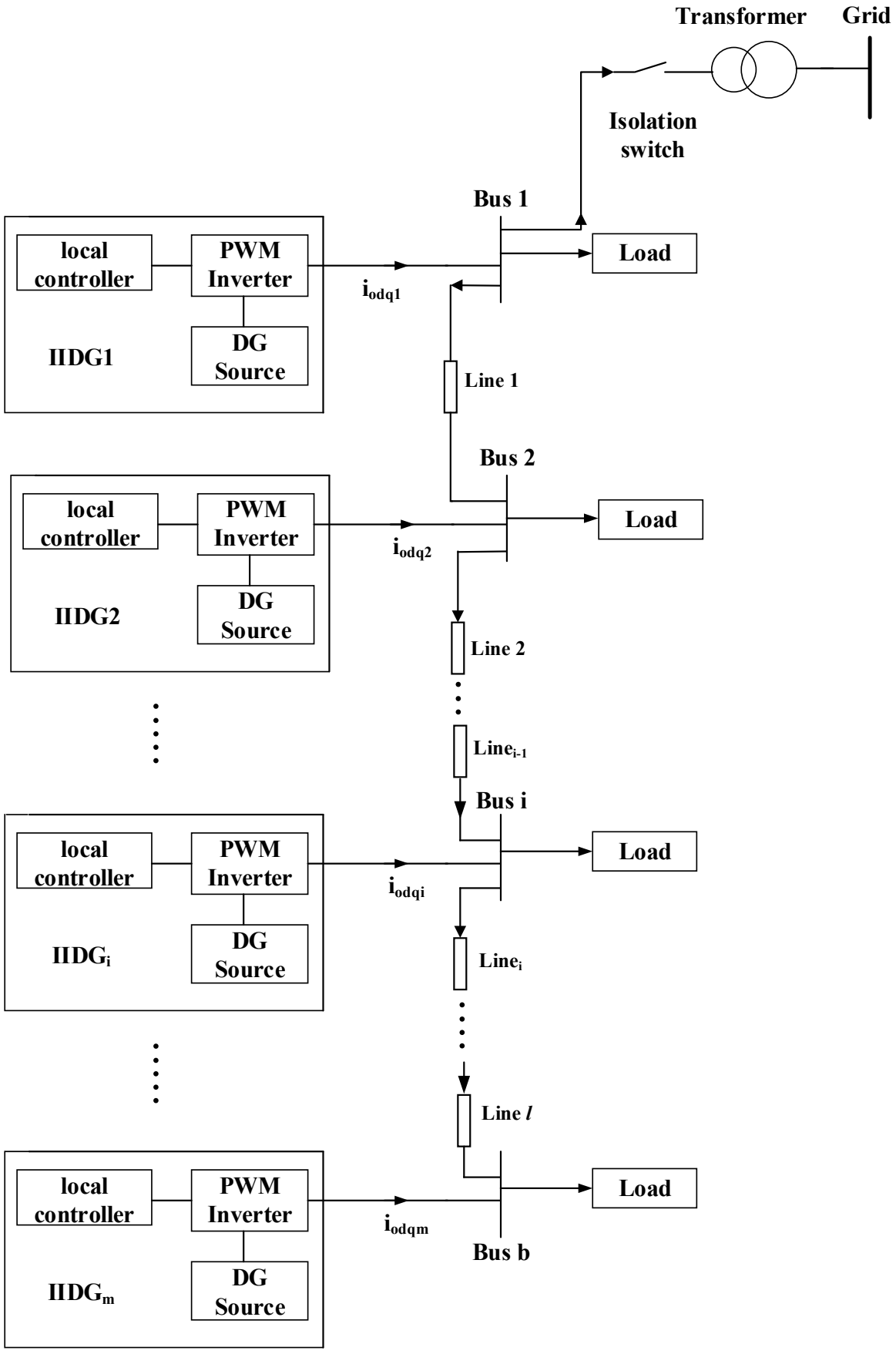

Figure 2.2: Schematic diagram of system with m DGs

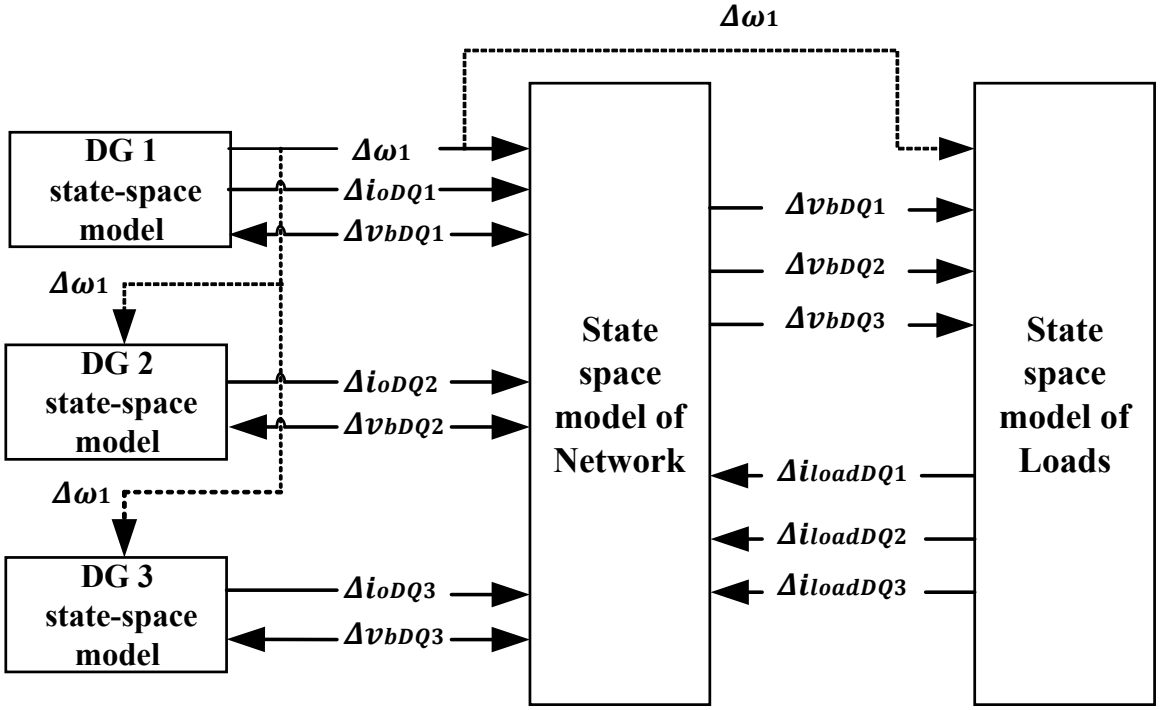

Figure 2.3: Block diagram representation of complete small signal state space model

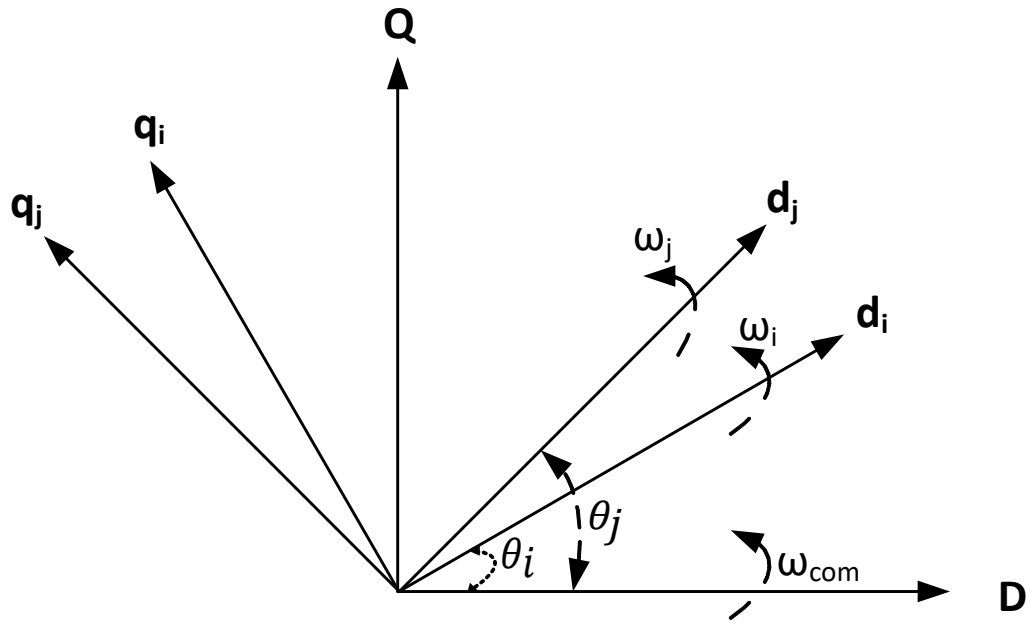

Figure 2.4: Reference frame transformation from local dq to common DQ

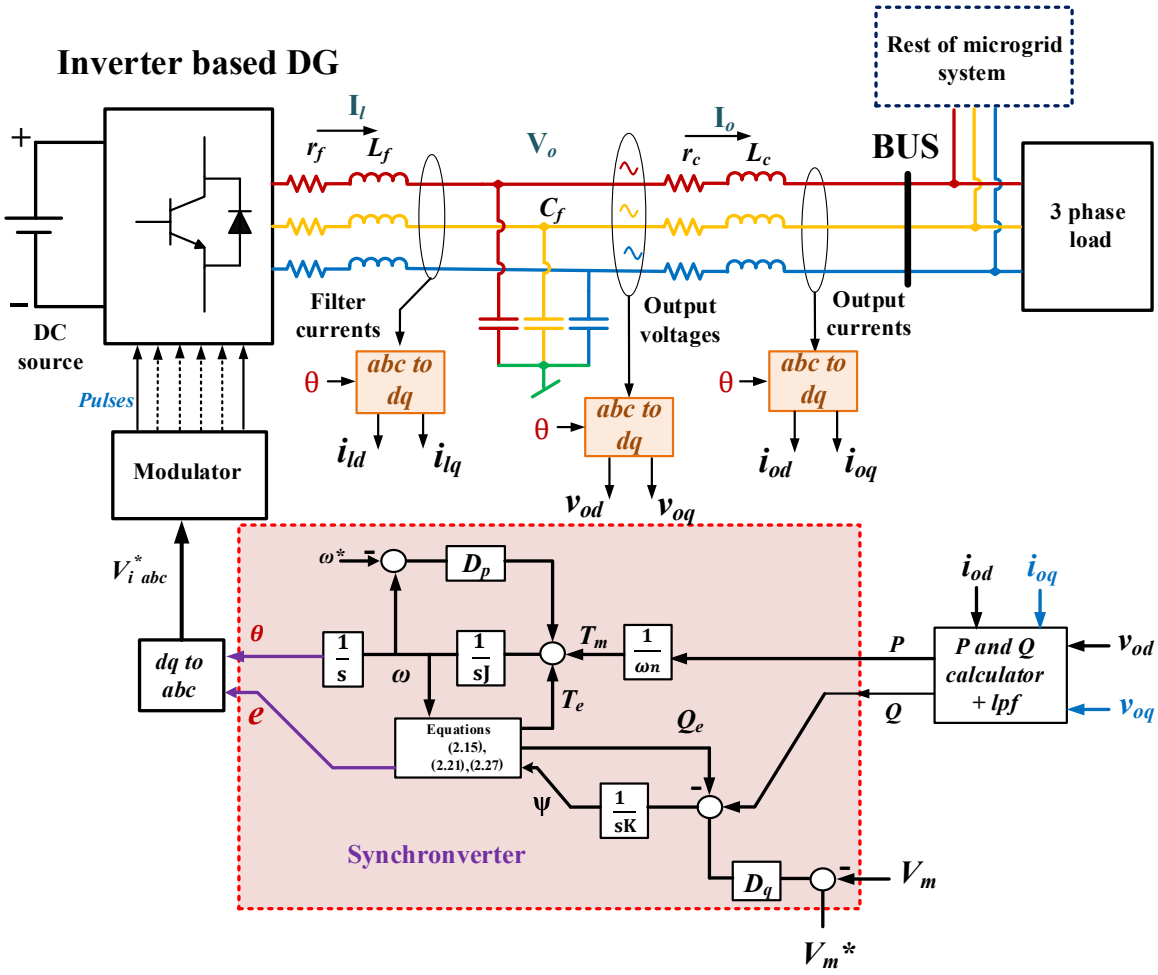

Figure 2.5: Synchronverter scheme for one DG

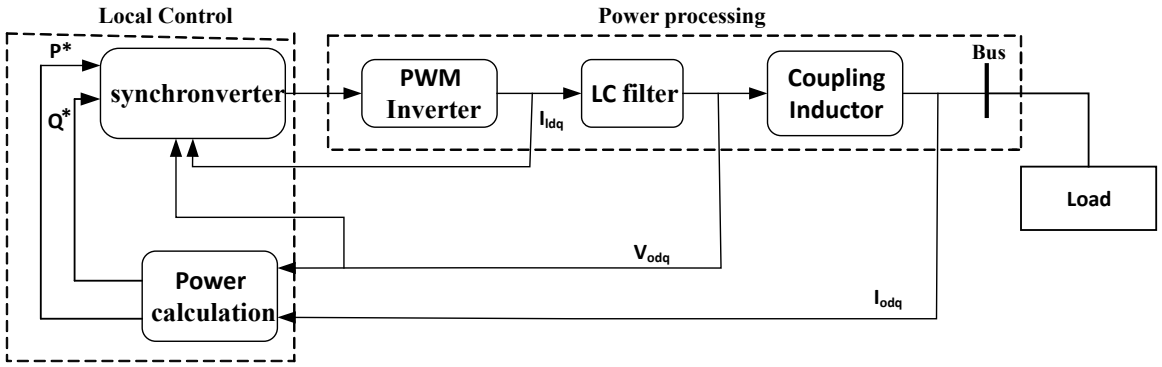

Figure 2.6: Local control and power control section of DG

2.3.1 Power Calculation

The outer block of local controller is power calculation block, which is shown in fig. 2.7. The reference active and reactive power for synchronverter is extracted from low pass filter as given in (2.8) and (2.9).

$$P_i = \frac{\omega_c}{s+\omega_c} \times 1.5 \underbrace{\left(V_{odi}I_{odi} + V_{oqi}I_{oqi}\right)}_{Instantaneous\ Active\ Power} \tag{2.8}$$

$$Q_i = \frac{\omega_c}{s+\omega_c} \times 1.5 \underbrace{\left(V_{oqi}I_{odi} - V_{odi}I_{oqi}\right)}_{Instantaneous\ Reactive\ Power} \tag{2.9}$$

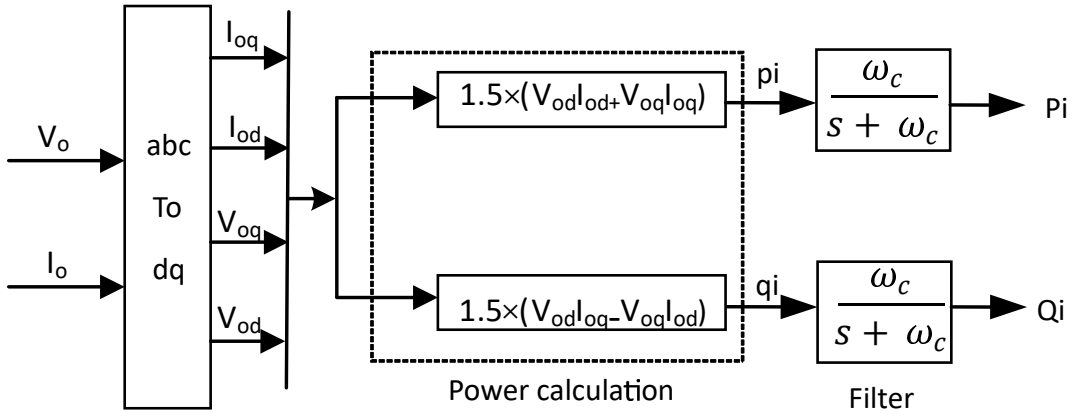

Figure 2.7: Power calculation block

Where V_{odi}, V_{oqi}, I_{odi} and I_{oqi} are the output voltages and currents of i^{th} DG unit in the individual dq reference frame, respectively, and ω_c is cut-off frequency of the low pass filter. This low pass filter is used to remove unwanted harmonics in the instantaneous active and reactive powers (p_i and q_i). Output of low pass filter is average active and reactive power (P_i and Q_i).

By linearizing and arranging above equations, small signal state space model for the power calculation block can be obtained as in (2.10) and (2.11).

$$\begin{bmatrix} \dot{\Delta P_i} \\ \Delta Q_i \end{bmatrix} = \mathbf{A_{pi}} \begin{bmatrix} \Delta P_i \\ \Delta Q_i \end{bmatrix} + \mathbf{B_{pi}} \begin{bmatrix} \Delta \mathbf{I_{ldqi}} \\ \Delta \mathbf{V_{odqi}} \\ \Delta \mathbf{I_{odqi}} \end{bmatrix} \tag{2.10}$$

$$\begin{bmatrix} \Delta P_i \\ \Delta Q_i \end{bmatrix} = \mathbf{C_{pi}} \begin{bmatrix} \Delta P_i \\ \Delta Q_i \end{bmatrix} \tag{2.11}$$

Here, $\mathbf{A_{pi}}$ represents state matrix of the power calculation block of the i^{th} DG unit, while $\mathbf{B_{pi}}$ is input matrix and $\mathbf{C_{pi}}$ is output matrix. Details of these DGs are given in the Appendix A.

2.3.2 Synchronverter

The synchronverter replicates mathematical model of the synchronous generator into the controller of the power electronic converter to emulate rotor dynamics of the synchronous generator and inject inertia in the grid [33]. Figure 2.8 shows the control implementation of the synchronverter. Synchronverter model includes Active Power Loop (APL) and Reactive Power Loop (RPL).

2.3.2.1 Active Power Loop

Active Power Loop of synchronverter implements swing equation of the synchronous generator with simplified governor droop action for frequency droop control.

$$J_i \frac{d\omega_i}{dt} = T_{mi} - T_{ei} - D_{pi}(\omega_i - \omega_r) \tag{2.12}$$

Here, J_i is the inertia constant for the i^{th} DG, T_{mi} is mechanical input torque for the i^{th} DG, T_{ei} is electromagnetic torque for the i^{th} DG, ω_i is the rotating speed of the synchronverter for the i^{th} DG, ω_r is reference rotating speed of the synchronverter and D_{pi} is the frequency droop coefficient for the i^{th} DG.

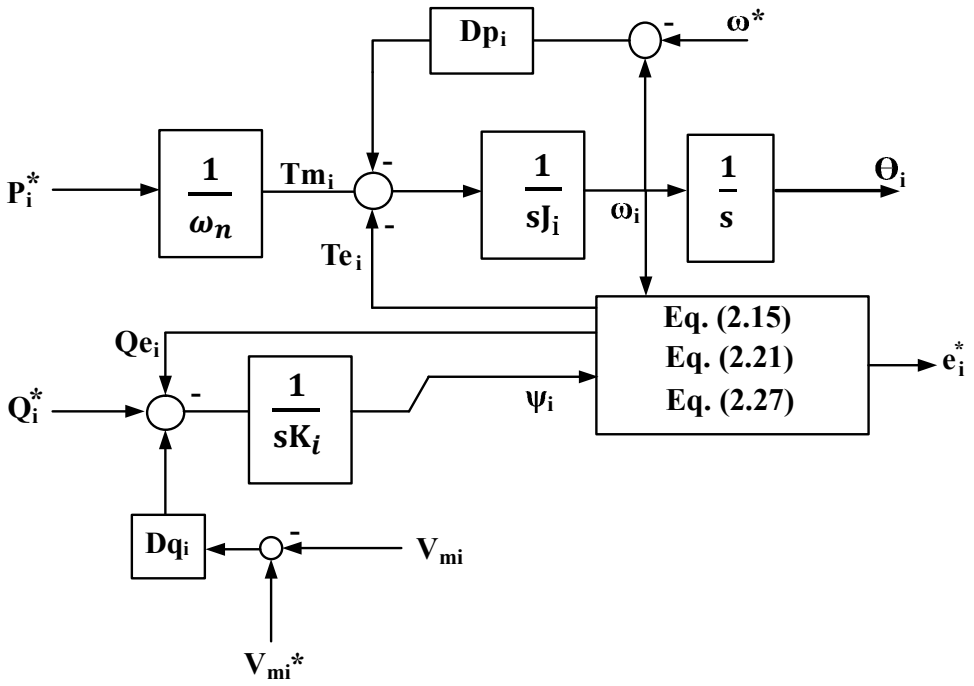

Figure 2.8: Synchronverter control

Here, D_{pi} is calculated as,

$$D_{pi} = \frac{\Delta T_{mi}}{\Delta \omega_r} \tag{2.13}$$

Where, ΔT_{mi} is the amount of change in the input torque for the i^{th} DG when there is $\Delta\omega_r$ change in the angular speed. Here, T_{mi} is dependent on the rating of DG and calculated as,

$$T_{mi} = \frac{P_i}{\omega_n} \tag{2.14}$$

Where, P_i is the reference input power for the i^{th} DG which is obtained from the power calculation block in (2.8) and ω_n is rated angular speed.

Now, the electromagnetic torque for i^{th} DG (T_{ei}) is calculated from the filtered excitation flux of i^{th} DG (Ψ_{ffi}), which is obtained from the reactive power loop of synchronverter and inverter output current I_{di} [31].

$$T_{ei} = 1.5\psi_{ffi} I_{di} \tag{2.15}$$

the rotor angle or torque angle of the i^{th} DG (θ_i) is calculated as

$$\theta_i = \int \omega_i - \omega_{com}\, dt \tag{2.16}$$

As given in [31], APL has a time constant τ_f, which decides the speed of response for APL . Also, time constant τ_f is useful to decide the inertia constant J_i of the system,

$$J_i = D_{pi}\tau_f \tag{2.17}$$

2.3.2.2 Reactive Power Loop

Reactive Power Loop (RPL) of synchronverter implements the similar equation as APL to regulate reactive power according to the voltage droop coefficient as given in (2.18)

$$\frac{d\psi_{fi}}{dt} = \frac{1}{K_i}\left(Q_{ri} - Q_i + D_{qi}\left(V_{ref} - V_{mi}\right)\right) \tag{2.18}$$

Where K_i is the control parameter to adjust the speed of response of RPL for i^{th} DG, D_{qi} is the voltage droop coefficient for the i^{th} DG, V_{mi} is the maximum voltage of the i^{th} DG and V_{ref} is reference max voltage.

Here, D_{qi} is calculated as,

$$D_{qi} = \frac{\Delta Q_i}{\Delta v_{mi}} \tag{2.19}$$

Where, ΔQ_i is the amount of change in the reactive power of i^{th} DG when there is Δv_{mi} change in output voltage.

Q_{ri} is the reference average reactive power for i^{th} DG and taken from power controller block, which is obtained from (2.9). Q_i is calculated as (2.20),

$$Q_i = -1.5\omega_i\psi_{ff}I_{qi} \tag{2.20}$$

RPL has the time constant of τ_v, which decides speed of response for the RPL and used to decide control parameter K_i of the i^{th} DG and calculated as,

$$K_i = \tau_v D_{qi}\omega_i \tag{2.21}$$

2.3.2.3 Measurement Filter

ψ_f , Q_e and T_{ei} are the sensing parameters, which contain harmonics due to the PWM switching. In order to remove these harmonics, these signals are passed through low pass filter. Due to this, there is signal processing communication delay and that can be modelled in the form of time constant τ [33, 37].

$$\frac{d\psi_{ff}}{dt} = \frac{1}{\tau}\psi_f + \frac{1}{\tau}\psi_{ff} \tag{2.22}$$

$$\frac{dQ_{ef}}{dt} = \frac{1}{\tau}Q_e + \frac{1}{\tau}Q_{ef} \tag{2.23}$$

$$\frac{dT_{ef}}{dt} = \frac{1}{\tau}T_e + \frac{1}{\tau}T_{ef} \tag{2.24}$$

ψ_{ff}, Q_{ef} and T_{efi} are the filter values for sensing parameters ψ_f, Q_i and T_{ei} respectively, which are used as state variables in synchronverter.

2.3.2.4 Small Signal Model for Synchronverter

Small signal linearized state space model for the synchronverter can be given as

$$\begin{bmatrix} \dot{\Delta\omega_i} \\ \Delta\psi_{fi} \\ \Delta\psi_{ff\ i} \\ \Delta T_{efi} \\ \Delta Q_{efi} \\ \Delta\theta_i \end{bmatrix} = \mathbf{A_{Ci}} \begin{bmatrix} \Delta\omega_i \\ \Delta\psi_{fi} \\ \Delta\psi_{ff\ i} \\ \Delta T_{efi} \\ \Delta Q_{efi} \\ \Delta\theta_i \end{bmatrix} + \mathbf{B_{C1i}} \begin{bmatrix} \Delta P_i \\ \Delta Q_i \end{bmatrix} + \mathbf{B_{C2i}} \begin{bmatrix} \Delta I_{ldi} \\ \Delta I_{lqi} \\ \Delta V_{odi} \\ \Delta V_{oqi} \\ \Delta I_{odi} \\ \Delta I_{oqi} \end{bmatrix} + \mathbf{BP_{comi}} \left[\Delta\omega_{com}\right] \tag{2.25}$$

Details of the above matrices, $\mathbf{A_{Ci}}$, $\mathbf{B_{C1i}}$, $\mathbf{B_{C2i}}$, $\mathbf{BP_{comi}}$, are given in the Appendix A.

Inner voltage (E_i) is given as,

$$E_i = \omega_i \psi_{ff} \tag{2.26}$$

The small signal model for output of the synchronverter is given as (2.27)

$$\begin{bmatrix} \Delta\omega_i \\ \Delta E_i \\ \Delta\theta_i \end{bmatrix} = \begin{bmatrix} \mathbf{C_{cwi}} \\ \mathbf{C_{cvi}} \end{bmatrix} \begin{bmatrix} \Delta\omega_i \\ \Delta\psi_{fi} \\ \Delta\psi_{ffi} \\ \Delta T_{ei} \\ \Delta Q_{ei} \\ \Delta\theta_i \end{bmatrix} \tag{2.27}$$

The details of matrices $\mathbf{C_{cwi}}$ and $\mathbf{C_{cvi}}$ are given in the Appendix A.

Inner voltage E_i along with angle θ_i is used as reference for the generation of pulses for the PWM inverter.

2.3.3 Output LC Filter and Coupling Inductor

Most of the DGs use renewable sources such as PV solar. The output voltage of these sources is DC. Three leg VSI converts this DC voltage into AC with the help of power electronic switches. Typically, switching frequency used for these switches is 2kHz to 15 kHz. Due to this switching action, harmonics are present in the output current and voltage. To attenuate these harmonics, LC filter along with coupling inductor, referred as output LCL filter, is used for DG as shown in fig. 2.9. Coupling inductor provide reasonable impedance between output of the inverter and bus with good bus voltage regulation. The current through inductors and voltage across capacitor are given in (2.28)- (2.33)

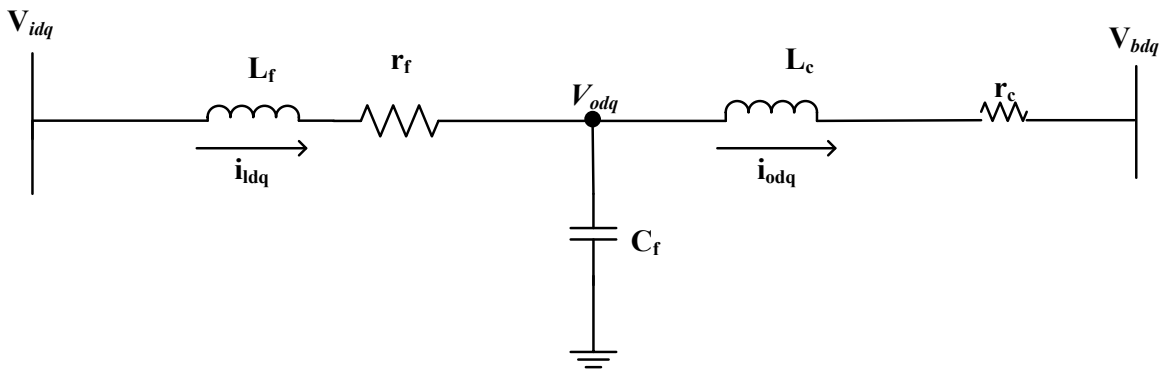

Figure 2.9: LC Filter and Coupling Inductor

$$\dot{I}_{ldi} = \frac{1}{L_f}\left(V_{idi} - V_{odi} - r_f I_{ldi}\right) + \omega I_{lqi} \tag{2.28}$$

$$\dot{I}_{lqi} = \frac{1}{L_f}\left(V_{iqi} - V_{oqi} - r_f I_{lqi}\right) - \omega I_{ldi} \tag{2.29}$$

$$\dot{V}_{odi} = \frac{1}{C_f}\left(I_{ldi} - I_{odi}\right) + \omega V_{oqi} \tag{2.30}$$

$$\dot{V}_{oqi} = \frac{1}{C_f}\left(I_{lqi} - I_{oqi}\right) - \omega V_{odi} \tag{2.31}$$

$$\dot{I}_{odi} = \frac{1}{L_c}\left(V_{odi} - V_{bdi} - r_c I_{odi}\right) + \omega I_{oqi} \tag{2.32}$$

$$\dot{I}_{oqi} = \frac{1}{L_c}\left(V_{oqi} - V_{bqi} - r_c I_{oqi}\right) - \omega I_{odi} \tag{2.33}$$

Here, r_f and r_c are the parasitic resistances of the inductors, L_f and L_c, respectively. C_f is the filter capacitor.

The small signal linearized state space model for the LC filter with coupling inductor is given in (2.34)-(2.35)

$$\begin{bmatrix} \dot{\Delta\mathbf{I}}_{\mathbf{ldqi}} \\ \Delta\mathbf{V}_{\mathbf{odqi}} \\ \Delta\mathbf{I}_{\mathbf{odqi}} \end{bmatrix} = \mathbf{A}_{\mathbf{LCLi}} \begin{bmatrix} \Delta\mathbf{I}_{\mathbf{ldqi}} \\ \Delta\mathbf{V}_{\mathbf{odqi}} \\ \Delta\mathbf{I}_{\mathbf{odqi}} \end{bmatrix} + \mathbf{B}_{\mathbf{LCL1i}} \begin{bmatrix} \Delta V_{id} \\ \Delta V_{iq} \end{bmatrix} + \mathbf{B}_{\mathbf{LCL2i}} \begin{bmatrix} \Delta\mathrm{Vbd} \\ \Delta\mathrm{Vbq} \end{bmatrix} + \mathbf{B}_{\mathbf{LCL3i}} \left[\Delta\omega\right] \tag{2.34}$$

$$\begin{bmatrix} \Delta\mathbf{I}_{\mathbf{ldqi}} \\ \Delta\mathbf{V}_{\mathbf{odqi}} \\ \Delta\mathbf{I}_{\mathbf{odqi}} \end{bmatrix} = \mathbf{C}_{\mathbf{LCLi}} \begin{bmatrix} \Delta\mathbf{I}_{\mathbf{ldqi}} \\ \Delta\mathbf{V}_{\mathbf{odqi}} \\ \Delta\mathbf{I}_{\mathbf{odqi}} \end{bmatrix} \tag{2.35}$$

Details of above matrices, $\mathbf{A}_{\mathbf{LCLi}}$, $\mathbf{B}_{\mathbf{LCL1i}}$, $\mathbf{B}_{\mathbf{LCL2i}}$, $\mathbf{B}_{\mathbf{LCL3i}}$, and $\mathbf{C}_{\mathbf{LCLi}}$, are given in Appendix A.

Assuming that VSI of the DG unit produces required voltage so that $V_i = V_i^*$. Here V_i is AC side voltage of the VSI. From the output of the synchronverter, which is given in (2.27), matrix $\mathbf{V}_{\mathbf{idqi}}$ is obtained as (2.36)

$$\begin{bmatrix} \Delta V_{idi} \\ \Delta V_{iqi} \end{bmatrix} = [\mathbf{T_M}] \begin{bmatrix} \Delta E_i \\ \Delta \theta_i \end{bmatrix} \tag{2.36}$$

Where in (2.36) matrix $\mathbf{T_M}$ is small signal linearized matrix and can be given as (2.37)

$$[\mathbf{T_M}] = \begin{bmatrix} cos(\theta_i) & -E_i sin(\theta_i) \\ sin(\theta_i) & E_i cos(\theta_i) \end{bmatrix} \tag{2.37}$$

2.3.4 Complete Model for Individual DG

The obtained output currents $\Delta\mathbf{I_{odqi}}$ of i^{th} DG are on the individual dq reference frame, which need to be transfered to the common DQ reference frame before connecting to the rest of MG. The small signal equivalent reference frame transformation is shown in fig. 2.10 [42]. Using transformation technique introduced in (2.5), the small signal output current, $\Delta\mathbf{I_{oDQi}}$ of i^{th} DG, on common reference frame can be obtained as (2.38)

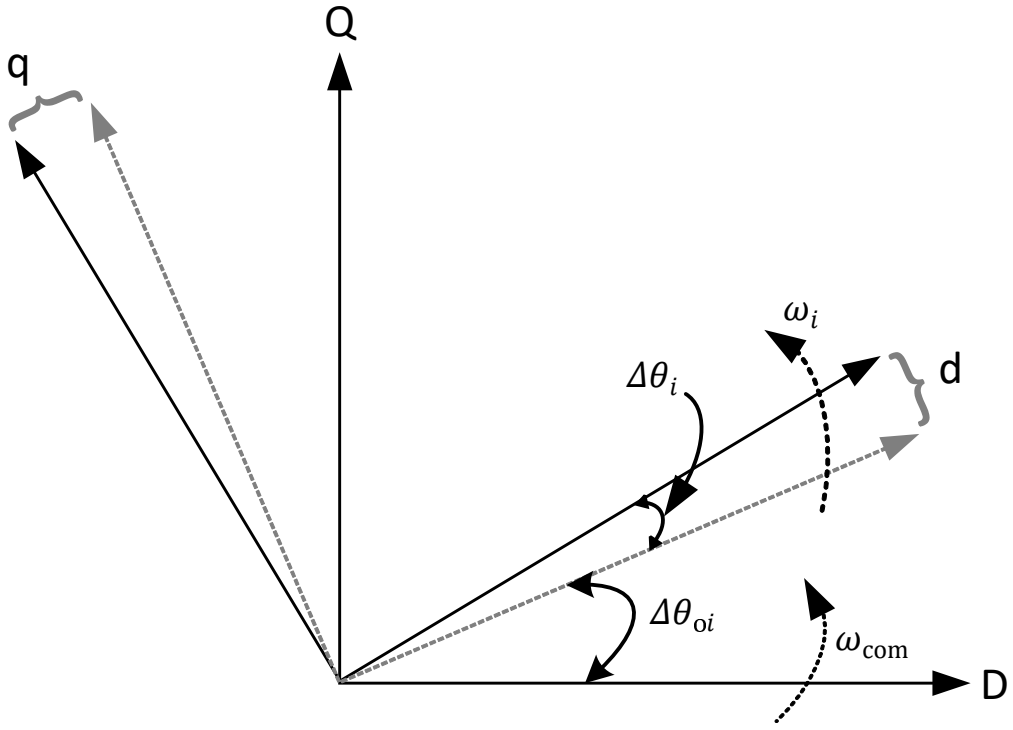

Figure 2.10: Small signal equivalent reference frame transformation

$$[\Delta I_{oDQi}] = [\mathbf{TS_i}] [\Delta I_{odqi}] + [\mathbf{TC_i}] [\Delta \theta_i] \tag{2.38}$$

Where $[\mathbf{TS_i}]$ and $[\mathbf{TC_i}]$ are given as eqs. (2.39) and (2.40), respectively.

$$[\mathbf{TS_i}] = \begin{bmatrix} cos(\theta_{oi}) & -sin(\theta_{oi}) \\ sin(\theta_{oi}) & cos(\theta_{oi}) \end{bmatrix} \tag{2.39}$$

$$[\mathbf{TC_i}] = \begin{bmatrix} -I_{od}sin(\theta_{oi}) - I_{oq}cos(\theta_{oi}) \\ I_{od}cos(\theta_{oi}) - I_{oq}sin(\theta_{oi}) \end{bmatrix} \tag{2.40}$$

Similarly, bus voltages, $\Delta\mathbf{V_{bDQi}}$, are the input to the i^{th} DG unit, which are expressed on common reference frame. These voltages need to be converted to the local dq frame of i^{th} DG unit, which can be done by reverse transformation, given by eq. (2.41).

$$\left[\Delta\mathbf{V_{bdqi}}\right] = \left[\mathbf{TS_i}^{-1}\right]\left[\Delta\mathbf{V_{bDQi}}\right] + \left[\mathbf{TV_i}^{-1}\right]\left[\Delta\theta_i\right] \tag{2.41}$$

Where, in (2.41) $\mathbf{TV_i^{-1}}$ is given as (2.42)

$$\left[\mathbf{TV_i}^{-1}\right] = \begin{bmatrix} -V_{bDi}sin(\theta_{oi}) + V_{bQi}cos(\theta_{oi}) \\ -V_{bDi}cos(\theta_{oi}) - V_{bQi}sin(\theta_{oi}) \end{bmatrix} \tag{2.42}$$

The complete small signal linearized state space model of an individual DG unit is obtained by combining the state space model of power calculation block, synchronverter and LCL filter, given by (2.10-2.11), (2.25-2.27), and (2.34- 2.35) respectively, and can be given as in (2.43-2.44). Total 14 states are obtained by combining all the sub modules.

$$\left[\Delta\dot{\mathbf{X}}_{\mathbf{geni}}\right] = \mathbf{A_{geni}}\left[\Delta\mathbf{X_{geni}}\right] + \mathbf{B_{geni}}\left[\Delta V_{bDQ}\right] + \mathbf{BW_{commi}}\left[\Delta\omega_{com}\right] \tag{2.43}$$

$$\begin{bmatrix} \Delta\omega \\ \Delta\mathbf{I_{oDQi}} \end{bmatrix}_{3\times1} = \begin{bmatrix} [\mathbf{C_{genw}}] \\ [\mathbf{C_{genc}}] \end{bmatrix}\left[\Delta\mathbf{X_{geni}}\right] \tag{2.44}$$

Here, $\mathbf{A_{geni}}$ is the state matrix of the i^{th} DG unit, $\mathbf{B_{geni}}$ and $\mathbf{BW_{commi}}$ are the input matrices of the i^{th} DG unit. $\mathbf{C_{genc}}$ and $\mathbf{C_{genw}}$ are output matrices for the two output currents $\Delta\mathbf{i_{oDQi}}$ and frequency $\Delta\omega$, respectively. These matrices are given in Appendix A. In eqs. (2.43) and (2.44), $\Delta\mathbf{X_{geni}}$ is the state vector, which includes the states of the power calculation block, synchronverter, and LCL filter, and given by 14 element vector as (2.45).

$$\left[\Delta \mathbf{X_{geni}}\right] = \begin{matrix}[\Delta P_i & \Delta Q_i & \Delta\omega & \Delta\psi_{fi} & \Delta\psi_{ffi} & \Delta T_{efi} \\ & & \Delta Q_{efi} & \Delta\theta_i & \Delta \mathbf{I_{ldqi}} & \Delta \mathbf{V_{odqi}} & \Delta \mathbf{I_{odqi}}]^T\end{matrix} \tag{2.45}$$

2.3.5 Complete Model of Generator Sub-module

In previous sections, small signal linearized model for one DG source is discussed, but in case of microgrid, there may be several DGs acting as sources and connected to network. Now, by combining all states of n_G number of DGs (given in eqs. (2.43) and (2.44)), complete small signal linearized state space model for generator module can be given on common reference frame as (2.46)-(2.48).

$$[\Delta \dot{\mathbf{X}}_{\mathbf{GEN}}] = \mathbf{A_{GEN}}\,[\Delta \mathbf{X_{GEN}}] + \mathbf{B_{GEN}}\left[\Delta \mathbf{V_{bDQ}}\right] \tag{2.46}$$

$$\left[\Delta \mathbf{I_{oDQ}}\right] = [\mathbf{C_{GENc}}]\,[\Delta \mathbf{X_{GEN}}] \tag{2.47}$$

$$[\Delta \omega_{\mathbf{com}}] = [\mathbf{C_{GENw}}]\,[\Delta \mathbf{X_{GEN}}] \tag{2.48}$$

Details of matrices $\mathbf{A_{GEN}}$, $\mathbf{B_{GEN}}$, $\mathbf{C_{GENc}}$ are given in Appendix A. Here $\mathbf{A_{GEN}}$ is state matrix of the generator sub-module, $\mathbf{B_{GEN}}$ is input matrix corresponding to the bus voltage for generator sub-module, and $\mathbf{C_{GENc}}$ is output matix to get output currents. Also, $\Delta\mathbf{X_{GEN}}$, $\Delta\mathbf{V_{bDQ}}$ and $\Delta\mathbf{I_{oDQ}}$ are given as (2.49), (2.50) and (2.51), respectively.

$$[\Delta \mathbf{X_{GEN}}] = \left[\Delta \mathbf{X_{gen1}} \quad \Delta \mathbf{X_{gen2}} \quad ..... \quad \Delta \mathbf{X_{genm}}\right]^{\mathbf{T}} \tag{2.49}$$

$$\left[\Delta \mathbf{V_{bDQ}}\right] = \left[\Delta \mathbf{V_{bDQ1}} \quad \Delta \mathbf{V_{bDQ2}} \quad ..... \quad \Delta \mathbf{V_{bDQm}}\right]^{\mathbf{T}} \tag{2.50}$$

$$\left[\Delta \mathbf{I_{oDQ}}\right] = \left[\Delta \mathbf{I_{oDQ1}} \quad \Delta \mathbf{I_{oDQ2}} \quad ..... \quad \Delta \mathbf{I_{oDQb}}\right]^{\mathbf{T}} \tag{2.51}$$

2.4 Network Module

Microgrid can have remotely placed multiple DGs acting as sources and connected through transmission line network. The small signal analysis of network is neglected in the small signal modelling of conventional power system due to presence of large rotating machines such as induction motors and synchronous generators and their controls have large time constants in comparison with the time constant of the network. In case of microgrid, most of the sources are renewable and use Power Electronic Converter (PEC) to interface with the rest of system, and these PECs have very small time constant. Due to the small time constant of VSI, the dynamics of the network can influence stability, and hence, the small signal modelling of network is needed in case of microgrid.

Figure 2.11 shows the i^{th} transmission line connected between j^{th} and k^{th} bus. The dynamic equation for this line on common reference frame is given in (2.52) and (2.53)

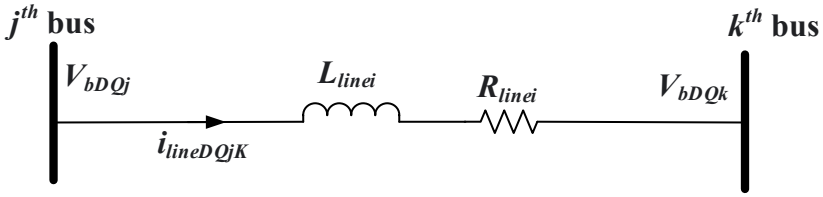

Figure 2.11: Transmission line

$$\dot{I}_{lineDi} = \frac{-R_{linei}}{L_{linei}} I_{lineDi} + \frac{1}{L_{linei}} \left(V_{bDj} - V_{bDk}\right) + \omega I_{lineQi} \tag{2.52}$$

$$\dot{I}_{lineQi} = \frac{-R_{linei}}{L_{linei}} I_{lineQi} + \frac{1}{L_{linei}} \left(V_{bQj} - V_{bQk}\right) - \omega I_{lineDi} \tag{2.53}$$

Linearizing eqs. (2.52) and (2.53), the small signal state space model for i^{th} line connected between j^{th} and k^{th} bus is obtained and given on common reference frame as shown in (2.54).

$$\left[\Delta \dot{\mathbf{I}}_{\mathbf{lineDQi}}\right] = \mathbf{A_{NETi}} \left[\Delta \mathbf{I_{lineDQi}}\right] + \mathbf{B_{1NETi}} \left[\Delta \mathbf{V_{bDQi}}\right] + \mathbf{B_{2NETi}} \left[\Delta \omega\right] \tag{2.54}$$

Details of matrices $\mathbf{A_{NETi}}$, $\mathbf{B_{1NETi}}$, $\mathbf{B_{2NETi}}$ are given in Appendix A. The small signal state space model for the network with n lines is obtained and given in common reference frame and shown in eqs. (2.55) to (2.58)

$$\left[\Delta \dot{\mathbf{I}}_{\mathbf{lineDQ}}\right] = \mathbf{A_{NET}}\left[\Delta \mathbf{I_{lineDQ}}\right] + \mathbf{B_{1NET}}\left[\Delta \mathbf{V_{bDQ}}\right] + \mathbf{B_{2NET}}\left[\Delta\omega\right] \tag{2.55}$$

$$\left[\Delta \mathbf{I_{lineDQ}}\right] = \mathbf{C_{NET}}\left[\Delta \mathbf{I_{lineDQ}}\right] \tag{2.56}$$

Where in eqs. (2.55) and (2.56)

$$\left[\Delta \mathbf{I_{lineDQ}}\right] = \begin{bmatrix}\Delta \mathbf{I_{lineDQ1}} & \Delta \mathbf{I_{lineDQ2}} & ..... & \Delta \mathbf{I_{lineDQn}}\end{bmatrix}^{\mathbf{T}} \tag{2.57}$$

$$\left[\Delta \mathbf{V_{bDQ}}\right] = \begin{bmatrix}\Delta \mathbf{V_{bDQ1}} & \Delta \mathbf{V_{bDQ2}} & ..... & \Delta \mathbf{I_{bDQb}}\end{bmatrix}^{\mathbf{T}} \tag{2.58}$$

Here, $\mathbf{A_{NET}}$ is the state matrix for network sub-module with n lines, $\mathbf{B_{1NET}}$ and $\mathbf{B_{2NET}}$ are the input matrices of network submodule for voltage input and frequency respectively. Details of these matrices are given in Appendix A.

2.5 Load Module

Microgrid can have different types of loads, such as combination of static passive loads like resistive (R) load, inductive (RL) load, Constant Power Load (CPL), and dynamic loads like induction motor. In this thesis, only static passive loads are assumed to be connected simultaneously to the system. The small signal state space linearized model is formed individualy for these loads and then combined on common reference frame to obtain complete small signal state space model for load sub module.

a) Resistive (R) and Inductive (RL) load

R and RL loads are the most common loads in power systems. Electrical motors, coils, toroid and solenoids can be modeled as RL load. Incandescent lamps and electrical heaters are some examples of the R loads. R load can also be modeled as RL load, with assumption of very small inductance connected in series with the resistance, to obtain the eigenvalues.

a) Constant Power Load (CPL) load

CPL draws constant power from the source. The instantaneous impedance of CPL is always positive but the incremental impedance of CPL is always negative which can be seen from fig. 2.12 [43, 44]. Due to this, there is a decrease in current when the voltage increases and vice vesa. This incremental negative impedance may lead the system to instability. CPL is modelled by giving negative sign to the impedance [45].

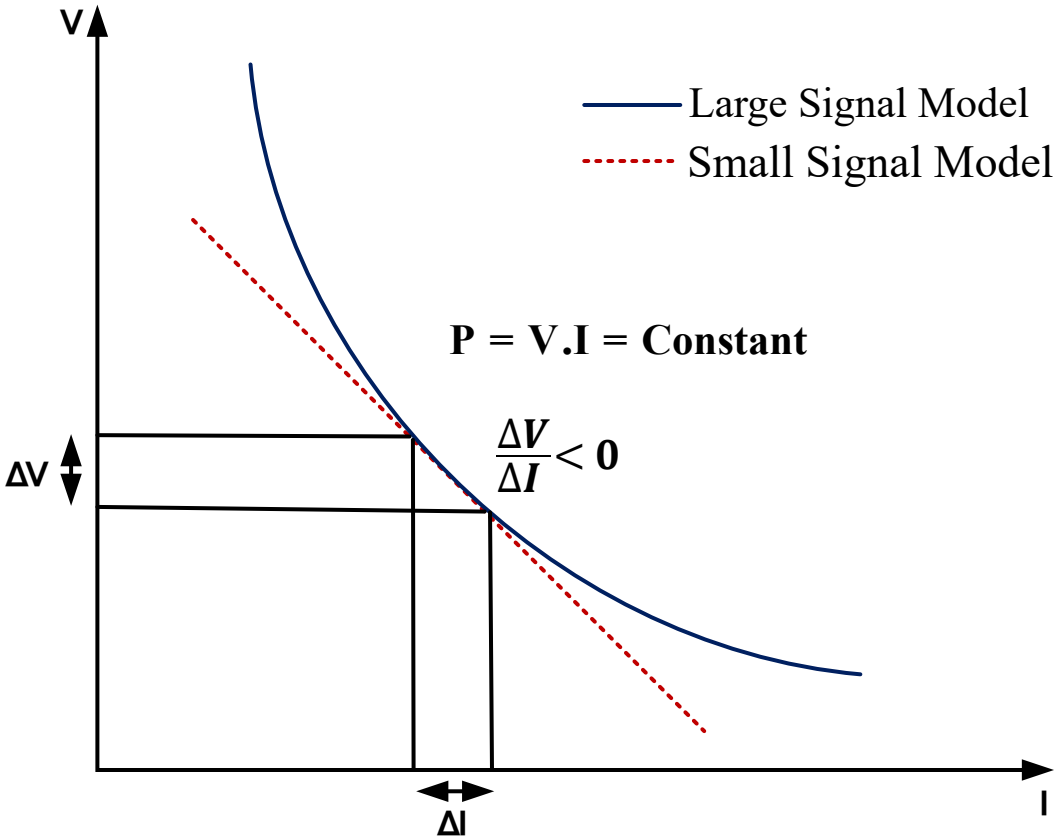

Figure 2.12: Characteristics of CPL

Figure 2.13 shows i^{th} passive load connected at b^{th} bus whose dynamic equations on common reference frame are given in (2.59) and (2.60)

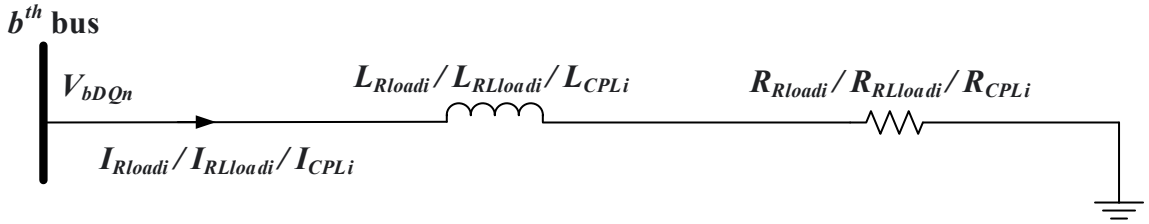

Figure 2.13: Passive loads configuration

$$\dot{I}_{LoadDi} = \frac{-R_{Loadi}}{L_{Loadi}} I_{LoadDi} + \frac{1}{L_{Loadi}} V_{bDj} + \omega I_{LoadDi} \tag{2.59}$$

$$\dot{I}_{LoadQi} = \frac{-R_{Loadi}}{L_{Loadi}} I_{LoadQi} + \frac{1}{L_{Loadi}} V_{bQj} - \omega I_{LoadQi} \tag{2.60}$$

Here, subscript *Load* will change according to the type of the load such as *Rload*, *RLload* and *CPL* for R load, RL load and CPL load, respectively. $R_{CPL} = -r_{CPL}cos(\alpha)$ and $X_{CPL} = -r_{CPL}sin(\alpha)$, where α is the firing angle of the converter and $r_{CPL} = \frac{{V_{rms}}^2}{P_{CPL}}$ [45]. For i^{th} passive load connected at b^{th} bus shown in fig. 2.13, the small signal state space model can be given as

$$\left[\Delta \dot{\mathbf{I}}_{\mathbf{LoadDQi}}\right] = \mathbf{A_{Loadi}} \left[\Delta \mathbf{I_{LoadDQi}}\right] + \mathbf{B_{1Loadi}} \left[\Delta \mathbf{V_{bDQ}}\right] + \mathbf{B_{2Loadi}} \left[\Delta \omega\right] \tag{2.61}$$

where, for i^{th} passive load connected at b^{th} bus, $\mathbf{A_{Loadi}}$ is a state matrix, and $\mathbf{B_{1Loadi}}$ and $\mathbf{B_{2Loadi}}$ are the input matrix corresponding to the input voltage and frequency. Details of these matrices are given in the Appendix A. The complete small signal state space model for l passive loads on common reference frame can be written as given in eqs. (2.62) and (2.63)

$$\left[\Delta \dot{\mathbf{I}}_{\mathbf{LoadDQ}}\right] = \mathbf{A_{Load}} \left[\Delta \mathbf{I_{LoadDQ}}\right] + \mathbf{B_{1Load}} \left[\Delta \mathbf{V_{bDQ}}\right] + \mathbf{B_{2Load}} \left[\Delta \omega\right] \tag{2.62}$$

$$\left[\Delta \mathbf{I_{LoadDQ}}\right] = \mathbf{C_{Load}} \left[\Delta \mathbf{I_{LoadDQ}}\right] \tag{2.63}$$

Where, $\mathbf{A_{Load}}$ is a state matrix for load module and $\mathbf{B_{1Load}}$ and $\mathbf{B_{2Load}}$ are the input matrices. The details of these matrices are given in Appendix A. In eqs. (2.62) and (2.63), $\Delta \mathbf{I_{LoadDQ}}$ is defined as given in (2.64)

$$\left[\Delta \mathbf{I_{LoadDQ}}\right] = \begin{bmatrix} \Delta \mathbf{I_{LoadDQ1}} & \Delta \mathbf{I_{LoadDQ2}} & ..... & \Delta \mathbf{I_{LoadDQl}} \end{bmatrix} \tag{2.64}$$

2.6 Complete Model of Microgrid

The complete model of microgrid is obtained by combining all sub modules. Mapping matrices are obtained by mapping the sub- modules, which connect the output currents to a node

[42]. In power system, each element either acts as source or load i.e it either gives power or current to the node or takes power or current from node. For the mapping, it is assumed that plus sign represents current flowing towards the node and minus represents current is flowing away from the load.

For all sub modules, mapping matrices are obtained for D and Q components. $\mathbf{M_{INV}}$ maps the connection of m generator modules to the b bus nodes. The size of $\mathbf{M_{INV}}$ can be given as $2b \times 2m$ and elements of matrix can be written as

$$\mathbf{M_{INV}}(\mathbf{i},\mathbf{j}) = \begin{cases} 1 & \text{if } j^{th} \text{ DG unit is connected at the } i^{th} \text{ bus node,} \\ 0 & \text{if } j^{th} \text{ DG unit is not connected at the } i^{th} \text{ bus node.} \end{cases}$$

Mapping matrix of the network module maps n transmission lines on to the b bus nodes. Order of mapping matrix is $2b \times 2n$ and represented by $\mathbf{M_{NET}}$ whose elements can be defined as

$$\mathbf{M_{NET}}(\mathbf{i},\mathbf{j}) = \begin{cases} 1 & \text{if } j^{th} \text{ transmission line is connected at the } i^{th} \text{ bus node and} \\ & \text{current is flowing towards the } i^{th} \text{ bus node,} \\ -1 & \text{if } j^{th} \text{ transmission line is connected at the } i^{th} \text{ bus node and} \\ & \text{current is flowing away from the } i^{th} \text{ bus node.} \end{cases}$$

Similarly, Mapping matrix of the load module maps l loads on to the b bus nodes. Size of mapping matrix is $2b \times 2l$ and represented by $\mathbf{M_{Load}}$ whose elements can be defined as

$$\mathbf{M_{Load}}(\mathbf{i},\mathbf{j}) = \begin{cases} 1 & \text{if } j^{th} \text{ passive load is connected at the } i^{th} \text{ bus node,} \\ 0 & \text{if } j^{th} \text{ passive load is not connected at the } i^{th} \text{ bus node.} \end{cases}$$

From eqs. (2.47), (2.56) and (2.63), it can be observed that, the currents are taken as output of the modules but in eqs. (2.46), (2.55) and (2.62) bus voltage $\Delta\mathbf{V_{bDQ}}$ is treated as input to each module. To obtain well defined bus voltage, a virtual resistance r_N is considered to be connected between bus and ground (shown in fig. 2.14). To minimize the effect of r_N on dynamic stability, the value of r_N is chosen sufficiently large [42]. The voltage at i^{th} bus,

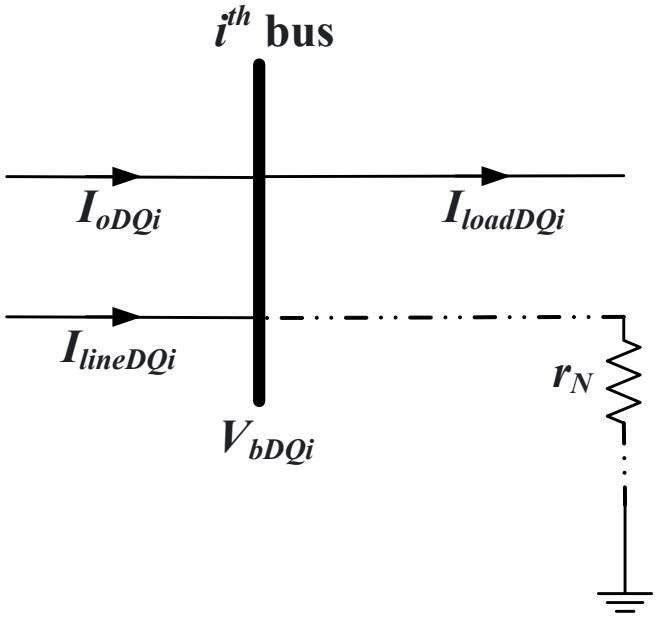

Figure 2.14: Virtual resistance at i^{th} bus

shown in fig. 2.14, can be obtained as

$$\mathbf{V_{bDQi}} = r_N(\mathbf{I_{oDQi}} - \mathbf{I_{LoadDQi}} + \mathbf{I_{lineDQ\ i}}) \tag{2.65}$$

The small signal state space representation for this bus voltage corresponding to the mapping matrices can be given as

$$\left[\Delta \mathbf{V_{bDQ}}\right] = \mathbf{R_N}\left(\mathbf{M_{INV}}\left[\Delta \mathbf{I_{oDQ}}\right] + \mathbf{M_{Load}}\left[\Delta\ \mathbf{I_{LoadDQ}}\right] + \mathbf{M_{NET}}\left[\Delta \mathbf{I_{NETDQ}}\right]\right) \tag{2.66}$$

Disturbance is needed to analyze the small signal stability and observe behavior of control scheme of microgrid. The most common disturbance in any power system is load change, so the load change is considered as a disturbance in the system. And hence, the load at i^{th} bus needs to be modelled as current as shown in fig. 2.15. Therefore, bus voltage given in (2.66) is modified as (2.67) including the load disturbance.

$$\begin{aligned}\left[\Delta \mathbf{V_{bDQ}}\right] = \mathbf{R_N}(&\mathbf{M_{INV}}\left[\Delta \mathbf{I_{oDQ}}\right] + \mathbf{M_{Load}}\left[\Delta\ \mathbf{I_{LoadDQ}}\right] \\ &+ \mathbf{M_{NET}}\left[\Delta \mathbf{I_{NETDQ}}\right] + \mathbf{M_{DIST}}\left[\Delta \mathbf{I_{distDQ}}\right]\end{aligned} \tag{2.67}$$

In (2.67), $\mathbf{M_{DIST}}$ is mapping matrix which maps the load distrubance on i^{th} bus node and whose size is $2b \times 2$. The elements of the $\mathbf{M_{DIST}}$ is given as

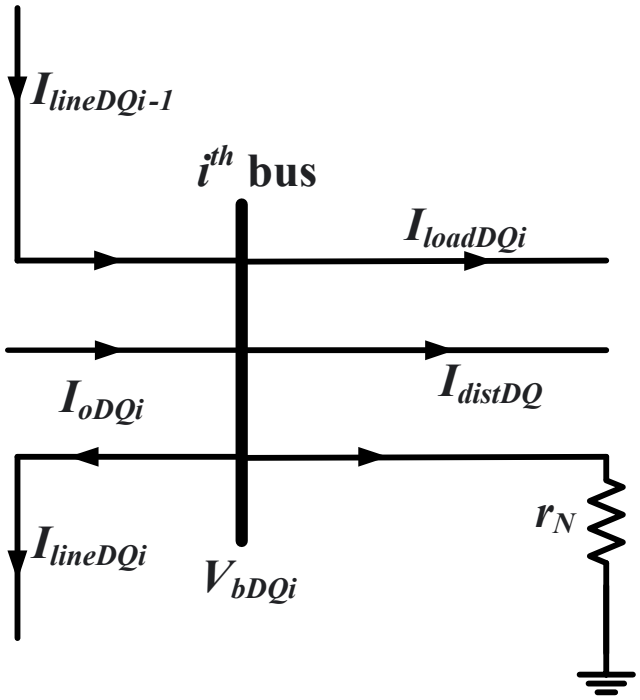

Figure 2.15: Disturbance at i^{th} bus

$$\mathbf{M_{DIST}(i,j)} = \begin{cases} -1 & \text{if } i = j \text{ and load disturbance is connected at } i^{th} \text{ bus node,} \\ 0 & \text{if } i \neq j. \end{cases}$$

Now, by combining individual small signal models given in (2.46) - (2.48) , (2.55) - (2.56) and (2.62) - (2.63), the complete small signal linearized state space mode for microgrid is obtained as defined in (2.68)

$$\left[\Delta \dot{\mathbf{X}}_{\mathbf{MG}}\right] = \mathbf{A_{MG}} \left[\Delta \mathbf{X_{MG}}\right] + \mathbf{B_{MG}} \left[\Delta \mathbf{I_{distDQ}}\right] \tag{2.68}$$

In (2.68), $\mathbf{A_{MG}}$ is the state matrix for microgrid and $\mathbf{B_{MG}}$ is the input matrix. Details of these matrices are given in Appendix A. Matrix $\left[\Delta \mathbf{X_{MG}}\right]$ can be given as

$$\left[\Delta \mathbf{X_{MG}}\right] = \left[\Delta \mathbf{X_{GEN}} \quad \Delta \mathbf{I_{LineDQ}} \quad \Delta \mathbf{I_{LoadDQ}}\right]^{\mathbf{T}} \tag{2.69}$$

Here, $\Delta \mathbf{X_{GEN}}$, $\Delta \mathbf{I_{LineDQ}}$ and $\Delta \mathbf{I_{LoadDQ}}$ are the state vectors corresponding to the generator module, network module and load module, respectively, which are previously obtained in eqs. (2.49), (2.57) and (2.64).

Hence, size of the $\left[\Delta \mathbf{X_{MG}}\right]$ can be given as $(14m + 2n + 2l) \times 1$ where m is number of DGs present in the system, n is number of transmission lines in the system and l is the

number of passive loads connected to the system. Also, size of $\mathbf{A_{MG}}$ is $(14m+2n+2l) \times (14m+2n+2l)$ and size of $\mathbf{B_{MG}}$ can be obtained as $(14m+2n+2l) \times (2m)$.

2.7 Conclusion

In this chapter, a generalized small signal state space model for microgrid with synchronverter as local controller is developed on synchronized rotating DQ reference frame. To obtain the complete state space model of the microgrid, the system is essentially divided in modules such as generator module, network module and load module. Generator module is further divided for obtaining state space model of power calculation block, synchronverter and LCL filter. All modules are modeled on individual dq reference frame and all are transferred to the common DQ reference frame to obtain the combined model. The obtained model is utilized for obtaining the eigenvalues and hence analyze stability of the system.

Chapter 3

Simulation Results

3.1 Introduction

For any technical system, stability is an essential aspect. The system should operate effectively under various disturbances. The most common disturbance in the microgrid is load change. Hence, system should maintain its stability and meet all the load demand under disturbance. Further, if power quality is taken into consideration, system should have good transient response with less number of oscillations.

To analyse stability of the non linear system, linear model has to be developed. This linear model is developed by linearizing system equations at steady state operating points. The procedure to obtain small signal linearized model is given in chapter 2. This chapter studies the stability analysis using the linearized model for DGs, as obtained in chapter 2, with synchronverter as their local controller. Further, this chapter also includes the real-time simulation results for various load disturbance cases.

3.2 Eigenvalues and their Properties

The concept of eigenvalue analysis from control system is widely used to analyse stability of conventional power system. Eigenvalues, also called as modes, are solution of the system characteristic equation. Eigenvalues obtained from state matrix, $\mathbf{A_{MG}}$ (2.69), can be given by scalar parameter λ for which there exists a non-trivial solution (i.e., $\boldsymbol{\phi} \neq 0$) to the equation (3.1)

$$\mathbf{A_{MG}}\boldsymbol{\phi} = \lambda\boldsymbol{\phi} \tag{3.1}$$

Here, $\mathbf{A_{MG}}$ is a square matrix with size $n \times n$ and $\boldsymbol{\phi}$ is $n \times 1$ vector termed as eigenvector. To find eigenvalue, equation (3.1) is written as (3.2)

$$(\mathbf{A_{MG}} - \lambda\mathbf{I})\,\boldsymbol{\phi} = 0 \tag{3.2}$$

Here, $\mathbf{I}$ is identity matrix of order $n \times n$. For a non-trivial solution,

$$det\,(\mathbf{A_{MG}} - \lambda\mathbf{I}) = 0 \tag{3.3}$$

Characteristic equation is obtained from the expansion of the determinant. The n solutions of $\lambda = \lambda_1, \lambda_2, \lambda_3, \cdots, \lambda_n$ are the eigenvalues of state matrix $\mathbf{A_{MG}}$. Eigenvalues may be real or complex but complex eigenvalue always exists in conjugate pair.

The imaginary part of the eigenvalues are related to the frequency of the oscillation of the mode, whereas real part is connected to the stability coefficient of the mode. A decaying mode is represented by the negative real eigenvalue. More away the eigenvalue is from the imaginary axis, faster is the decay. The positive eigenvalue results in an aperiodic monotonic instability. Each conjugate pair corresponds to the oscillatory behavior. Damping is provided by the real part of the complex eigenvalue, while frequency of oscillation is given by the imaginary part. The frequency of oscillation in (Hz) and the damping ratio (ζ) is given by (3.5) and (3.7), respectively. A positive real part of the complex mode indicates the increasing amplitude of the oscillations, while negative part shows damped oscillations.

$$\lambda = \sigma \pm j\omega \tag{3.4}$$

$$f = \frac{\omega}{2\pi} \tag{3.5}$$

$$\zeta = \frac{-\sigma}{\sqrt{\sigma^2 + \omega^2}} \tag{3.6}$$

Here, λ is described as a neper frequency (neper/s) whereas ω is frequency in rad/s. The damping coefficient ζ defines the rate of decay of the oscillations. $\frac{1}{|\sigma|}$ gives time constant of

the amplitude decay.

3.3 Sensitivity Analysis and Participation Factors

The frequency and the damping of the mode can be obtained from a given eigenvalue but more information about the origin of the mode can be obtained by observing the participation of the different state variables in a particular mode, and hence making it possible to find the reason behind the excitation of the mode [20]. This can be done by sensitivity analysis on the state matrix. Participation factor is a measure of the relation between the modes and the state variables. (3.7) gives participation of the j^{th} state variable in i^{th} mode, which is the sensitivity of the eigenvalue, λ_i, to the diagonal element, a_{jj}, of the state matrix, A_{MG}.

$$P_{ji} = \frac{\partial \lambda_i}{\partial a_{jj}} = \frac{\phi_{ji}\psi_{ji}}{\underline{\phi}_j \underline{\psi}_j} \tag{3.7}$$

Here, ϕ_{ji} is j^{th} entry of right eigenvector ϕ_i and ψ_{ji} is j^{th} entry of left eigenvector ψ_i, respectively and $\underline{\phi}_j \underline{\psi}_j$ is a scalar, which is used to normalize the eigenvector.

3.4 Stability Analysis and Dynamic Performance

Small signal state space model for the test system, shown in fig. 3.1, has been developed in the MATLAB environment using the procedure given in chapter 2. To investigate the stability of the system, eigenvalues analysis is performed on the state matrix of the system.

3.4.1 System Under Study

Figure 3.1 shows the schematic diagram of the system under study operating at 50 Hz and 230 V (per phase Root Mean Square (RMS)). Each IIDG consist of the DG source, an inverter, and a local controller, which is synchronverter in this case . The DG source may be wind turbine generator, photovoltaic or fuel cell generator, etc. The microgrid is operating in

isolated mode i.e islanded mode which can be realized by opening the isolation switch, shown in fig. 3.1, which disconnects the microgrid from the utility grid.

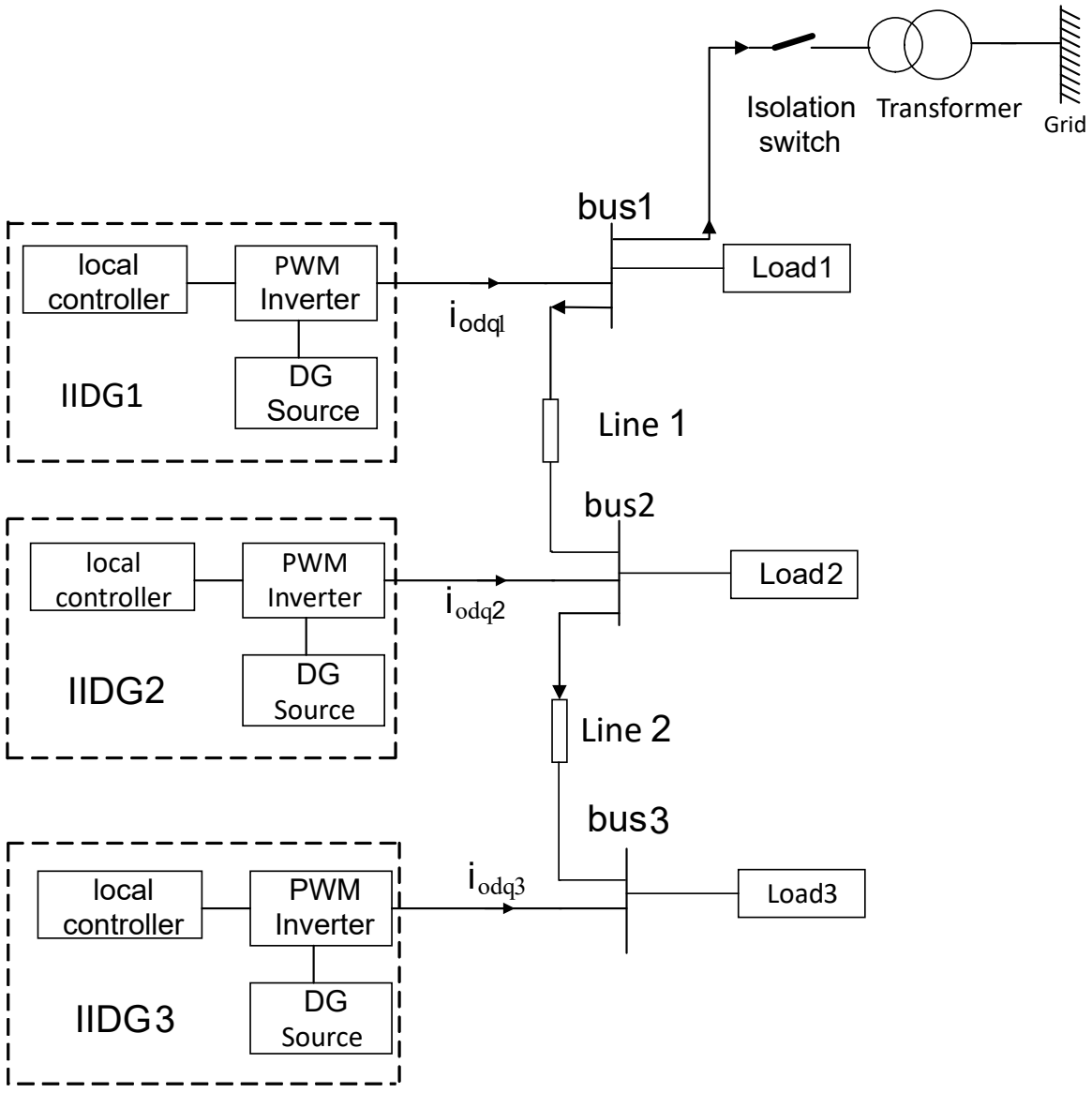

Figure 3.1: Schematic diagram of the test system

In the island mode of operation, the DG units are responsible to maintain system frequency and voltage within permissible limit while supplying the load demand. The system parameters used for analysis is given in table 3.1. The inverter parameters such as filter parameters are referred from [42, 46].

Table 3.1: System Parameters of the Test System

Equal Power Ratings	**Unequal Power Ratings**
DG Unit Ratings	
$DG_1 = DG_2 = DG_3$ = (20+j12) kVA.	DG_1 = (5+j3) kVA; DG_2 = (15+j15) kVA; DG_3 = (20+j12) kVA.
Frequency Droop Coefficients	
$DG_1 = DG_2 = DG_3$ =40.5284 N.m/rad/sec.	D_{P1} = 10.1321 N.m/rad/sec; D_{P2} = 30.3963 N.m/rad/sec; D_{P3} = 40.5284 N.m/rad/sec.
Inertia Constants	
$J_1 = J_2 = J_3$ = 0.405284 N.m/rad/sec^2.	J_1= 0.101321 N.m/rad/sec^2; J_2= 0.303963 N.m/rad/sec^2; J_3 = 0.405284 N.m/rad/sec^2.
Static Reactive Power Droop Gains	
$D_{q1} = D_{q2} = D_{q3}$ = 368.9252 VAR/V.	D_{q1} = 92.2313 VAR/V; D_{q2} = 276.6939 VAR/V; D_{q3} = 368.9252 VAR/V.
Control Parameter for Adjustment of RPL Response Speed	
$K_1 = K_2 = K_3$ = 1159.0116 VAR.rad/V.	K_1 = 289.7529 VAR.rad/V; K_2 = 869.2587 VAR.rad/V; K_3 = 1159.0116 VAR.rad/V.
Inverter parameters	
f_{sw} = 10 kHz, ω_c = 31.41 rad/s.	
Filter and Coupling Inductor Parameters	
L_f = 1.35 mH, C_f = 50 µF, r_f = 0.1 Ω, r_c = 0.3 Ω, L_c = 0.35 mH, τ = 10 ms.	
Line Parameters	
R_{line1} = 0.23 Ω; L_{line1} = 0.318 mH, R_{line2} = 0.35 Ω; L_{line2} = 1.84 mH.	
Load Parameters	
R load = 13.5 kW; R_{load} = 11.75 Ω, CPL 12 kVA; R_{CPL} = 15.87 Ω, L_{CPL}= 70.16 mH, RL Load 12 kVA; R_{RL}= 17.63 Ω, L_{RL} = 63.68 mH.	

3.4.2 Calculation of the Synchronverter Parameters

As discussed in subsection 2.3.2, synchronverter has two control loop APL and RPL, and parameters of these loops are calculated as given below.

3.4.2.1 Active Power Loop Design

APL has the two main parameters; frequency droop coefficient D_p and inertia constant J. To share active power, droop gains D_{p1}, D_{p2}, D_{p3} are considered. (3.8) shows calculation of D_{p1} and similarly, D_{p2} and D_{p3} are calculated.

$$D_{p1} = \frac{\Delta T_{m1}}{\Delta \omega_r} \tag{3.8}$$

Where, ΔT_{m1} is the amount of change in the input torque for the 1^{st} DG when there is change in the angular speed of $\Delta\omega_r$. Here, 100% change in the input torque is considered for the 0.5% change in the reference frequency. Also, ΔT_{m1} can be given as 100% change in the rated active power divided by natural frequency ω_n, as given in (3.9).

$$\Delta T_{m1} = \frac{\Delta P_1}{\omega_n} \tag{3.9}$$

Active power rating of 1^{st} DG is taken as 5kW and $\Delta\omega_r = 0.5\%\ of(2 \times \pi \times 50)$

$$\Delta T_{m1} = \frac{5 \times 10^3}{2 \times \pi \times 50} = 15.915$$

and, from (3.8), D_{p1} can be calculated as,

$$D_{P1} = \frac{15.915}{0.005 \times 2 \times \pi \times 50} = 10.1321\ Nm/rad/sec$$

Now, considering APL time constant $\tau_f = 10\ ms$, the inertia constant for 1^{st} DG can be calculated as

$$J_1 = D_{P1}\tau_f \tag{3.10}$$

$$J_1 = 10.1321 \times (10 \times 10^{-3}) = 0.101321\ Nm/rad/sec^2$$

Similarly, parameters of APL are calculated for other DGs.

3.4.2.2 Reactive Power Loop Design

RPL also has the two main design parameters; voltage droop coefficient D_q and RPL speed control parameter K.

$$D_{q1} = \frac{\Delta Q_1}{\Delta V_m} \tag{3.11}$$

Here, ΔQ_1 is a amount of change in the input reactive power and ΔV_m is net change in nominal voltage magnitude.

In this thesis, 100% change in the reactive power is considered for 10% change in the nominal voltage. The reactive power capacity of the first DG is taken as 3 kVAR. Hence, from (3.11) D_{q1} is calulated as,

$$D_{q1} = \frac{3000}{0.1 \times 230\sqrt{2}} = 92.2313\ VAR/V$$

RPL speed constant is dependent on D_{q1}, ω_n and the RPL time constant τ_v. Here, τ_v is taken same as τ_f, Hence, considering RPL time constant $\tau_v = 10\ ms$, K_1 for 1^{st} DG can be given as,

$$K_1 = D_{q1}\tau_v\omega_n \tag{3.12}$$

$$K_1 = 92.2313 \times 0.01 \times 314.159 = 289.7529\ VAR.rad/V$$

Similarly, parameters of RPL of other DGs are obtained.

3.4.3 Small Signal Model Development

Small signal linearized state space model for the test system, shown in fig. 3.1, is obtained by using the generalized model approach described in chapter 2.

$$\left[\Delta\dot{\mathbf{X}}_{\mathbf{MG}}\right]_{52\times1} = [\mathbf{A_{MG}}]_{52\times52}\left[\Delta\mathbf{X_{MG}}\right]_{52\times1} + [\mathbf{B_{MG}}]_{52\times6}\left[\Delta\mathbf{I_{distDQ}}\right]_{6\times1} \tag{3.13}$$

Where, $\mathbf{A_{MG}}$ is a state matrix and $\mathbf{B_{MG}}$ is input matrix.

3.4.4 Steady-State Initial Conditions

Steady state operating points are required to linearize all non linear equations. These operating points can be found by means of load flow solution. In this work, steady state operating conditions are obtained by performing simulation in RSCAD within substep environment, the results for which are shown in section 3.6. The system parameters used to obtain the steady state parameters are given in Table 3.1. The steady state conditions are obtained by considering equal as well as unequal ratings of DGs and given in Table 3.2 and Table 3.3, respectively.

Table 3.2: Steady State Initial Conditions For DGs with equal ratings

Parameters	DG units
	[DG_1 DG_2 DG_3]
Internal Parameters	
V_{oD}	[326.53 326.95 326.05]
V_{oQ}	[0 0 0]
I_{oD}	[22.08 21.71 22.9]
I_{oQ}	[-7.19 -1.9 7.66]
I_{lD}	[22.63 22.19 23.35]
I_{lQ}	[-1.5 -1.31 1.17]
δ_0	[0 0.0019 0.0045]
External Parameters	
V_{bD}	[319.13 318.72 320.23]
V_{bQ}	[0.4 -2.8 -3.7]
Steady State Parameters of Transmission Line	
I_{lineD}	[-4.68 1.46]
I_{lineQ}	[-7.42 9.4]
Steady State Parameters of R, CPL and RL loads	
I_{loadD}	[26.35 16.84 16.52]
I_{loadQ}	[-2.60 -6.48 -9.96]

3.4.5 Eigenvalue Analysis of the Test System

This section presents the eigenvalue analysis performed on the test system. The system parameters are kept same for all DG units as given in Table 3.1. Eigenvalue analysis was similar for both equal and unequal rating of DGs hence, eigenvalue analysis is presented only for the unequal ratings of DGs.

Fig. 3.2 shows the complete eigenvalues for the unequal rating of DGs. It can be ob-

Table 3.3: Steady State Initial Conditions For DGs with unequal ratings

Parameters	DG units
	[DG_1 DG_2 DG_3]
Internal Parameters	
V_{oD}	[323.22 324.00 325.93]
V_{oQ}	[0 0 0]
I_{oD}	[7.13 23.74 34.9]
I_{oQ}	[-6.15 4.62 8.16]
I_{lD}	[8.12 25.6 37.51]
I_{lQ}	[-0.7 6.43 9.46]
δ_0	[0 0.006 0.012]
External Parameters	
V_{bD}	[319.23 318.40 318.32]
V_{bQ}	[-0.8 -2.3 -3.1]
Steady State Parameters of Transmission Line	
I_{lineD}	[-18.08 -9.7]
I_{lineQ}	[-2.89 -4.89]
Steady State Parameters of R, CPL and RL loads	
I_{loadD}	[26.23 17.04 15.82]
I_{loadQ}	[-2.54 -7.21 -9.8]

served that the eigenvalues can be grouped in four clusters. Following the procedure given in section 3.3, participation analysis is performed on the eigenvalues. It is found that 12 high frequency modes, which are present in cluster '2', are sensitive to the state variables of LCL filter. Moreover, six dominant eigenvalues are shown in cluster '1'. The 28 eigenvalues sensitive to the parameters of synchronverter and transmission lines are grouped in cluster '3'. Whereas, cluster '4' contains six modes sensitive to the load currents.

3.4.5.1 Effect of Parameter Variation on Dominant Poles

To verify stability of the system, it is necessary to observe the behavior of the dominant poles with respect to the variation in system parameters. Since these eigenvalues are very close to the imaginary axis, they are prone to instability.

Fig. 3.3 shows the trajectory of dominant poles with change in inertia constant (J), which is the design parameter in APL. J is changed from 0.5 $N.m/rad/sec^2$ to 0.05 $N.m/rad/sec^2$, and it can be observed that the dominant poles, λ_{12} - λ_{15}, are not much sensitive to the parameter variation in APL. Fig. 3.4 shows the trajectory of the dominant poles with change in reactive power droop coefficient (D_q), which is the design parameter in RPL. D_q is increased

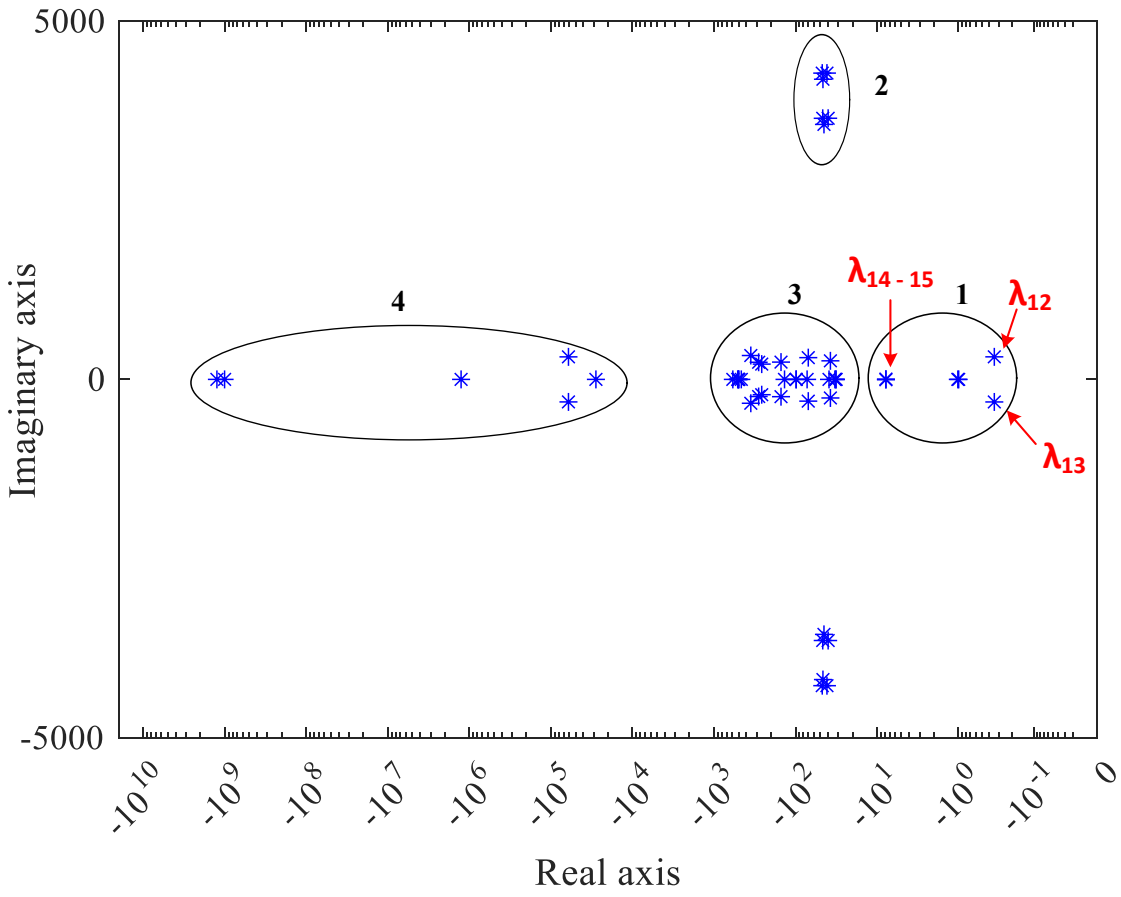

Figure 3.2: Eigenvalue spectrum of the system

from 80 VAR/V to 500 VAR/V. It can be seen that, in this case also the dominant poles, λ_{12} - λ_{15}, are not much sensitive to the parameter variation in RPL. From fig. 3.3 and fig. 3.4, it can be concluded that the system remains in stable condition unlike in droop control technique shown in ref [42], where the system becomes unstable with change in the droop coefficients.

3.5 Real Time Digital Simulation Results

This section presents the real-time simulation results for the test system. Various case studies are considered to obtain the results, which are given in the following subsections. Further, the performance of the synchronverter has been compared with the droop control scheme given in [42], keeping all the parameters same in both the control techniques.

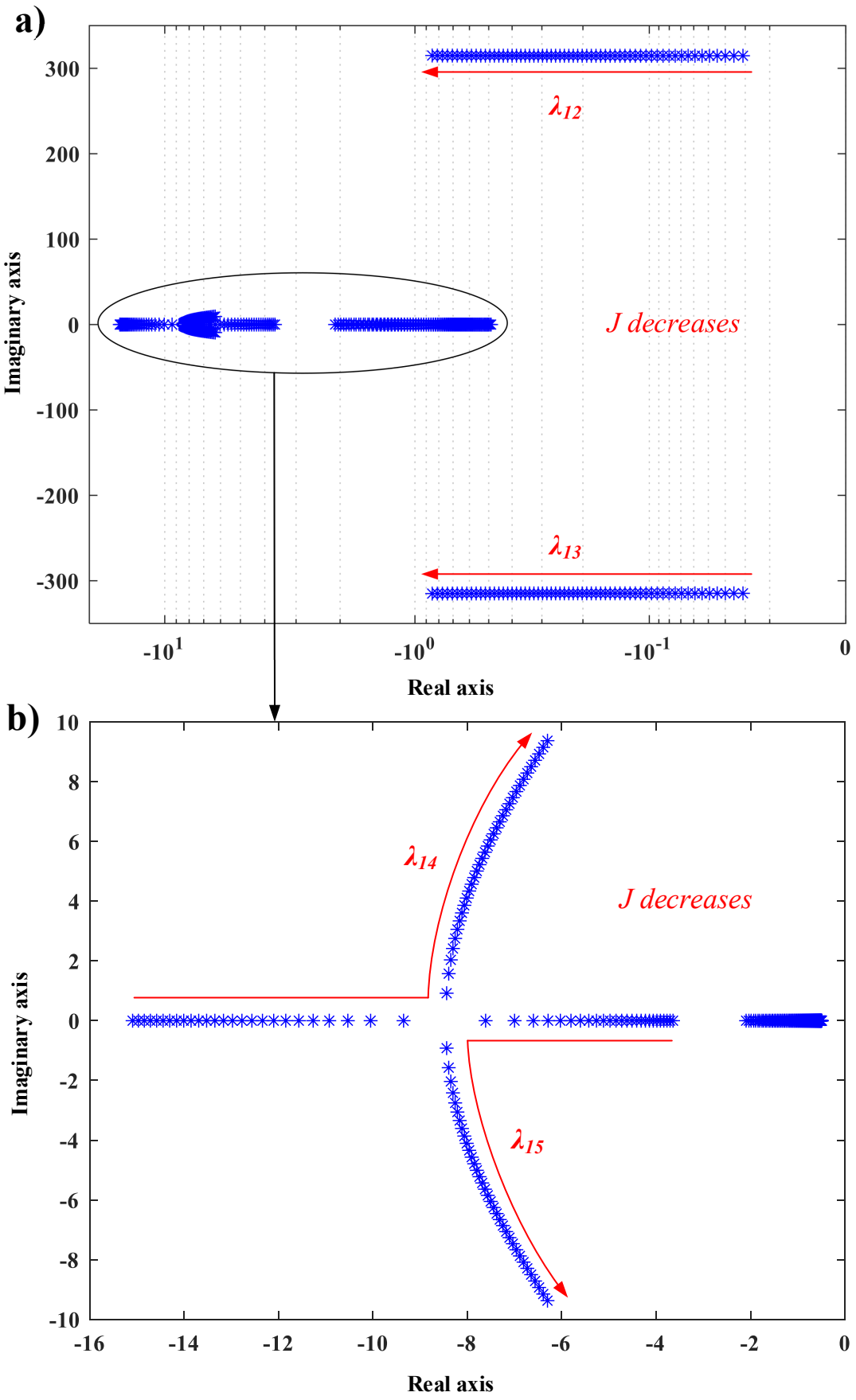

Figure 3.3: (a) Tracing of eigenvalues with variation in J. (b) Magnified plot of dominant poles

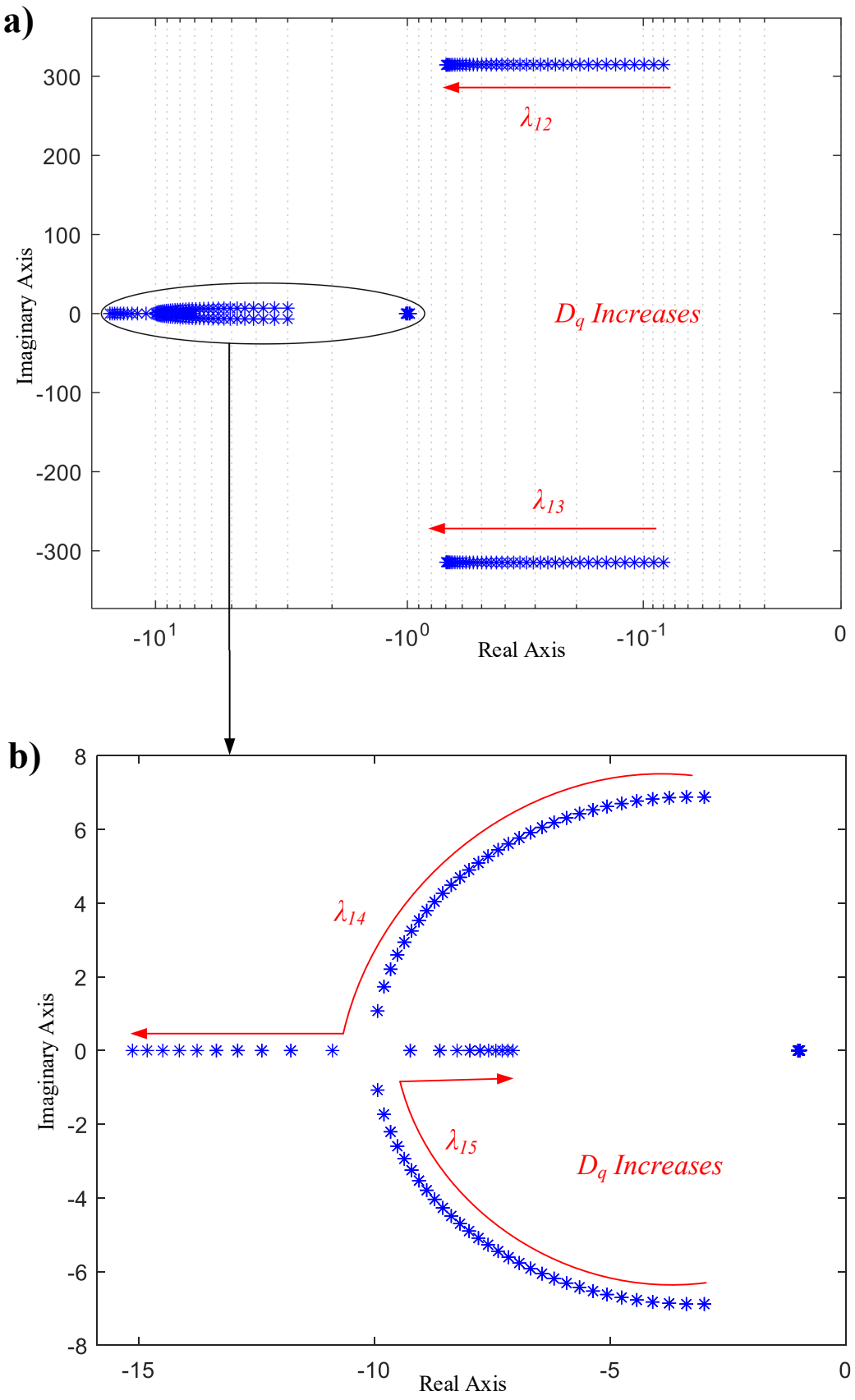

Figure 3.4: (a) Tracing of eigenvalues with variation in D_q. (b) Magnified plot of dominant poles

3.5.1 Concept of Real Time Simulation

Various offline simulation tools are available for performing simulation of power system and power electronics. During simulation, several complex non-linear differential equations need to be solved, and for offline simulation tool, it takes more time to simulate the whole system than the time taken by the real system. Time required to perform any task is not fixed and depends on the complexity of the system.

For these reasons, real-time simulation tools are becoming more popular in the power system and power electronic studies. Real-time simulations provide more accurate and reliable results than the offline simulation.

In this, Real Time Digital Simulator (RTDS) has been used for the real-time simulation studies. All components of the system are implemented in RTDS using RSCAD.

3.5.2 Real Time Digital Simulator (RTDS)

RTDS is the real-time power system simulator developed by RTDS technologies. It has state-of-the-art POWER8TM processor from IBM. RTDS is a specialized parallel processing hardware to simulate the power system and power electronics model in real time using its high-speed processors. It can solve hundreds of nodes in single core. Substep environment provides reduced time-steps in scale of nanoseconds for high precision simulation. RTDS has various Input/Output (I/O) cards such as Giga Transceiver Analog Output (GTAO), Giga Transceiver Digital Input (GTDI), Giga Transceiver Analog Input (GTAI) and Giga Transceiver Digital Output (GTDO), which allows user to connect any external hardware to perform Hardware In Loop (HIL) or Controller Hardware In Loop(CHIL) studies.

The system under study is simulated in RSCAD-Draft and then RSCAD-Runtime feature is used to upload it on RTDS processor cards. The test system is simulated in the substep environment, which is an integral fraction of the main step (μs), thus giving time step of *nanoseconds*.

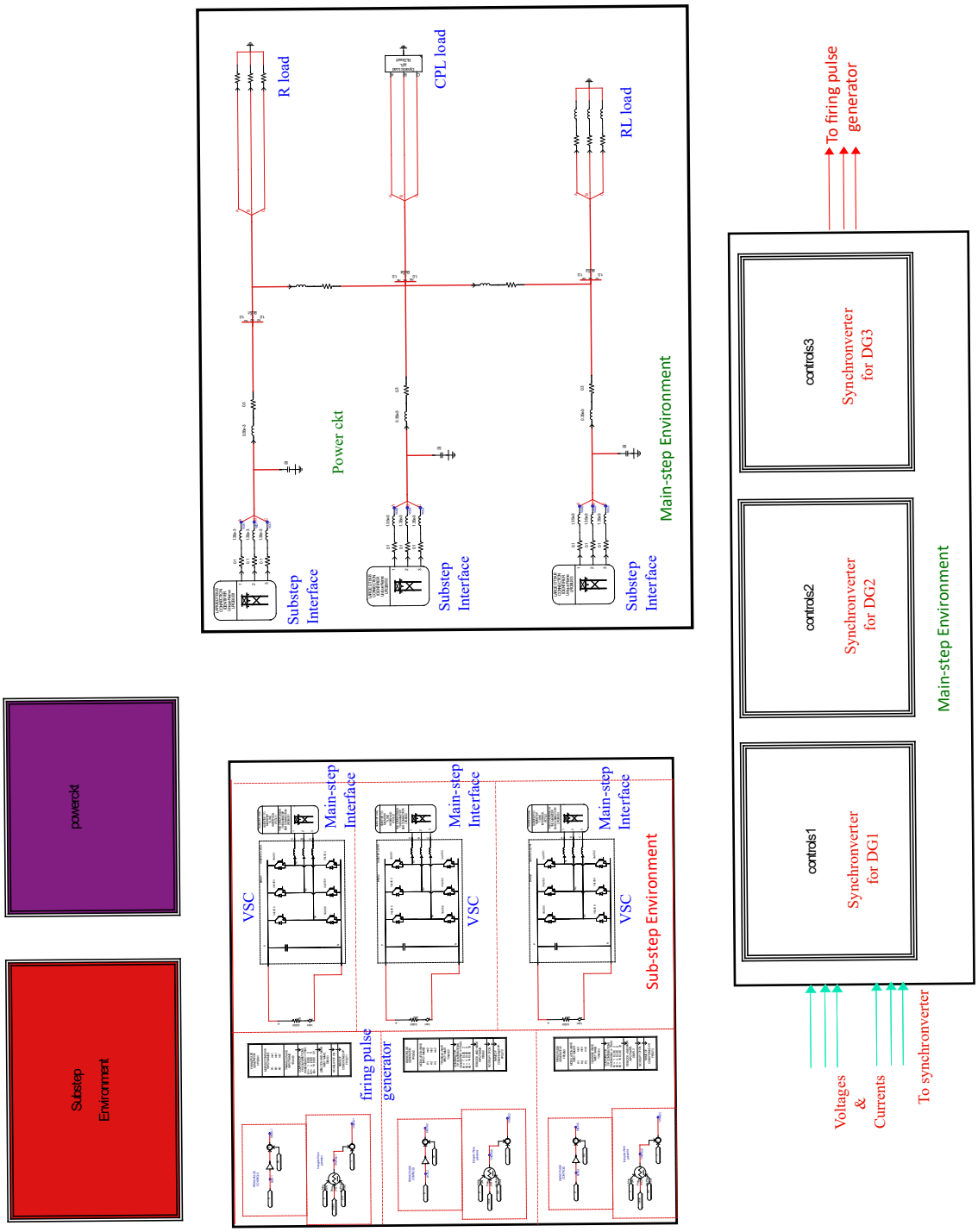

Figure 3.5: Schematic diagram of simulation build in RSCAD

3.5.3 RTDS Study Results

To obtain the steady state operating conditions of the system, system is simulated in RSCAD. Fig. 3.5 shows the whole structure of the implemented test system in RSCAD. The system parameters are given in Table 3.1. Figures 3.6 to 3.8 show the dynamic response of the three phase load voltages and three phase currents for R, RL, and CPL loads.

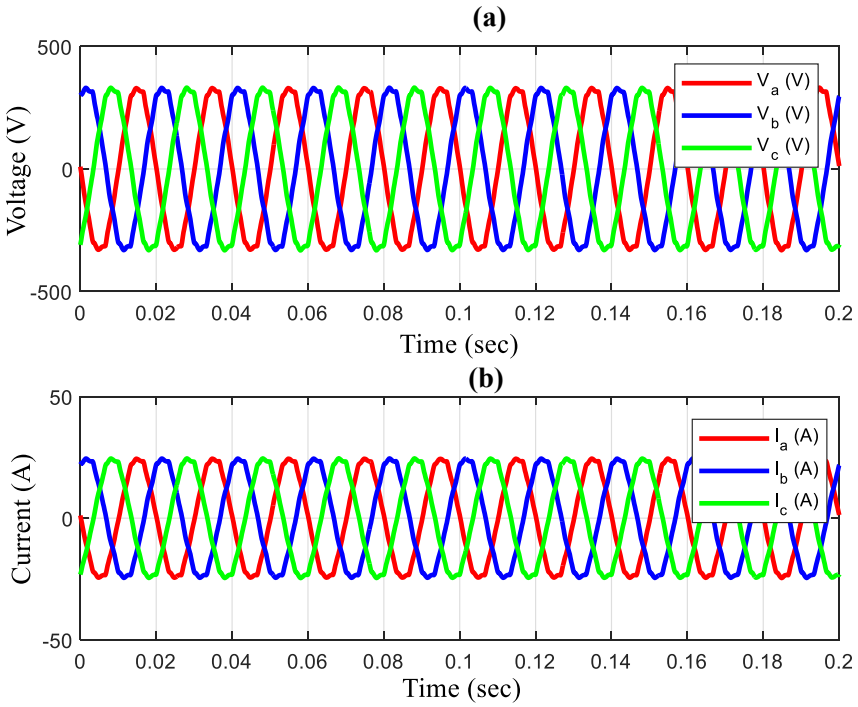

Figure 3.6: Response of the three-phase voltages and currents of R load. (a) Voltages (V_{Rabc}). (b) Currents (I_{Rabc})

From fig. 3.6, it can be seen that voltages and currents are in phase with each other while in fig. 3.7, current lags behind the voltages, thus proving the basic properties of R and RL loads, respectively. It can be observed from fig. 3.8 that, due to the negative incremental resistance of CPL, there is an increase in current when voltage decreases and a decrease in current when voltage increases.

The most common disturbance on microgrid is load change. To analyse the performance of synchronverter during various disturbances, following three case have been considered for both equal ratings as well as unequal rating of DGs,

Case 1: Step load is applied at bus 3.

Case 2: Step load is applied at all buses at the same time.

Case 3: Step load is applied first at bus 3 and then at bus 2.

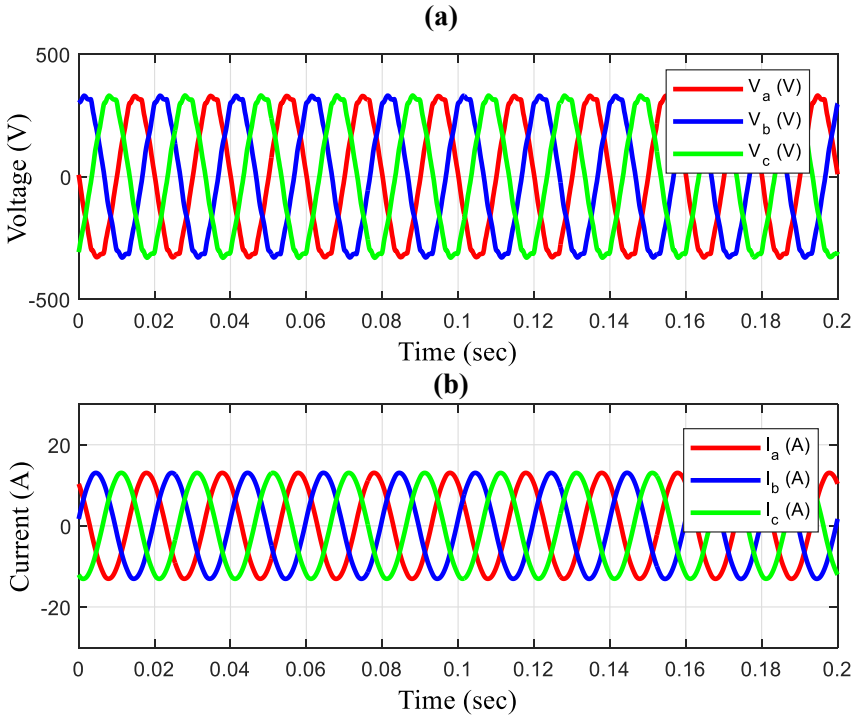

Figure 3.7: Response of the three-phase voltages and currents of RL load. (a) Voltages (V_{RLabc}). (b) Currents (I_{RLabc})

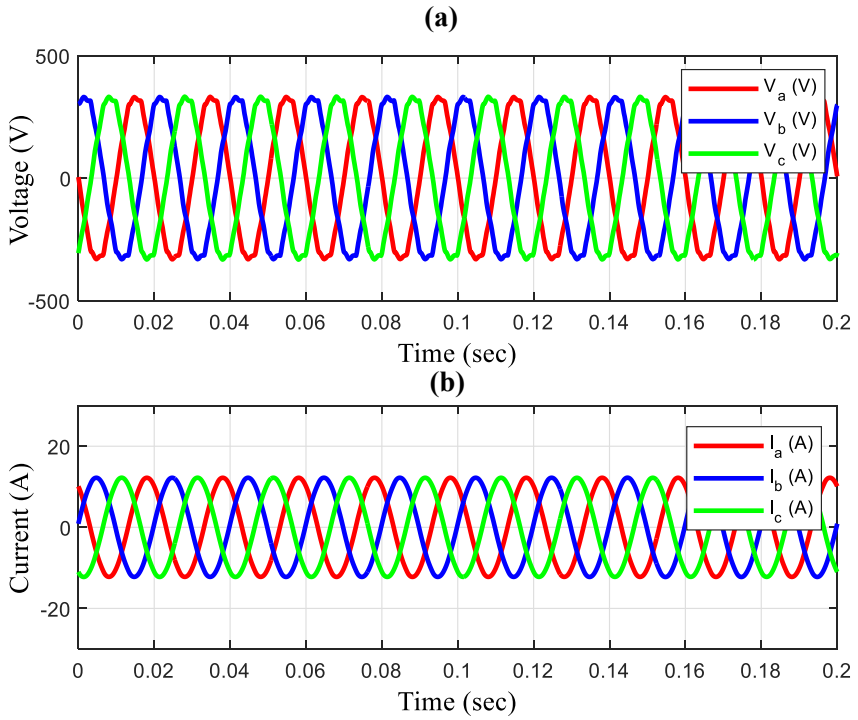

Figure 3.8: Response of the three-phase voltages and currents of CPL load. (a) Voltages (V_{CPLabc}). (b) Currents (I_{CPLabc})

Case 1: Step load is applied at bus 3

Load change on any bus is the most frequent disturbance for the system. In this case, an additional R load of 10 kW is connected at bus 3 in parallel to the existing loads shown in fig. 3.1. Dynamics of the system is recorded for 20 sec; the extra load is added to the system at t = 1.5 sec and removed at t = 11.5 sec. The response of the system is observed for both equal and unequal rating of DGs.

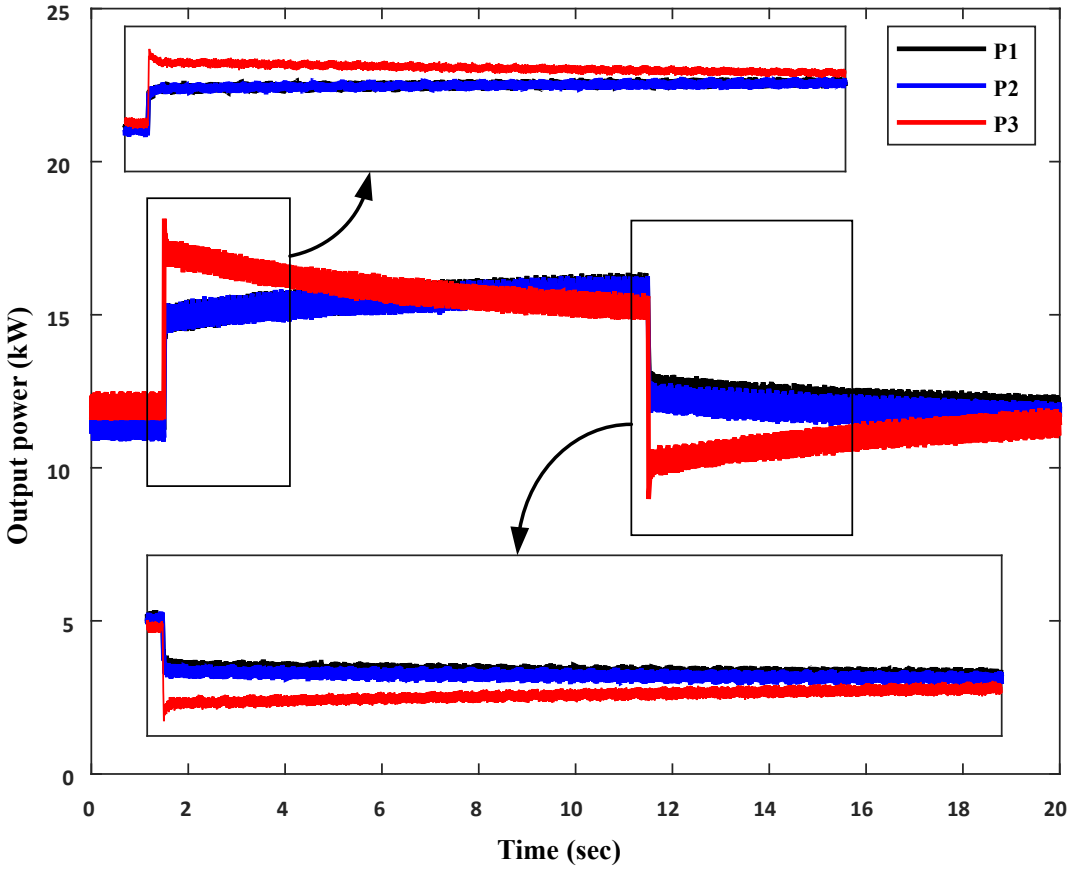

Figure 3.9: Change in output power for case 1 with equal ratings of DGs

a) DGs with equal ratings

DG ratings along with other system parameters are given in table 3.1. Figures 3.9 and 3.10 show the output power and frequency of the system for this case. DG inverter 3 shares more power for a transient period of time, and subsequently, the power sharing among all DG inverters become nearly equal as can be seen in fig. 3.9. Fig. 3.10 shows change in frequency at all buses. It can be confirmed that the deviation of frequency for 3rd DG is little more than others in transient period. This is because the disturbance is nearest to this DG.

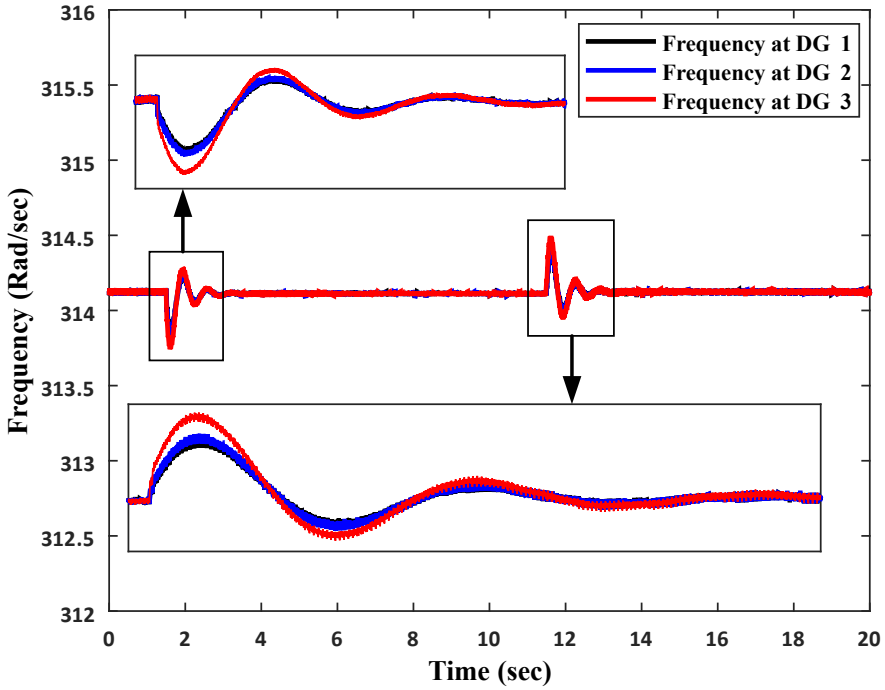

Figure 3.10: Change in output frequency for case 1 with equal ratings of DGs

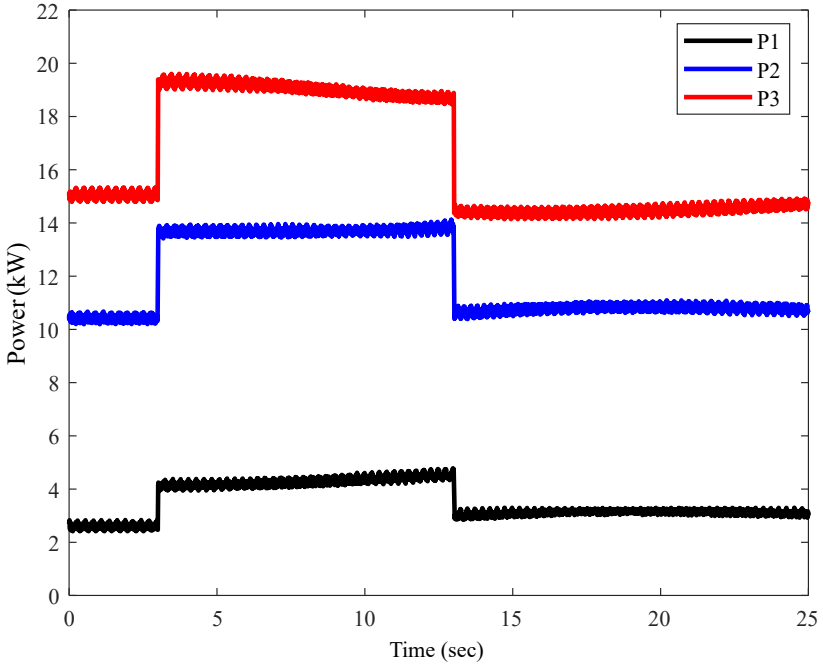

Figure 3.11: Change in output power for case 1 with unequal ratings of DGs

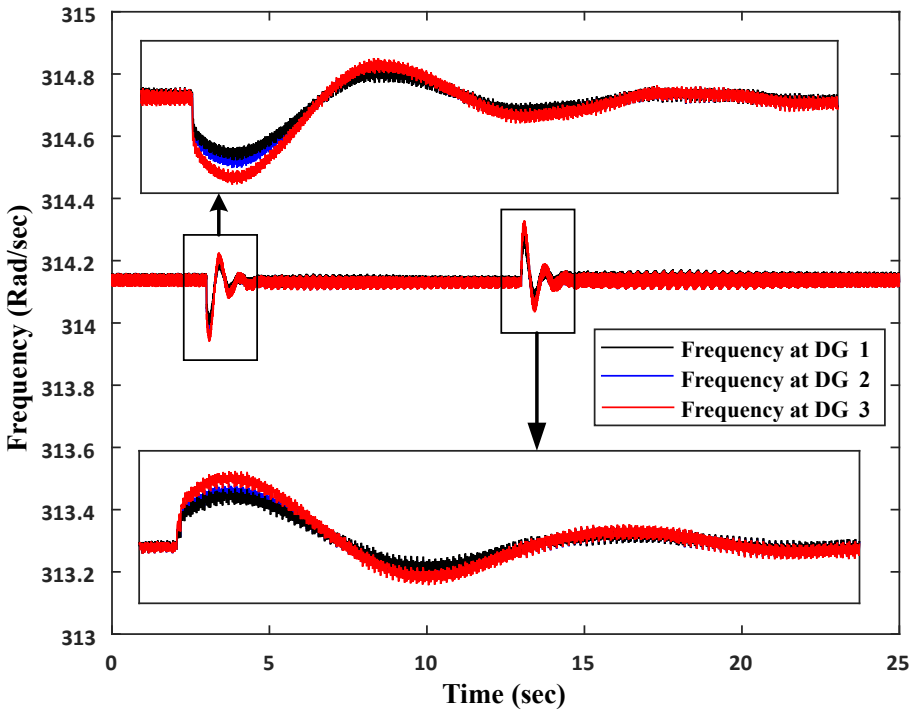

Figure 3.12: Change in output frequency for case 1 with unequal ratings of DGs

b) DGs with unequal ratings

In power system, rating of each DG may not be same. Hence, the study is done for unequal ratings of DGs also. Output power and frequency response is shown in figs. 3.11 and 3.12. From fig. 3.11, it can be observed that the output power of DG is unequal and proportional to the rating of each DG. Variation in the output frequency of DGs is shown in fig. 3.12 and it can be seen that the frequency variation is more at DG 3 since it is nearest to the disturbance. For steady state, the frequency at all buses are equal.

Case 2 : Step load is applied at all buses at the same time.

This is a case of special disturbance, which may occur in microgrid. This case study observes behaviour of the system when there is a simultaneous load change at all the buses. This case discusses the performance of system for additional R load of 3.3 kW connected at all buses in parallel to the existing loads shown in fig. 3.1. Load disturbance is applied at the same time. Load is connected to the system at t = 1.5 sec and removed at t = 11.5 sec. The response of the system is observed for both the cases i.e., for equal as well as unequal ratings of DGs.

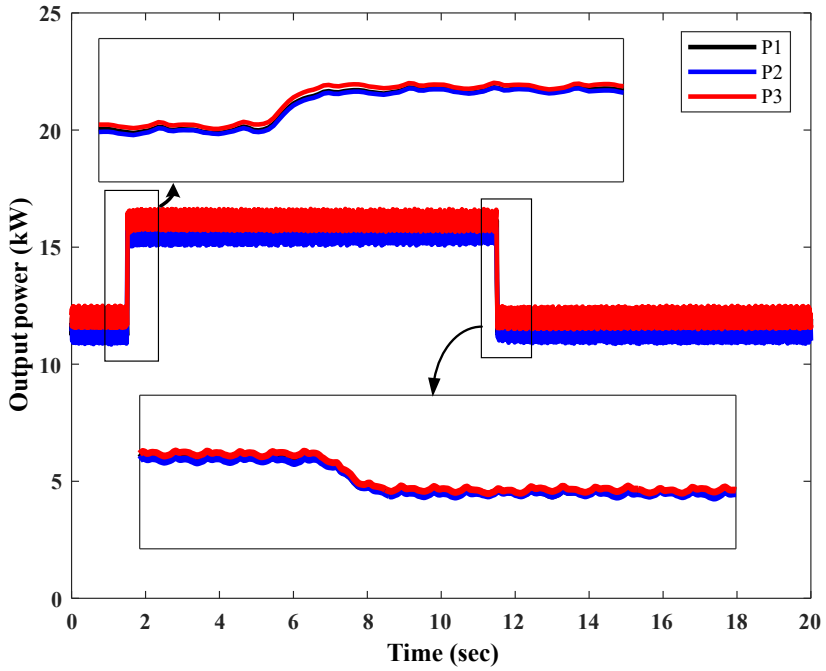

Figure 3.13: Change in output power for case 2 with equal ratings of DGs

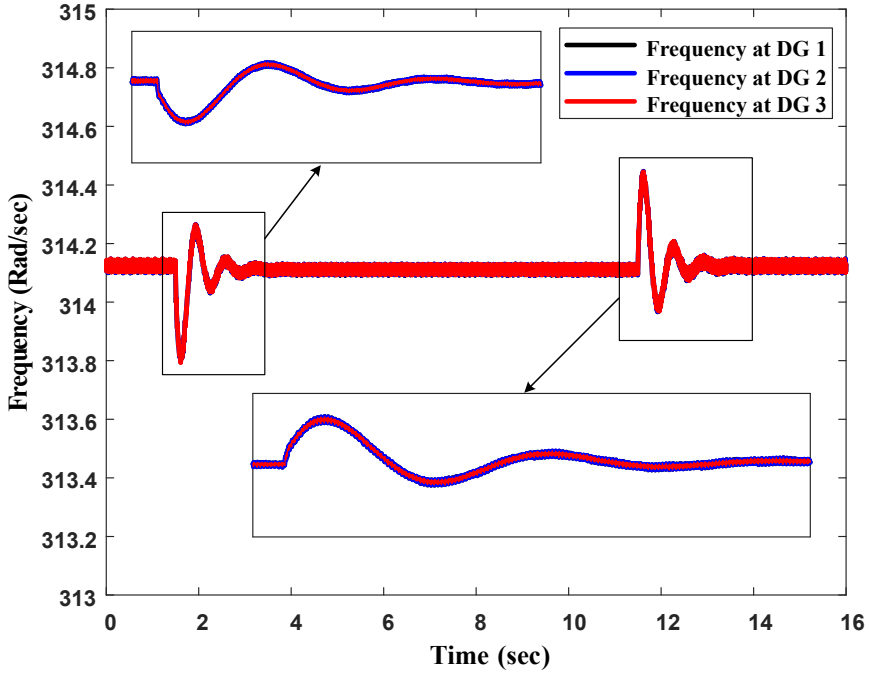

Figure 3.14: Change in output frequency for case 2 with equal ratings of DGs

a) DGs with equal ratings

The output power and frequencies of all DGs are shown in figs. 3.13 and 3.14, respectively. It can be observed from fig. 3.13 that the power sharing is equal in the transient period as well as in steady state. Fig. 3.14 shows that the frequency deviation is equal for all the DGs, since the disturbance is applied at all the buses.

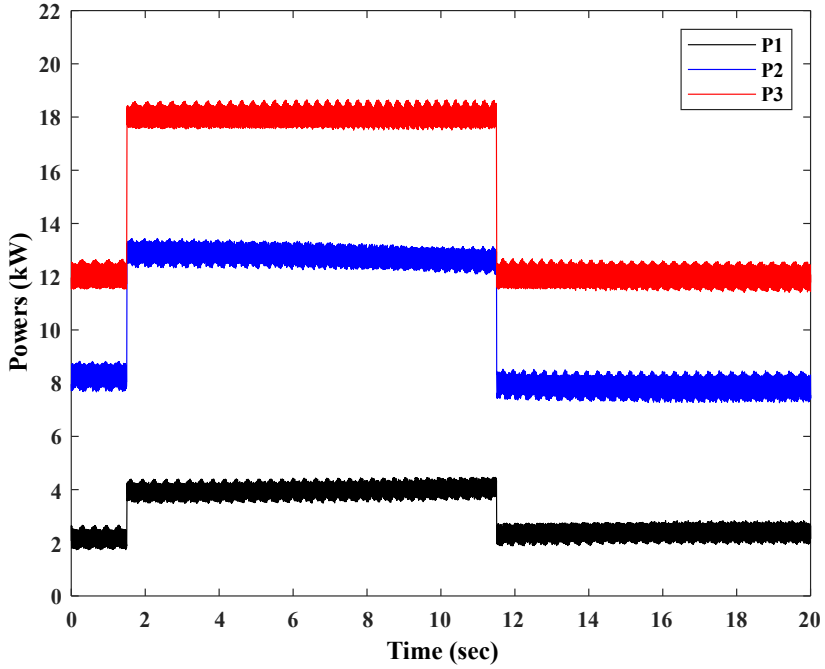

Figure 3.15: Change in output power for case 2 with unequal ratings of DGs

b) DGs with unequal ratings

This case observes the response of the system with unequal DG ratings for simultaneous load disturbance at all buses. The response of the system for this case is shown in figs. 3.15 and 3.16. In fig. 3.15, DGs share unequal powers, which depends on the rating of individual DGs. Fig. 3.16 shows change in the frequency of the DGs for the simultaneous load change at all the buses and it can be observed that the deviation in frequencies at all DGs are equal.

Case 3 : Step load is applied first at bus 3 and then at bus 2.

This case studies the response of the system for the the disturbance consecutively occurring on bus 3 and bus 2. This case focuses not only on R load disturbance but also RL load. First the load disturbance is applied at bus 3 and subsequently on bus 2. R load of 5 kW is connected at bus 3 at t =1.5 sec in parallel to the existing loads and RL load of 5 kVA

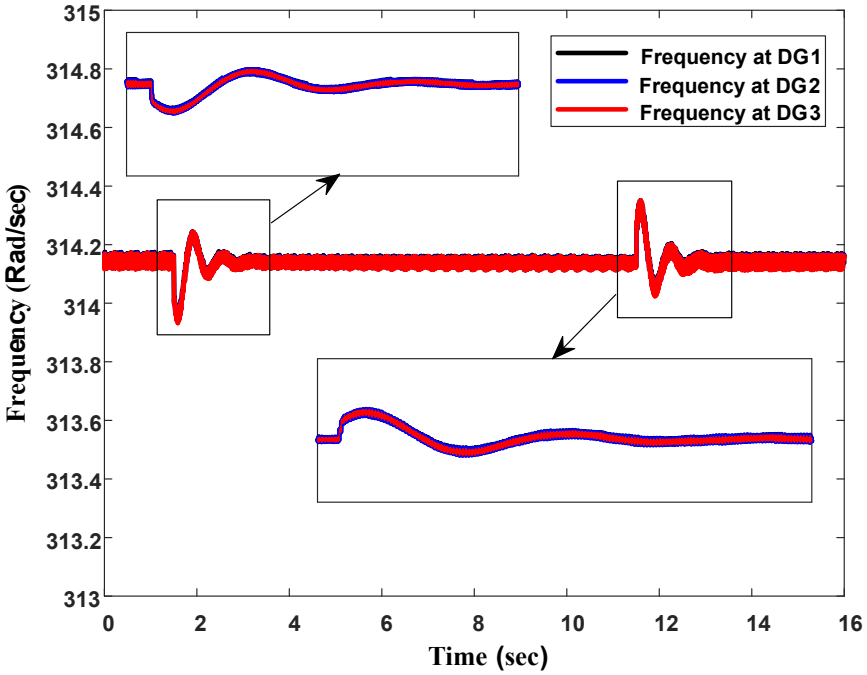

Figure 3.16: Change in output frequency for case 2 with unequal ratings of DGs

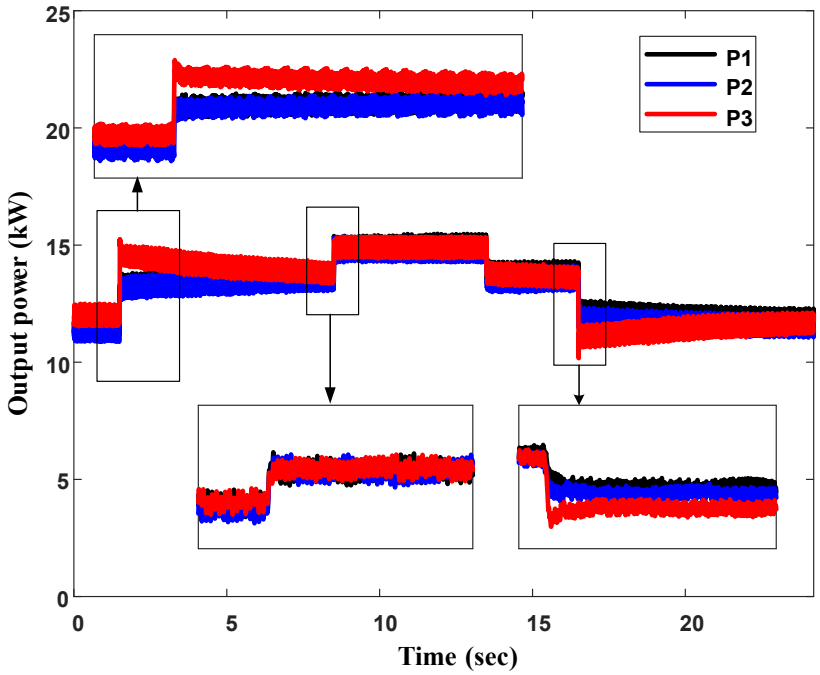

Figure 3.17: Change in output power for case 3 with equal ratings of DGs

is connected to bus 2 at t = 8.5 sec. RL load is disconnected at t = 13.5 sec, and R load is disconnected at t = 16.5 sec. The response of the system is recorded for both equal and unequal ratings of DGs.

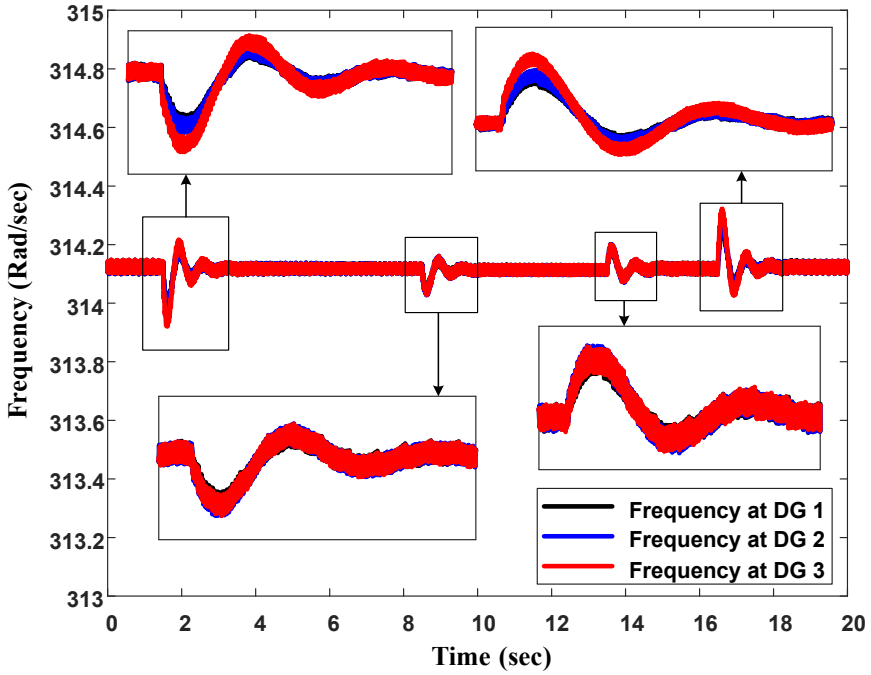

Figure 3.18: Change in output frequency for case 3 with equal ratings of DGs

a) DGs with equal ratings

Figures 3.17 and 3.18 shows output voltage and frequency response of the system, respectively, for equal rating of DGs. It can be seen in fig. 3.17, the output power of DG 3 is more for transient period but only for the first disturbance since it is the nearest DG. But, for the second disturbance, all DGs share power equally in transient period. This is because, bus 2 is at the centre of the system and all DGs contribute in the power sharing during disturbance. Similar variations can be observed in fig. 3.18, where frequency variation for the first disturbance is more and unequal during transient but, there is less effect on frequency for the second disturbance.

a) DGs with unequal ratings

Study of response of the system, for consequent load changes, with unequal DG ratings is done in this case. The response of the system is given in figs. 3.19 and 3.20. The output powers for all DGs are given in fig. 3.19, which again confirms that the output power of each DG is in proportional to their ratings. For the first load disturbance, DG 3 has more variation

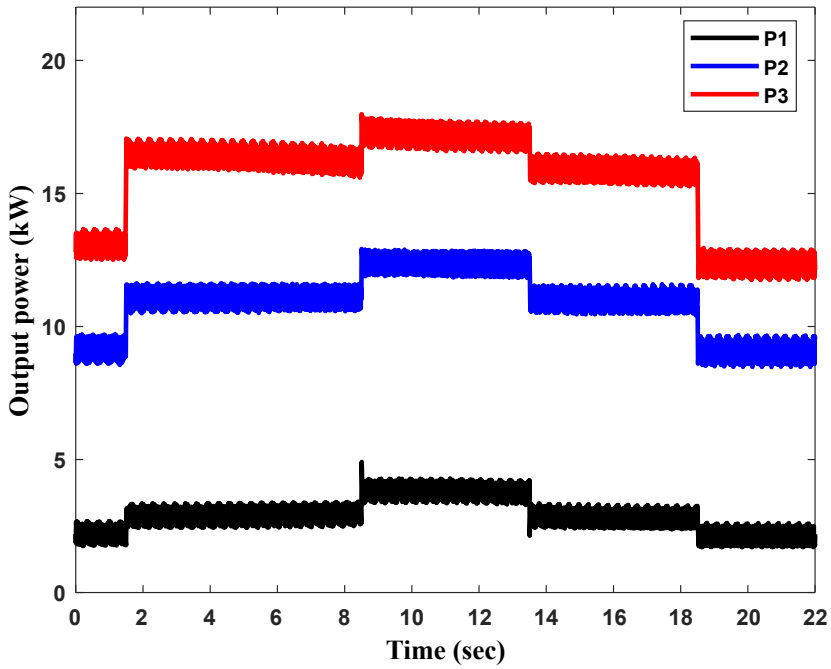

Figure 3.19: Change in output power for case 3 with unequal ratings of DGs

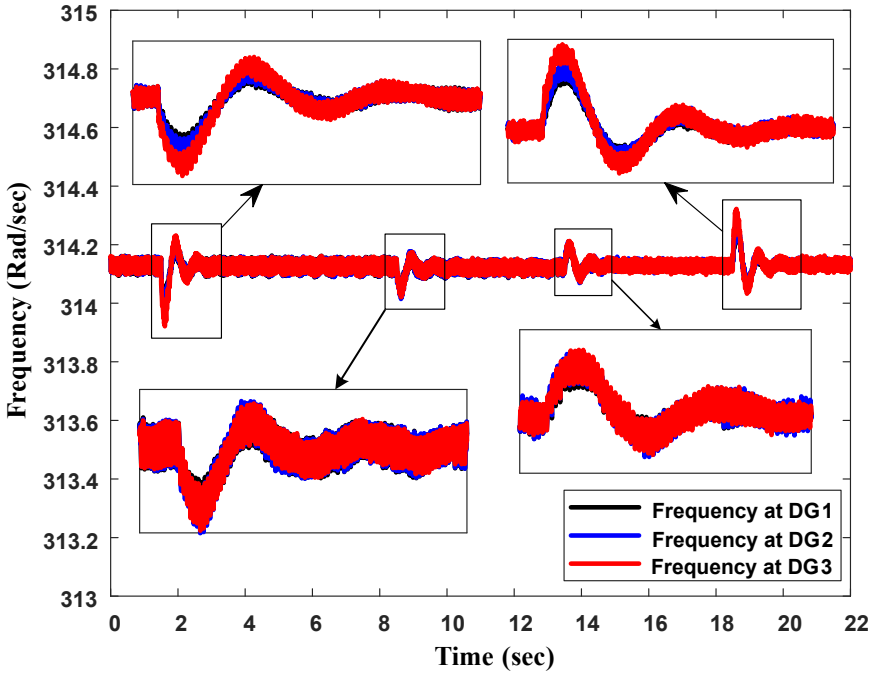

Figure 3.20: Change in output frequency for case 3 with unequal ratings of DGs

in frequency which can be seen in fig. 3.20, and for the second disturbance, the frequency deviation is similar for all DGs.

3.5.4 Comparison with Droop Control

Droop control scheme along with inner voltage and current controller, given in [42], is widely used to control the microgrid, where multiple DGs are operating simultaneously and share common loads. The control scheme given in [42] is simulated in RSCAD within substep environment keeping all the parameters same as given in table 3.1. This subsection compares the performance of the synchronverter control with the droop control scheme on the test system. The comparison has been made for all the three cases considered in subsection 3.5.3, considering both equal as well as unequal rating of DGs.

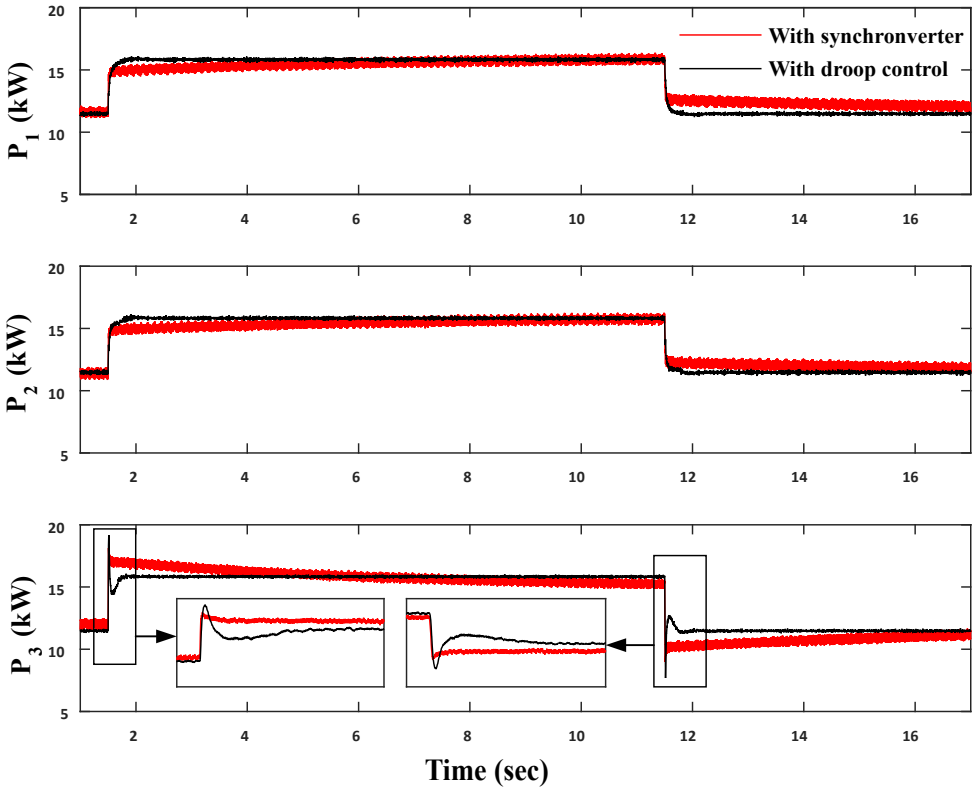

Figure 3.21: Comparison of output power for case 1 with equal ratings of DGs

Case 1 : Step load is applied at bus 3.

In this case, response of the system for both the control techniques is recorded and compared for the disturbance at bus 3. For both the control techniques, the additional R load of

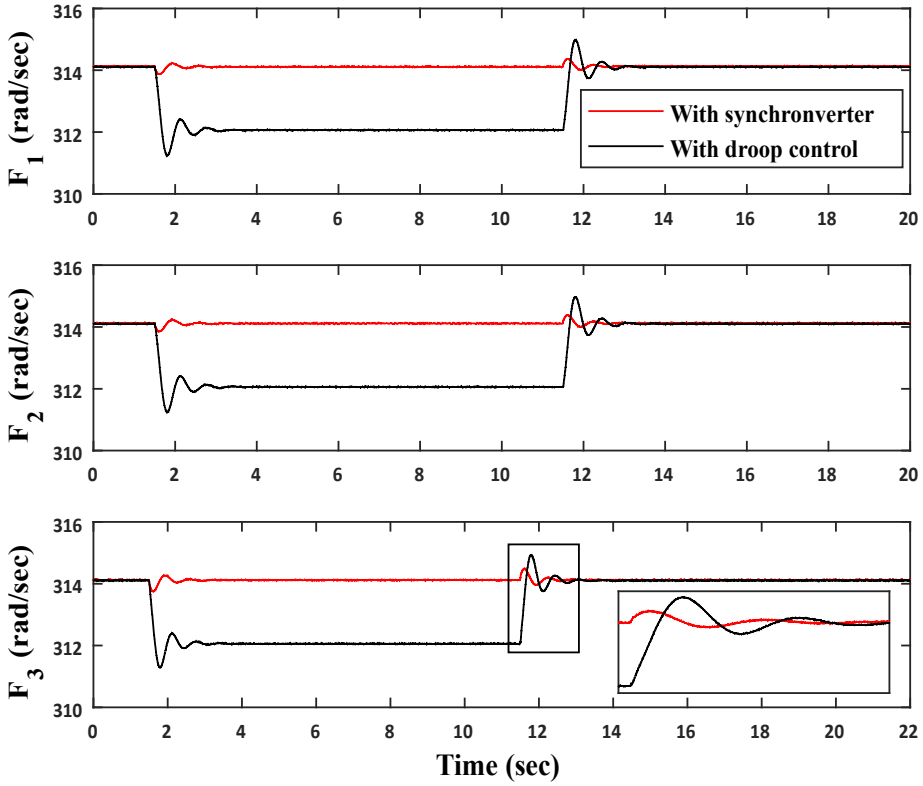

Figure 3.22: Comparison of output frequency for case 1 with equal ratings of DGs

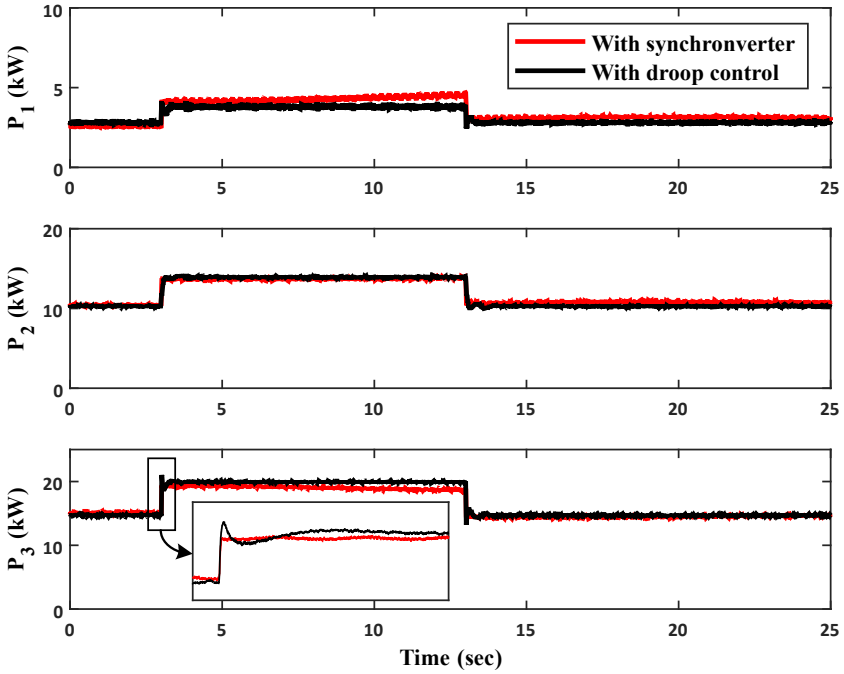

Figure 3.23: Comparison of output power for case 1 with unequal ratings of DGs

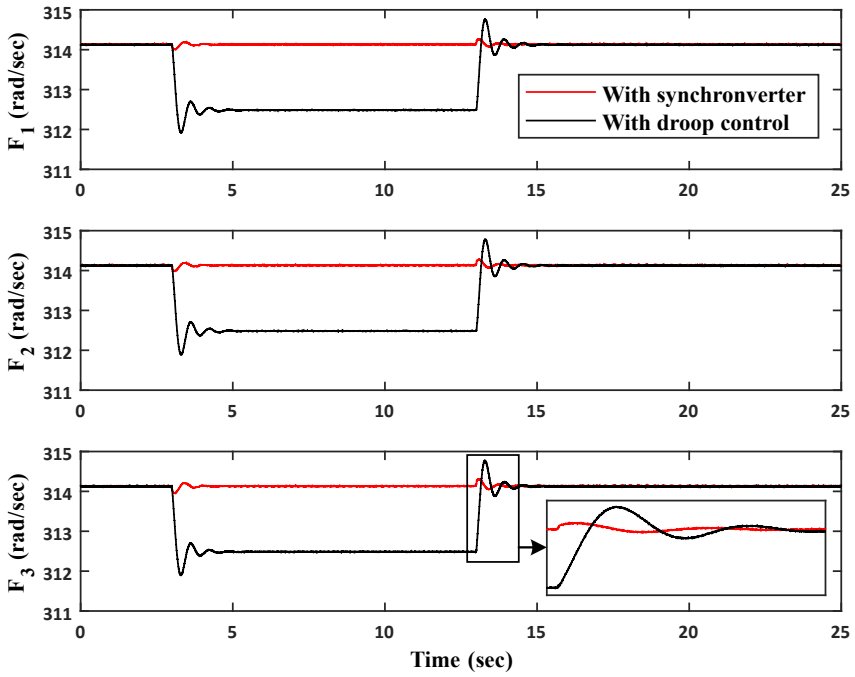

Figure 3.24: Comparison of output frequency for case 1 with unequal ratings of DGs

10 kW is connected to the system at t = 1.5 sec and removed at t = 11.5 sec.

a) DGs with equal ratings

The comparison of output power and frequency response for equal rating of DGs is shown in figs. 3.21 and 3.22, respectively. It can be observed from fig. 3.21 that the power sharing between DGs is similar in both the cases for steady state. For the droop control scheme, overshoot is present at a power output of DG3 in the transient period, but in the case of synchronverter, no such oscillations are visible. The comparison of frequency output is shown in fig. 3.22, which shows that the deviation in frequency in case of the synchronverter is very less than the droop control scheme. Also, it can be seen from fig. 3.22 that the oscillation in frequency is very small with synchronverter.

b) DGs with unequal ratings

This case compares the response of the system for droop control and synchronverter control techniques having DGs with unequal ratings. Figures 3.23 and 3.24 compare output power and frequency for the droop control and synchronverter. For this case also, power sharing among DGs are similar for both the techniques which can be seen in fig. 3.23. It can be observed that small oscillations are present in the power output of DG3 for droop control scheme but absent in case of synchronverter. Fig. 3.24 shows that there is very small change

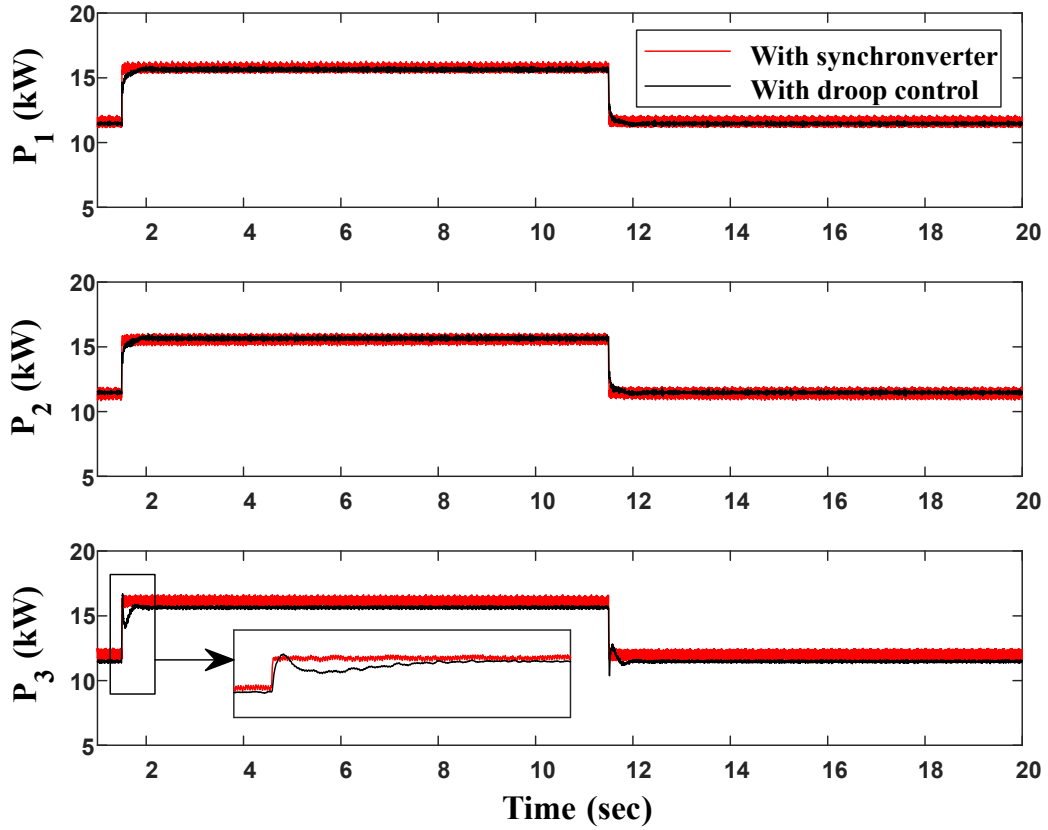

Figure 3.25: Comparison of output power for case 2 with equal ratings of DGs

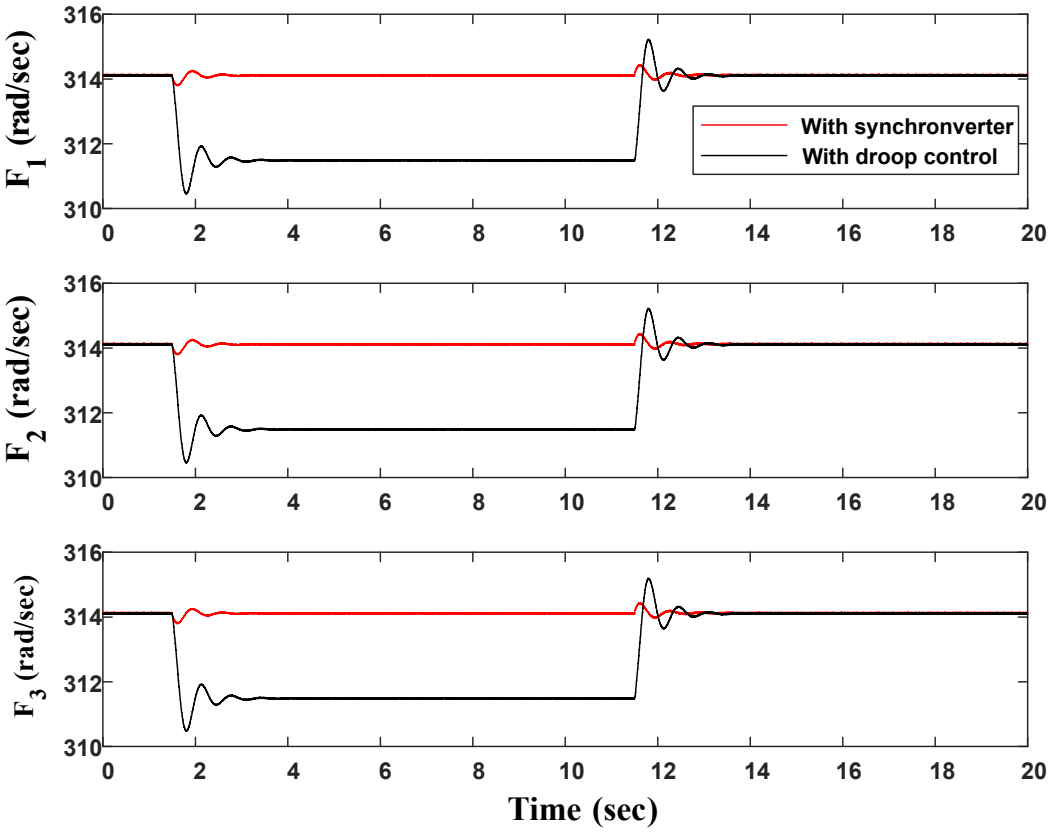

Figure 3.26: Comparison of output frequency for case 2 with equal ratings of DGs

in the output frequency with the synchronverter when compared to the change in frequency with the droop control scheme. Oscillations in output frequency are very less in case of synchronverter than the droop control.

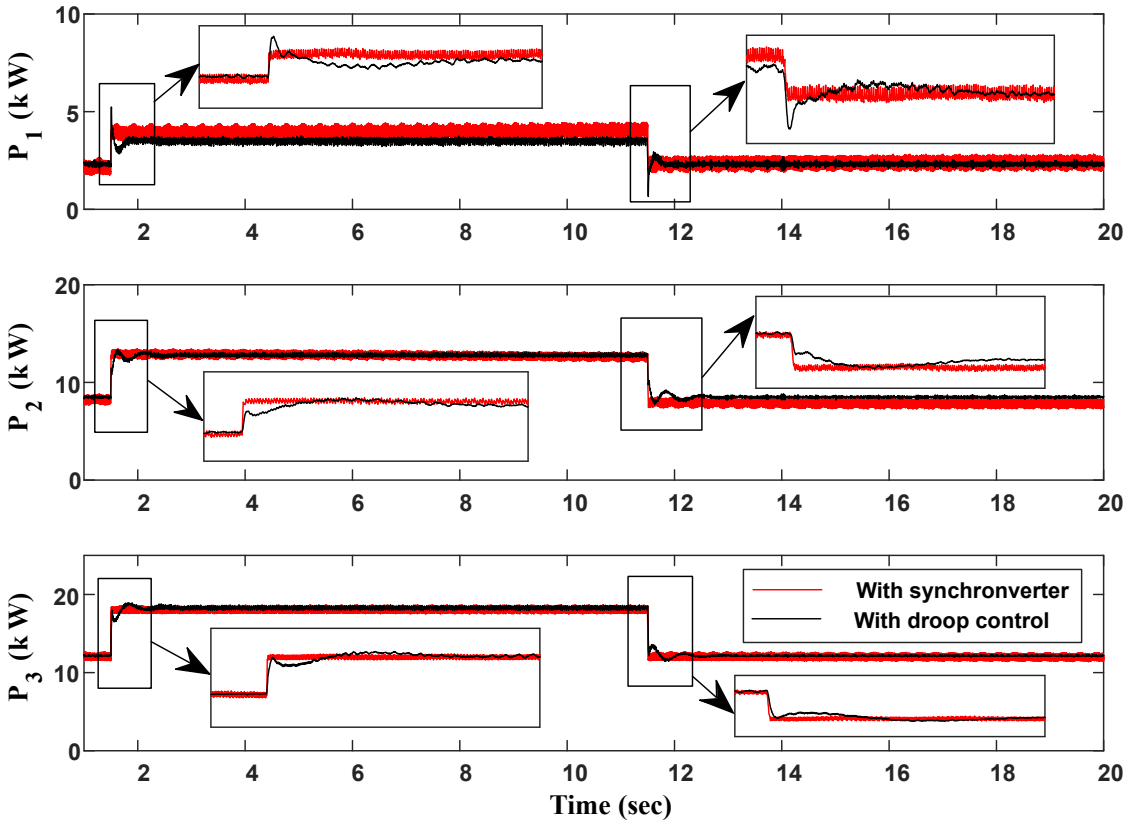

Figure 3.27: Comparison of output power for case 2 with unequal ratings of DGs

Case 2 : Step load is applied at all buses at the same time.

The particular type of disturbance is applied to observe the behavior of the system with synchronverter and droop control scheme. For both the control techniques, the additional R load of 3.3 kW is connected to all the buses in the system. Load is connected to the system at t = 1.5 sec and removed at t = 11.5 sec. The response of the system is compared for both equal and unequal ratings of DGs.

a) DGs with equal ratings

Figures 3.25 and 3.26 show the comparison of output power and frequency, respectively, for the synchronverter and the droop control technique with equal ratings of DGs. Fig. 3.25 shows that for both the techniques, power sharing between DGs are similar. Further, oscillations seen in power output for case 1 are absent in this case. Fig. 3.26 confirms that the

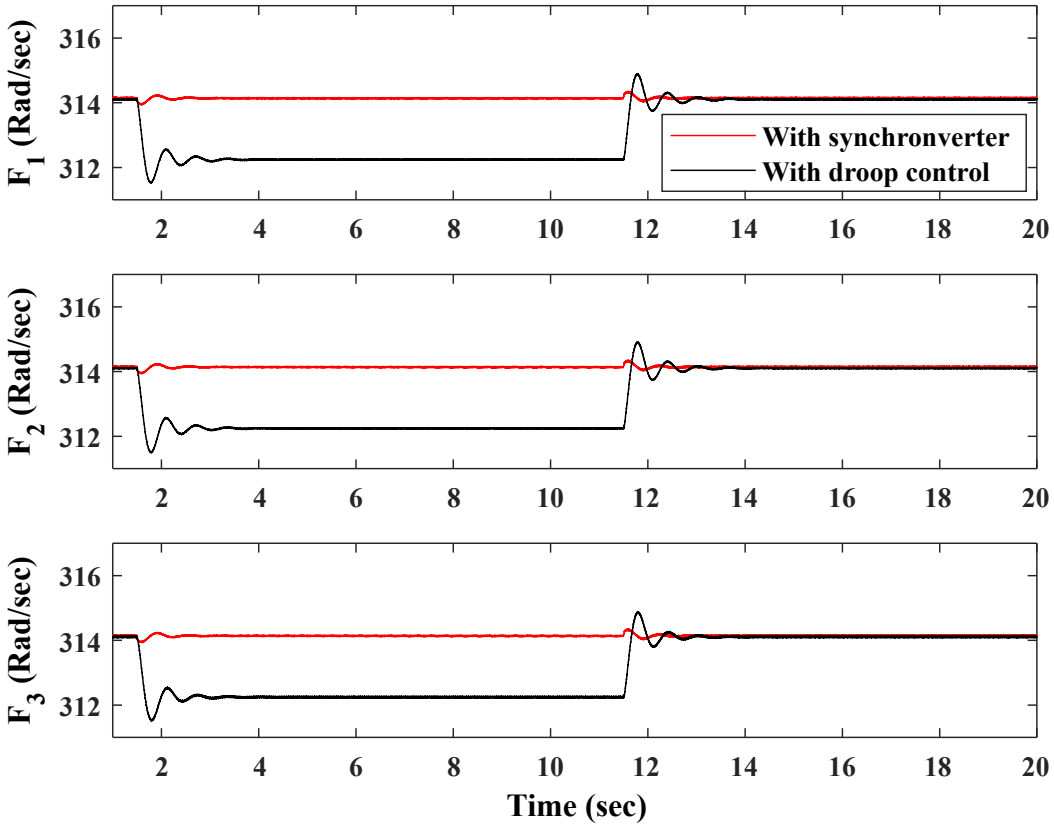

Figure 3.28: Comparison of output frequency for case 2 with unequal ratings of DGs

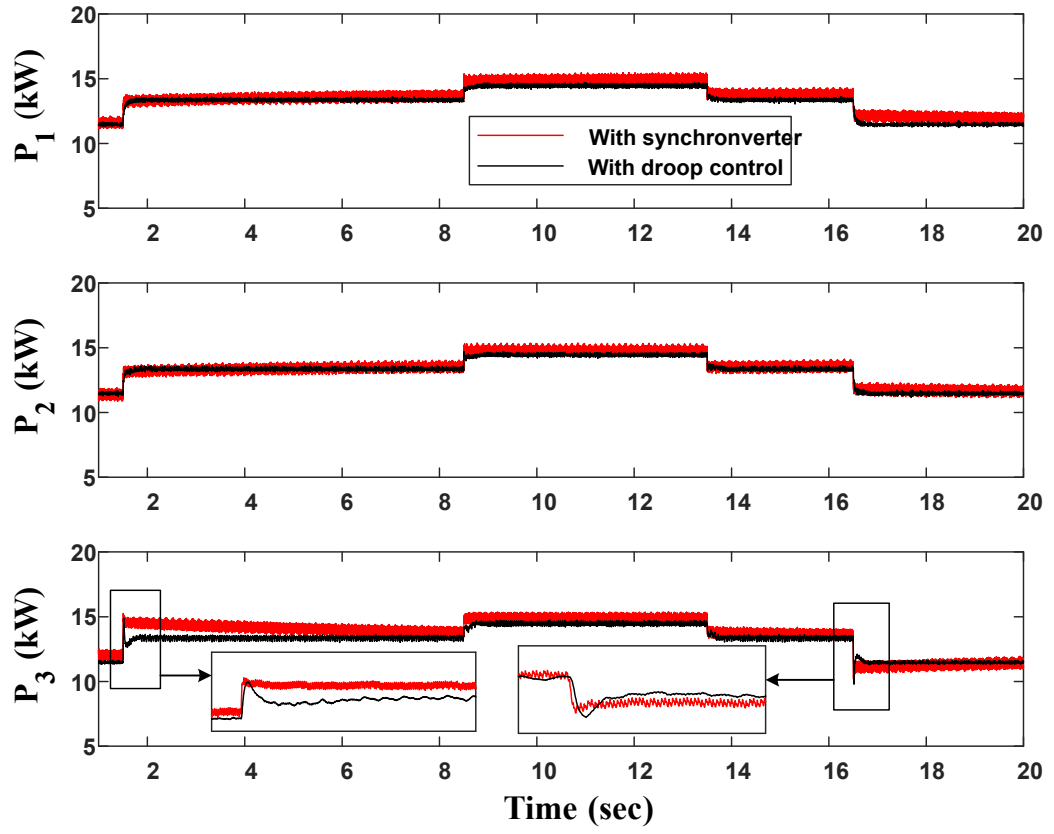

Figure 3.29: Comparison of output power for case 3 with equal ratings of DGs

oscillations and variation in frequency is minor in case of the synchronverter compared to the droop control technique.

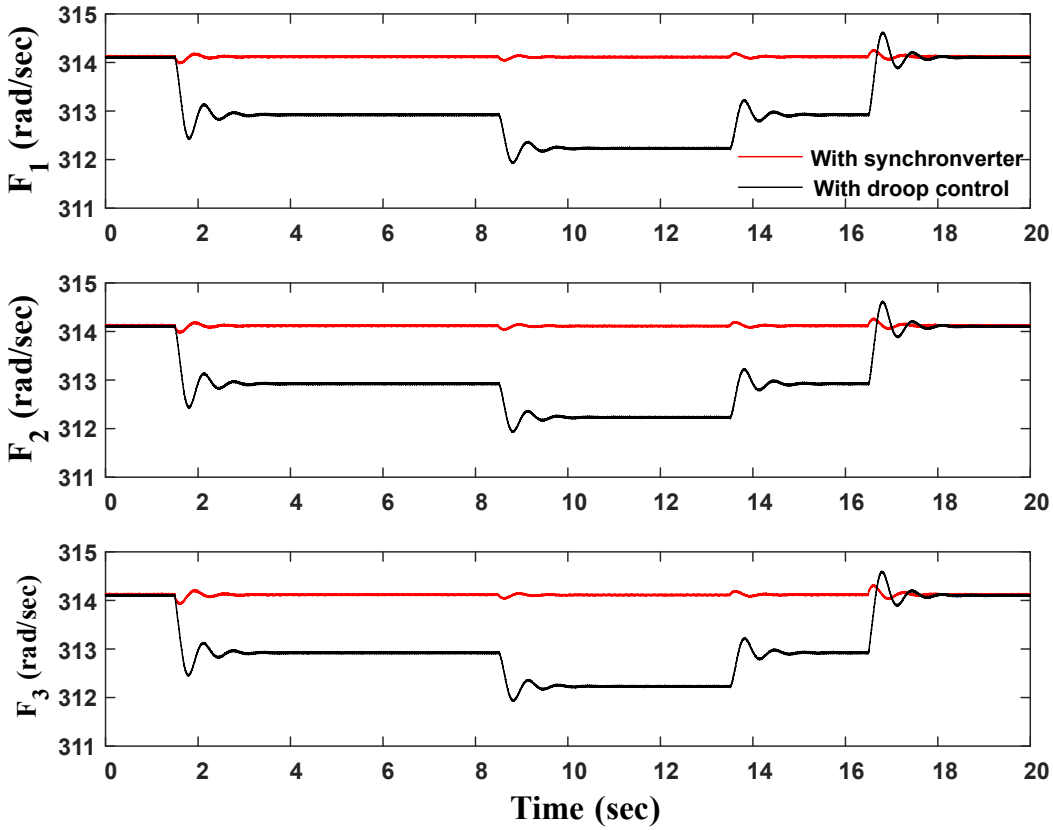

Figure 3.30: Comparison of output frequency for case 3 with equal ratings of DGs

b) DGs with unequal ratings

This case compares the response of the synchronverter and the droop control for this particular disturbance with unequal ratings of the DGs. Fig. 3.27 shows that there are small oscillations in power output during transient period in case of the droop control but they are absent in synchronverter control. Steady state power sharing between DGs are similar in both the control techniques. With the synchronverter, deviation in frequency is very small compared to the droop control scheme as can be seen in fig. 3.28.

Case 3 : Step load is applied first at bus 3 and then at bus 2.

This case presents the study of comparison of the response when a consecutive disturbance is applied on the system. The output of the system is observed by applying the load disturbance first at the third bus and then at the second bus. Additional R load of 5 kW is connected to the system at t = 1.5 sec and 5 kVA RL load is connected to the system at t =

8.5 sec. The response of the system is observed for both equal and unequal ratings of DGs.

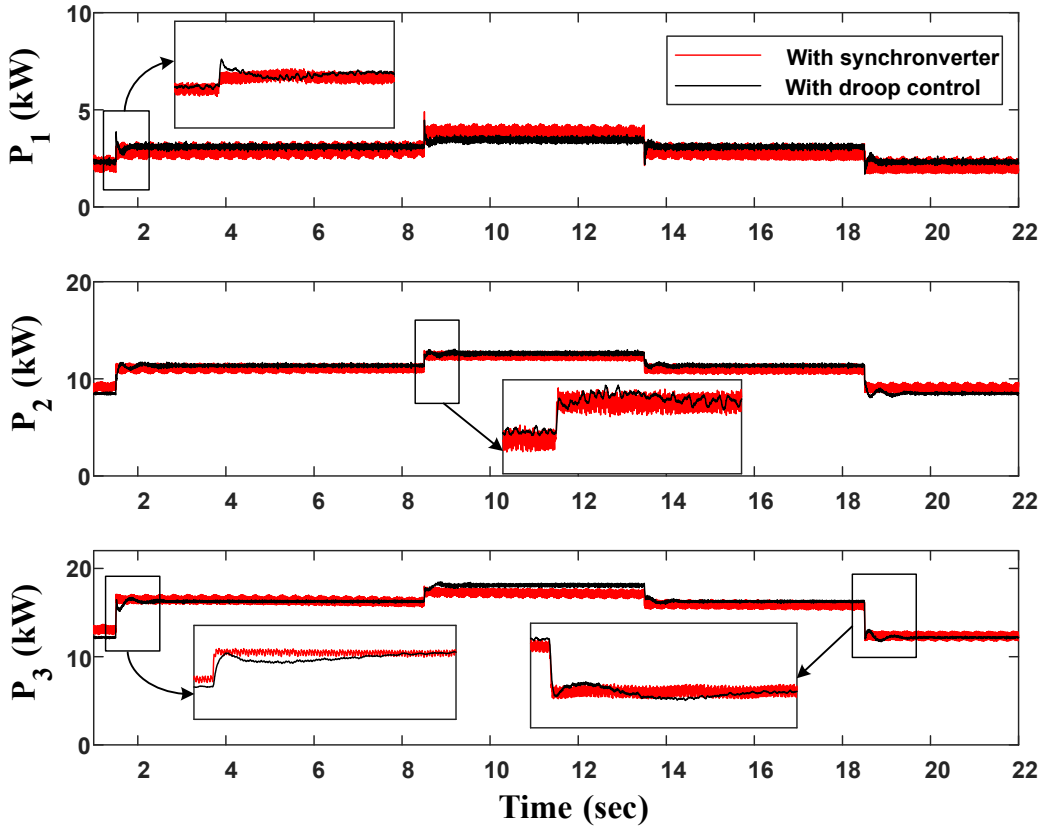

Figure 3.31: Comparison of output power for case 3 with unequal ratings of DGs

a) DGs with equal ratings

Comparison of output power and frequency is given in figs. 3.29 and 3.30, respectively, for the synchronverter and the droop control scheme with equal ratings of DGs. It can be observed from fig. 3.29 that the power sharing between DGs are similar in both the control techniques in steady state. During transient period, there are small oscillations in output power for load disturbance at bus 3 with the droop control but with the synchronverter control, oscillations are absent. Fig. 3.30 shows that the frequency response with synchronverter is better than the droop control technique. Oscillations in frequency is very less in case of the synchronverter compared to those with the droop control scheme.

b) DGs with unequal ratings

Figures 3.31 and 3.32 present the comparison of output power and frequency, respectively, for the synchronverter and the droop control technique. It can be seen from fig. 3.31 that in steady state, both the techniques share power according to the rating of individual

DG. In this case also, oscillations in output power for transient period are absent in case of the synchronverter control. Fig. 3.32 shows the comparison of output frequency for the synchronverter and the droop control scheme. One can observe from fig. 3.32 that the deviation in frequency with the synchronverter is very less in comparison to the deviation in frequency for the droop control technique.

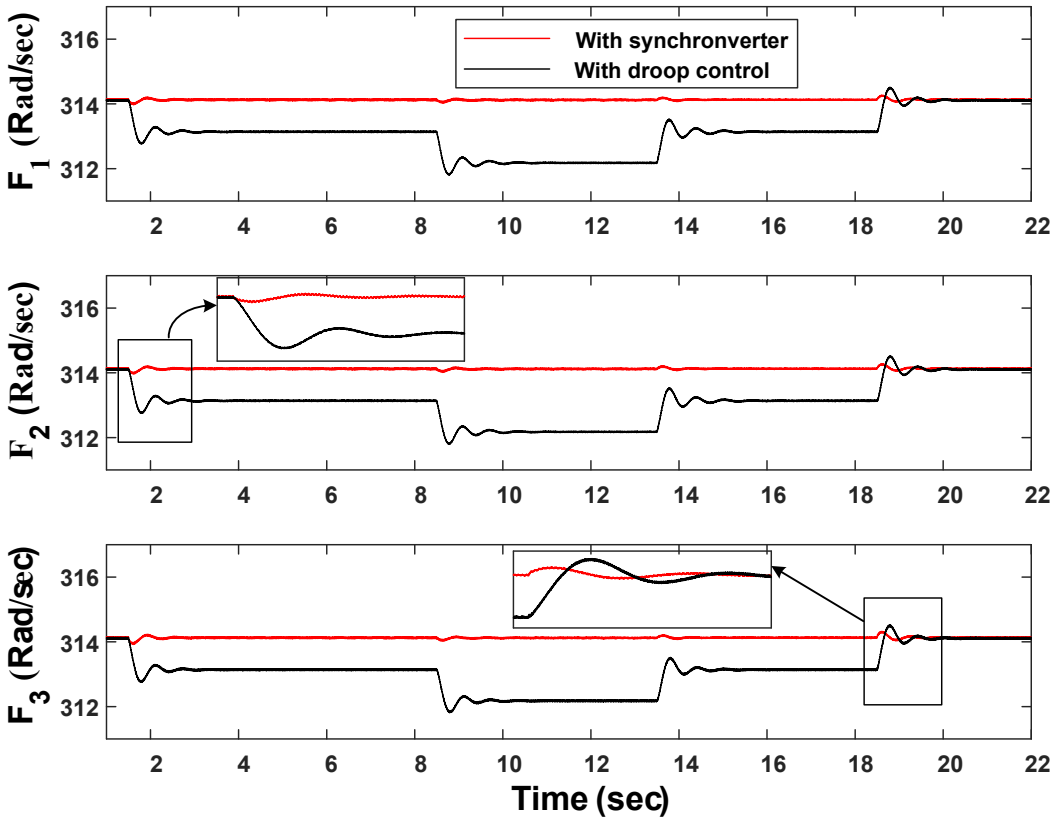

Figure 3.32: Comparison of output frequency for case 3 with unequal ratings of DGs

3.6 Conclusion

This chapter presents the results obtained by performing eigenvalue analysis and simulation in RSCAD. The eigenvalue analysis has been performed by developing the linearized small signal state space model for the test system using the procedure given in chapter 2. Further, the design of a synchronverter is explained for both APL and RPL. The real-time simulation results are presented for various disturbance cases. Finally, the results obtained with the synchronverter control are compared with the droop control technique. Following conclusions can be drawn from the study

- The effect of parameter variation on the dominant modes is very less.
- Synchronverter has similar power sharing capabilities as compared to the droop control.
- On applying the load disturbance, the change in frequency with the synchronverter control is less.

Chapter 4

Conclusions and Future Scope

4.1 Conclusion

The stability of MG is an important concern especially in the island mode of operation. The main focus of this thesis is to analyse stability of ACMG with multiple DGs in an islanded microgrid with synchronverter as a decentralized controller. This is accompanied, by developing a linearized small signal model **in chapter 2** for individual sub modules and then combining all submodules on common reference frame to obtain the complete model of the microgrid. This methodology can be extended to a microgrid with n number of DGs.

In chapter 3, eigenvalue analysis is performed on the test system with synchronverter control strategy. It is found that the dominant modes are less sensitive to the variation in system parameters such as inertia constant (J) and damping factor (D_q). Further, simulation results show that the synchronverter control has similar power sharing capabilities as the droop control, with an added advantage of better frequency regulation. This demonstrates the superiority of the synchronverter control over the droop control for multiple DG inverters.

4.2 Scope for Future Research

The following topics are identified for the future work, related to the research work carried out in this thesis.

- **In chapter 2**, it was assumed that the energy source of DG unit provides a con-

stant DC voltage. But, in the practical DG, it may not be possible for the RESs to provide constant DC source. Hence, the effect of the disturbance on the primary energy source needs to be investigated. Also, there may be additional controller equipped to obtain DC voltage, the dynamics of these controllers should be considered.

• **In chapter 2**, only DGs are considered as sources, however, energy storage system is an integral part of the MG. Hence, the dynamics and control of energy sources are important to consider.

• **In chapter 3**, the test system considers only passive loads. However, in ACMG there may be dynamic loads such as induction machines, and investigation of small signal stability for these loads is necessary.

• Finally, the proposed system can be validated by performing hardware-in-loop (HIL) as well as controller hardware-in-loop (CHIL) using real-time simulators such as RTDS [47].

Appendix A

Appendix

A.1 Generator Module

A.1.1 Power Calculation

$$\mathbf{A_{pi}} = \begin{bmatrix} -\omega_c & 0 \\ 0 & -\omega_c \end{bmatrix} \quad \mathbf{B_{pi}} = 1.5\omega_c \begin{bmatrix} 0 & 0 & I_{odi} & I_{oqi} & V_{odi} & V_{oqi} \\ 0 & 0 & I_{oqi} & -I_{odi} & -V_{oqi} & V_{odi} \end{bmatrix}$$

$$\mathbf{C_{pi}} = \begin{bmatrix} 1 & 0 \\ 0 & 1 \end{bmatrix}$$

A.1.2 Synchronverter

$$\mathbf{A_{Ci}} = \begin{bmatrix} \frac{-D_{pi}}{J_i} & 0 & 0 & \frac{-1}{J_i} & 0 & 0 \\ 0 & 0 & 0 & 0 & \frac{-1}{K_i} & 0 \\ 0 & \frac{1}{\tau} & \frac{-1}{\tau} & 0 & 0 & 0 \\ 0 & 0 & \frac{1.5I_{ldi}}{\tau} & \frac{-1}{\tau} & 0 & 0 \\ \frac{-1.5\psi_{ffi}I_{lqi}}{\tau} & 0 & \frac{-1.5\omega_o I_{lqi}}{\tau} & 0 & \frac{-1}{\tau} & 0 \\ 1 & 0 & 0 & 0 & 0 & 0 \end{bmatrix} \quad \mathbf{B_{C2i}} = \begin{bmatrix} \frac{-1}{J_i\ \omega_o} & 0 \\ 0 & \frac{-1}{K_i} \\ 0 & 0 \\ 0 & 0 \\ 0 & 0 \\ 0 & 0 \end{bmatrix}$$

$$\mathbf{B_{C1i}} = \begin{bmatrix} 0 & 0 & 0 & 0 & 0 & 0 \\ \frac{-D_{qi}R_d}{K_i} & 0 & \frac{-D_{qi}}{K_i} & 0 & \frac{D_{qi}R_d}{K_i} & 0 \\ 0 & 0 & 0 & 0 & 0 & 0 \\ \frac{1.5\psi_{ffi}}{\tau} & 0 & 0 & 0 & 0 & 0 \\ 0 & \frac{-1.5\omega_o\psi_{ffi}}{\tau} & 0 & 0 & 0 & 0 \\ 0 & 0 & 0 & 0 & 0 & 0 \end{bmatrix} \quad \mathbf{BP_{comi}} = \begin{bmatrix} [0]_{1\times 5} & -1 \end{bmatrix}^T$$

$$\mathbf{C_{cwi}} = \begin{bmatrix} 1 & 0 & 0 & 0 & 0 & 0 \end{bmatrix} \quad \mathbf{C_{cvi}} = \begin{bmatrix} \psi_{ffi} & 0 & \omega_o & 0 & 0 & 0 \\ 0 & 0 & 0 & 0 & 0 & 1 \end{bmatrix}$$

A.1.3 LC Filter and Coupling Inductor

$$\mathbf{A_{LCLi}} = \begin{bmatrix} \frac{-r_f}{L_f} & \omega_o & \frac{-1}{L_f} & 0 & 0 & 0 \\ -\omega_o & \frac{-r_f}{L_f} & 0 & \frac{-1}{L_f} & 0 & 0 \\ \frac{1}{C_f} & 0 & 0 & \omega_o & \frac{-1}{C_f} & 0 \\ 0 & \frac{1}{C_f} & -\omega_o & 0 & 0 & \frac{-1}{C_f} \\ 0 & 0 & \frac{1}{L_c} & 0 & \frac{-r_c}{L_c} & \omega_o \\ 0 & 0 & 0 & \frac{1}{L_c} & -\omega_o & \frac{-r_c}{L_c} \end{bmatrix} \quad \mathbf{B_{LCL1i}} = \begin{bmatrix} \frac{1}{L_f} & 0 \\ 0 & \frac{1}{L_f} \\ 0 & 0 \\ 0 & 0 \\ 0 & 0 \\ 0 & 0 \end{bmatrix}$$

$$\mathbf{B_{LCL2i}} = \begin{bmatrix} 0 & 0 \\ 0 & 0 \\ 0 & 0 \\ 0 & 0 \\ \frac{-1}{L_c} & 0 \\ 0 & \frac{-1}{L_c} \end{bmatrix} \quad \mathbf{B_{LCL3i}} = \begin{bmatrix} I_{lqi} \\ -I_{ldi} \\ V_{oqi} \\ -V_{odi} \\ I_{oqi} \\ -I_{odi} \end{bmatrix} \quad \mathbf{C_{LCLi}} = [I]_{6\times 6}$$

A.1.4 Complete Model for Individual DG

$$\mathbf{A_{geni}} = \begin{bmatrix} \mathbf{A_{pi}} & [0]_{\mathbf{2*6}} & \mathbf{B_{Pi}} \\ \mathbf{B_{C2i}} & \mathbf{A_{Ci}} & \mathbf{B_{C1i}} \\ [0]_{\mathbf{6\times 2}} & \mathbf{B_{LCL1i}T_{mi}C_{CVi}} + \begin{bmatrix} \mathbf{B_{LCL3i}} & [0]_{\mathbf{6*5}} \end{bmatrix} + \mathbf{B_{LCL2i}} \begin{bmatrix} [0]_{\mathbf{2*5}} & \mathbf{TV_i} \end{bmatrix} & \mathbf{A_{LCLi}} \end{bmatrix}$$

$$\mathbf{B_{geni}} = \begin{bmatrix} [0]_{8\times 2} \\ B_{LCL2i} TS_i^{-1} \end{bmatrix}_{14\times 2} \qquad \mathbf{BP_{wcomi}} = -1$$

$$\mathbf{BW_{commi}} = \begin{bmatrix} [0]_{1\times 7} & \mathbf{BP_{wcomi}} & [0]_{1\times 6} \end{bmatrix}^T$$

$$\mathbf{C_{genci}} = \begin{bmatrix} [0]_{2\times 7} & \mathbf{TC_i} & [0]_{2\times 4} & \mathbf{TS_i} \end{bmatrix} \quad \mathbf{C_{genwi}} = \begin{cases} \begin{bmatrix} [0]_{1\times 2} & \mathbf{Ccwi} & [0]_{1\times 6} \end{bmatrix}_{1\times 13} & \text{if i = 1} \\ \begin{bmatrix} 0 & 0 & \cdots & 0 \end{bmatrix}_{1\times 13} & \text{if i} \neq 1 \end{cases}$$

A.1.5 Complete Model for generator Sub-module

$$\mathbf{A_{GEN}} = \begin{bmatrix} \mathbf{A_{gen1}} + \mathbf{BW_{comm1}} \mathbf{C_{genw1}} & 0 & \cdots & 0 \\ \mathbf{BW_{comm2}} \mathbf{C_{genw1}} & \mathbf{A_{gen2}} & \cdots & 0 \\ \cdots & \cdots & \cdots & \cdots \\ \mathbf{BW_{comm_m}} \mathbf{C_{genw1}} & 0 & \cdots & \mathbf{A_{gen_m}} \end{bmatrix}$$

$$\mathbf{B_{GEN}} = \begin{bmatrix} \mathbf{B_{gen1}} & 0 & \cdots & 0 \\ 0 & \mathbf{B_{gen2}} & \cdots & 0 \\ \cdots & \cdots & \cdots & \cdots \\ 0 & 0 & \cdots & \mathbf{B_{gen_m}} \end{bmatrix} \quad \mathbf{C_{GENc}} = \begin{bmatrix} \mathbf{C_{genc1}} & 0 & \cdots & 0 \\ 0 & \mathbf{C_{genc2}} & \cdots & 0 \\ \cdots & \cdots & \cdots & \cdots \\ 0 & 0 & \cdots & \mathbf{C_{genc_m}} \end{bmatrix}$$

$$\mathbf{C_{GENw}} = \begin{bmatrix} \mathbf{C_{genw1}} & \mathbf{C_{genw2}} & \cdots & \mathbf{C_{genw_m}} \end{bmatrix}$$

A.2 Network Module

$$\mathbf{A_{NETi}} = \begin{bmatrix} \frac{-R_{linei}}{L_{linei}} & \omega_o \\ -\omega_o & \frac{-R_{linei}}{L_{linei}} \end{bmatrix} \quad \mathbf{B_{2NETi}} = \begin{bmatrix} I_{lineQi} \\ -I_{lineDi} \end{bmatrix} \quad \mathbf{C_{NETi}} = \begin{bmatrix} 1 & 0 \\ 0 & 1 \end{bmatrix}$$

$$\mathbf{B_{1NETi}} = \begin{bmatrix} \cdots & \frac{1}{L_{linei}} & 0 & \cdots & \frac{-1}{L_{linei}} & 0 & \cdots \\ \cdots & 0 & \frac{1}{L_{linei}} & \cdots & 0 & \frac{-1}{L_{linei}} & \cdots \end{bmatrix}$$

$$\mathbf{A_{NET}} = \begin{bmatrix} \mathbf{A_{NET1}} & 0 & \cdots & 0 \\ 0 & \mathbf{A_{NET2}} & \cdots & 0 \\ \cdots & \cdots & \cdots & \cdots \\ 0 & 0 & \cdots & \mathbf{A_{NETn}} \end{bmatrix} \quad \mathbf{B_{1NET}} = \begin{bmatrix} \mathbf{B_{1NET1}} \\ \mathbf{B_{1NET2}} \\ \cdots \\ \cdots \\ \mathbf{B_{1NETn}} \end{bmatrix}$$

$$\mathbf{B_{2NET}} = \begin{bmatrix} \mathbf{B_{1NET1}} \\ \mathbf{B_{2NET2}} \\ \cdots \\ \cdots \\ \mathbf{B_{2NETn}} \end{bmatrix} \quad \mathbf{C_{NET}} = \begin{bmatrix} \mathbf{C_{NET1}} & 0 & \cdots & 0 \\ 0 & \mathbf{C_{NET2}} & \cdots & 0 \\ \cdots & \cdots & \cdots & \cdots \\ 0 & 0 & \cdots & \mathbf{C_{NETn}} \end{bmatrix}$$

A.3 Load Module

$$\mathbf{A_{Loadi}} = \begin{bmatrix} \frac{-R_{loadi}}{L_{loadi}} & \omega_o \\ -\omega_o & \frac{-R_{loadi}}{L_{loadi}} \end{bmatrix} \quad \mathbf{B_{Loadi}} = \begin{bmatrix} \cdots & \frac{1}{L_{linei}} & 0 & \cdots \\ \cdots & 0 & \frac{1}{L_{linei}} & \cdots \end{bmatrix}$$

$$\mathbf{B_{2Loadi}} = \begin{bmatrix} I_{loadQi} \\ -I_{loadDi} \end{bmatrix} \quad \mathbf{C_{Loadi}} = [I]_{2\times 2}$$

$$\mathbf{A_{Load}} = \begin{bmatrix} \mathbf{A_{Load1}} & 0 & \cdots & 0 \\ 0 & \mathbf{A_{Load2}} & \cdots & 0 \\ \cdots & \cdots & \cdots & \cdots \\ 0 & 0 & \cdots & \mathbf{A_{Load_l}} \end{bmatrix} \quad \mathbf{B_{1Load}} = \begin{bmatrix} \mathbf{B_{1Load1}} \\ \mathbf{B_{1Load2}} \\ \cdots \\ \cdots \\ \mathbf{B_{1Load_l}} \end{bmatrix}$$

$$\mathbf{B_{2Load}} = \begin{bmatrix} \mathbf{B_{1Load1}} \\ \mathbf{B_{2Load2}} \\ \cdots \\ \cdots \\ \mathbf{B_{2Load_l}} \end{bmatrix} \quad \mathbf{C_{Load}} = \begin{bmatrix} \mathbf{C_{Load1}} & 0 & \cdots & 0 \\ 0 & \mathbf{C_{Load2}} & \cdots & 0 \\ \cdots & \cdots & \cdots & \cdots \\ 0 & 0 & \cdots & \mathbf{C_{Load_l}} \end{bmatrix}$$

A.4 Complete Model of Microgrid

$$\mathbf{A_{MG}} = \begin{bmatrix} A_{GEN} + & & \\ B_{GEN}R_N M_{GEN} C_{GENC} & B_{GEN}R_N M_{NET} C_{NET} & B_{GEN}R_N M_{Load} C_{Load} \\ + BW_{COMM} C_{GENW} & & \\ B_{1NET}R_N M_{GEN} C_{GENC} & A_{NET} + & \\ + B_{2NET} C_{GENW} & B_{1NET}R_N M_{NET} C_{NET} & B_{1NET}R_N M_{Load} C_{Load} \\ B_{1Load}R_N M_{GEN} C_{GENC} & & A_{Load} + \\ + B_{2Load} C_{GENW} & B_{1Load}R_N M_{NET} C_{NET} & B_{1Load}R_N M_{Load} C_{Load} \end{bmatrix}$$

$$\mathbf{B_{MG}} = \begin{bmatrix} B_{GEN}R_N M_{DIST} & 0 & 0 \\ 0 & B_{1NET}R_N M_{DIST} & 0 \\ 0 & 0 & B_{GEN}R_N M_{DIST} \end{bmatrix}$$

References

[1] W. Elkhattam, "Distributed generation technologies, definitions and benefits," *Electric Power Systems Research*, vol. 71, pp. 119–128, 10 2004.

[2] R. Lasseter, A. Akhil, C. Marnay, J. Stephens, J. Dagle, R. Guttromsom, A. S. Meliopoulous, R. Yinger, and J. Eto, "Integration of distributed energy resources. the certs microgrid concept."

[3] R. H. Lasseter, "Microgrids," in *Proc. 2002 IEEE Power Eng. Soc. Winter Meeting*, p. 305–308.

[4] B. Zhao, X. Zhang, and J. Chen, "Integrated microgrid laboratory system," *Power Systems, IEEE Transactions on*, vol. 27, pp. 2175–2185, 11 2012.

[5] G. Pepermans, J. Driesen, D. Haeseldonckx, R. Belmans, and W. D'haeseleer, "Distributed generation: definition, benefits and issues," *Energy Policy*, vol. 33, no. 6, pp. 787–798, 2005.

[6] K. B. H. Zareipour and C. Canizares, "Distributed generation: current status and challenges," in *Proceedings of the 36th Annual North American Power Symposium (NAPS)*, 2004.

[7] "Standard for interconnecting distributed resources with electric power systems," *IEEE Std 1547-2003*, pp. 1–28, 2003.

[8] M. Mahmoud, S. Azher Hussain, and M. Abido, "Modeling and control of microgrid: An overview," *Journal of the Franklin Institute*, vol. 351, no. 5, pp. 2822–2859, 2014.

[9] J. Dyer, "Consortium for electric reliability technology solutions (certs)," Mar 2003.

[10] S. Parhizi, H. Lotfi, A. Khodaei, and S. Bahramirad, "State of the art in research on microgrids: A review," *IEEE Access*, vol. 3, pp. 890–925, 2015.

[11] S. P. Chowdhury and P. Crossley, "Microgrids and active distribution networks," *London, U.K.: Institution of Engineering and Technology*, 2009.

[12] A. Trivedi and M. Singh, "Repetitive controller for vsis in droop-based ac-microgrid," *IEEE Transactions on Power Electronics*, vol. 32, no. 8, pp. 6595–6604, 2017.

[13] I.-Y. Chung, W. Liu, D. A. Cartes, E. G. Collins, and S.-I. Moon, "Control methods of inverter-interfaced distributed generators in a microgrid system," *IEEE Transactions on Industry Applications*, vol. 46, no. 3, pp. 1078–1088, 2010.

[14] N. Eghtedarpour and E. Farjah, "Control strategy for distributed integration of photovoltaic and energy storage systems in dc micro-grids," *Renewable Energy*, vol. 45, pp. 96–110, 2012.

[15] N. N. Eghtedarpour and E. Farjah, "Distributed charge/discharge control of energy storages in a renewable-energy-based dc micro-grid," *IET Renewable Power Generation*, vol. 8, 01 2013.

[16] K. Sun, X. Wang, Y. W. Li, F. Nejabatkhah, Y. Mei, and X. Lu, "Parallel operation of bidirectional interfacing converters in a hybrid ac/dc microgrid under unbalanced grid voltage conditions," *IEEE Transactions on Power Electronics*, vol. 32, no. 3, pp. 1872–1884, 2017.

[17] F. Nejabatkhah and Y. W. Li, "Overview of power management strategies of hybrid ac/dc microgrid," *IEEE Transactions on Power Electronics*, vol. 30, no. 12, pp. 7072–7089, 2015.

[18] J. Rocabert, A. Luna, F. Blaabjerg, and P. Rodríguez, "Control of power converters in ac microgrids," *IEEE Transactions on Power Electronics*, vol. 27, no. 11, pp. 4734–4749, 2012.

[19] K. De Brabandere, B. Bolsens, J. Van den Keybus, A. Woyte, J. Driesen, and R. Belmans, "A voltage and frequency droop control method for parallel inverters," *IEEE Transactions on Power Electronics*, vol. 22, no. 4, pp. 1107–1115, 2007.

[20] P. Kundur, *Power system stability and control*. New York: McGrawHill, 1994.

[21] P. Kundur, J. Paserba, V. Ajjarapu, G. Andersson, A. Bose, C. Canizares, N. Hatziargyriou, D. Hill, A. Stankovic, C. Taylor, T. Van Cutsem, and V. Vittal, "Definition and classification of power system stability ieee/cigre joint task force on stability terms and definitions," *IEEE Transactions on Power Systems*, vol. 19, no. 3, pp. 1387–1401, 2004.

[22] F. Katiraei and M. Iravani, "Power management strategies for a microgrid with multiple distributed generation units," *IEEE Transactions on Power Systems*, vol. 21, no. 4, pp. 1821–1831, 2006.

[23] M. Hamzeh, S. Emamian, H. Karimi, and J. Mahseredjian, "Robust control of an islanded microgrid under unbalanced and nonlinear load conditions," *IEEE Journal of Emerging and Selected Topics in Power Electronics*, vol. 4, no. 2, pp. 512–520, 2016.

[24] R. Bakhshi-Jafarabadi, J. Sadeh, J. d. J. Chavez, and M. Popov, "Two-level islanding detection method for grid-connected photovoltaic system-based microgrid with small non-detection zone," *IEEE Transactions on Smart Grid*, vol. 12, no. 2, pp. 1063–1072, 2021.

[25] G. G. . S. U. Das, D., "Transition between grid-connected mode and islanded mode in VSI-fed microgrids," *Sādhanā 42*, p. 1239–1250, 2017.

[26] Y. Hirase, K. Abe, K. Sugimoto, and Y. Shindo, "A Grid Connected Inverter with Virtual Synchronous Generator Model of Algebraic Type," *IEEJ Transactions on Power and Energy*, vol. 132, no. 4, pp. 371–380, Jan. 2012.

[27] J. Driesen and K. Visscher, "Virtual synchronous generators," in *2008 IEEE Power and Energy Society General Meeting - Conversion and Delivery of Electrical Energy in the 21st Century*, 2008, pp. 1–3.

[28] K. Visscher and S. De Haan, "Virtual synchronous machines (vsg's) for frequency stabilisation in future grids with a significant share of decentralized generation," in *CIRED Seminar 2008: SmartGrids for Distribution*, 2008, pp. 1–4.

[29] R. Hesse, D. Turschner, and H.-P. Beck, "Micro grid stabilization using the virtual synchronous machine (visma)," *Renewable Energy and Power Quality Journal*, vol. 1, pp. 676–681, 04 2009.

[30] H.-P. Beck and R. Hesse, "Virtual synchronous machine," in *2007 9th International Conference on Electrical Power Quality and Utilisation*, 2007, pp. 1–6.

[31] Q.-C. Zhong and G. Weiss, "Synchronverters: Inverters that mimic synchronous generators," *IEEE Transactions on Industrial Electronics*, vol. 58, no. 4, pp. 1259–1267, 2011.

[32] H. Wu, X. Ruan, D. Yang, X. Chen, W. Zhao, Z. Lv, and Q.-C. Zhong, "Small-signal modeling and parameters design for virtual synchronous generators," *IEEE Transactions on Industrial Electronics*, vol. 63, no. 7, pp. 4292–4303, 2016.

[33] S. Dong and Y. C. Chen, "Adjusting synchronverter dynamic response speed via damping correction loop," *IEEE Transactions on Energy Conversion*, vol. 32, no. 2, pp. 608–619, 2017.

[34] S. D'Arco and J. A. Suul, "Virtual synchronous machines — classification of implementations and analysis of equivalence to droop controllers for microgrids," in *2013 IEEE Grenoble Conference*, 2013, pp. 1–7.

[35] Z. Shuai, Y. Hu, Y. Peng, C. Tu, and Z. J. Shen, "Dynamic stability analysis of synchronverter-dominated microgrid based on bifurcation theory," *IEEE Transactions on Industrial Electronics*, vol. 64, no. 9, pp. 7467–7477, 2017.

[36] J. Alipoor, Y. Miura, and T. Ise, "Power system stabilization using virtual synchronous generator with alternating moment of inertia," *Emerging and Selected Topics in Power Electronics, IEEE Journal of*, vol. 3, pp. 451–458, 06 2015.

[37] A. J. Sonawane and A. C. Umarikar, "Small-signal stability analysis of pv-based synchronverter including pv operating modes and dc-link voltage controller," *IEEE Transactions on Industrial Electronics*, vol. 69, no. 8, pp. 8028–8039, 2022.

[38] M. Ashabani and Y. A.-R. I. Mohamed, "Novel comprehensive control framework for incorporating vscs to smart power grids using bidirectional synchronous-vsc," *IEEE Transactions on Power Systems*, vol. 29, no. 2, pp. 943–957, 2014.

[39] R. Rosso, J. Cassoli, G. Buticchi, S. Engelken, and M. Liserre, "Robust stability analysis of lcl filter based synchronverter under different grid conditions," *IEEE Transactions on Power Electronics*, vol. 34, no. 6, pp. 5842–5853, 2019.

[40] J. Liu, Y. Miura, H. Bevrani, and T. Ise, "Enhanced virtual synchronous generator control for parallel inverters in microgrids," *IEEE Transactions on Smart Grid*, vol. 8, no. 5, pp. 2268–2277, 2017.

[41] Z. Shuai, Y. Peng, J. M. Guerrero, Y. Li, and Z. J. Shen, "Transient response analysis of inverter-based microgrids under unbalanced conditions using a dynamic phasor model," *IEEE Transactions on Industrial Electronics*, vol. 66, no. 4, pp. 2868–2879, 2019.

[42] N. Pogaku, M. Prodanovic, and T. C. Green, "Modeling, analysis and testing of autonomous operation of an inverter-based microgrid," *IEEE Transactions on Power Electronics*, vol. 22, no. 2, pp. 613–625, 2007.

[43] N. Bottrell, M. Prodanovic, and T. Green, "Dynamic stability of a microgrid with an active load," *Power Electronics, IEEE Transactions on*, vol. 28, pp. 5107–5119, 11 2013.

[44] N. Bottrell, "Small-signal analysis of active loads and large-signal analysis of faults in inverter interfaced microgrid applications," PhD dissertation, University of London, Imperial College London, London, United Kingdom, 2015.

[45] D. P. Ariyasinghe and D. M. Vilathgamuwa, "Stability analysis of microgrids with constant power loads," in *2008 IEEE International Conference on Sustainable Energy Technologies*, 2008, pp. 279–284.

[46] P. E. S. N. Raju and T. Jain, "Centralized supplementary controller to stabilize an islanded ac microgrid," in *2014 Eighteenth National Power Systems Conference (NPSC)*, 2014, pp. 1–6.

[47] *RTDS Hardware Manual*, Rev. 2 ed., RTDS Technologies, Winnipeg, 2012.